3 2 1
8-31-62

IDO-16787

MASTER

ORGANIC COOLANT REACTOR PROGRAM QUARTERLY REPORT

January 1 - March 31, 1962

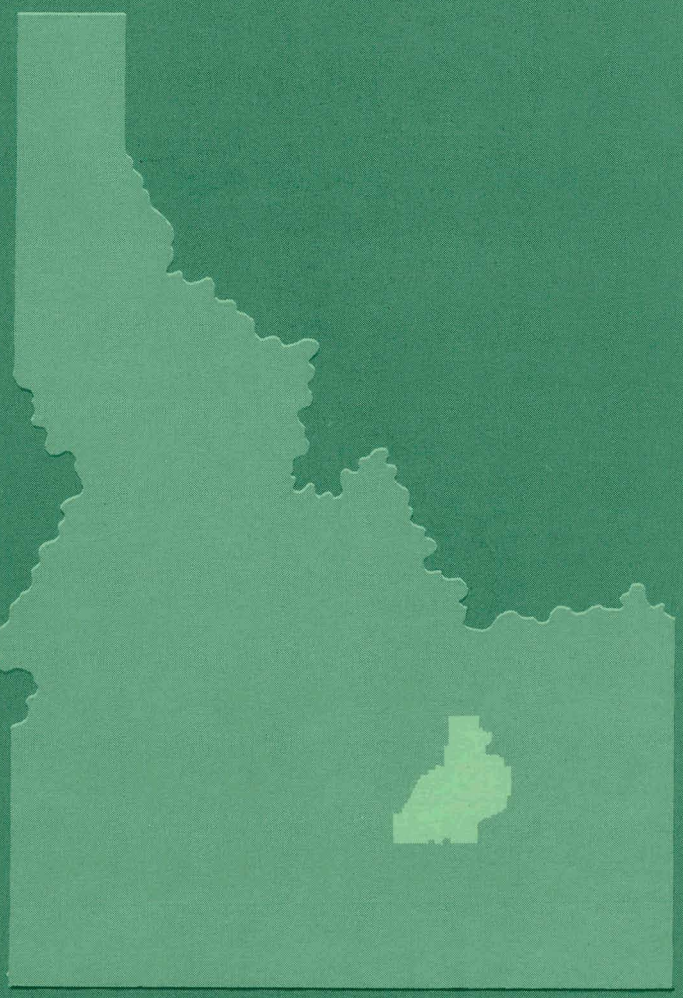

PHILLIPS PETROLEUM COMPANY

ATOMIC ENERGY DIVISION

NATIONAL REACTOR TESTING STATION

US ATOMIC ENERGY COMMISSION

DISCLAIMER

PRICE $2.50

Available from the
Office of Technical Services
U. S. Department of Commerce
Washington 25, D. C.

Printed in USA

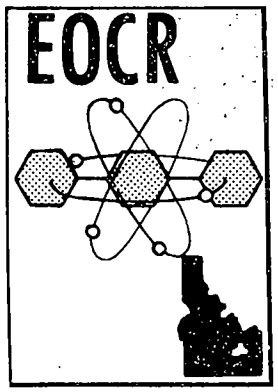

IDO-16787
AEC Research and Development Report
Reactor Technology
TID-4500 (17th Ed.)
Issued: June 29, 1962

ORGANIC COOLANT REACTOR PROGRAM

QUARTERLY REPORT

January 1 - March 31, 1962

J. R. Huffman
Assistant Manager, Technical

J. A. McBride
Manager, Chemical Technology

J. C. Hillyer
Manager, OCR Project, Bartlesville

J. W. Dykes
Superintendent, EOCR Operations

W. B. Lewis
Manager, EOCR Technical Branch

PHILLIPS
PETROLEUM
COMPANY

Atomic Energy Division

Contract AT(10-1)-205
Idaho Operations Office
U. S. ATOMIC ENERGY COMMISSION

Organic Coolant Research (Part I of this report) was carried out by Phillips Petroleum Company, Research and Development Department, Bartlesville, Oklahoma under Contract AT(10-1)-1080 with the Idaho Operations Office, U.S. Atomic Energy Commission.

Previous Quarterly Reports in the OCR Series

1960

Quarter	Number
4	IDO-16675

1961

Quarter	Number
1	IDO-16705
2	IDO-16713
3	IDO-16734
4	IDO-16761

ORGANIC REACTOR TECHNOLOGY
QUARTERLY REPORT
JANUARY 1 - MARCH 31, 1962

SUMMARY

The possible effects of a hydrogen atmosphere in reducing film deposition were studied in the large circulating loop and in rocking cell and pyrolytic capsule tests. At hydrogen pressures of 200 to 400 psig no reduction in film weight deposited was observed in the loop tests, and in the pyrolytic tests film deposits were doubled. Heat conductivity of the films was much higher however. In these high ash films the inorganic constituent was found to be α-iron rather than the usual magnetite, which seems to account for the heat conductivity.

Separation of benzene insoluble material from high boiler and coolant was accomplished by centrifugation and by deposition on glass. The material was closely related to film formation. The nature of the inorganic and organic constituents of this material was examined in several analytical studies. Advances in the techniques of nuclear magnetic resonance, oxygen analysis, measurement of chromatograms, application of computers, and other methods were made.

It was demonstrated by use of Fe-59 that irradiated terphenyl under air attacks iron rapidly and possibly the iron is in solution as a chelate or other complex. It also was indicated by some tests that such a soluble form of iron can figure in the formation of film and of the iron percarbide observed.

The program of synthesis of pure samples of polyphenyls neared completion, and the attention was shifted to synthesis of new candidate coolants. Fused-ring structures, partially hydrogenated, such as dihydrophenanthrene have been made and proved of interest. Some similar studies from the stabilizer investigation indicate the same thing. Other groups in which synthetic activity has been initiated are the substituted triazines, pyridines, and other heterocyclic non-benzenoid types. The industrial coolant candidates from petroleum and coal tar were found to be lacking in thermal stability above 700°F. Only the hydrodealkylated decant oil appeared to have promise for future development.

The study of hydrocracking high boiler neared completion. Very good results were obtained using unfractionated coolants, and with the most recent high boiler produced at OMRE. An economic survey of processing high boiler to reclaim coolant is nearing completion.

Close technical liaison continued throughout the quarter with AEC-IDO and Fluor Corp on the Title II design of the Coolant Technology Loop (CTL) and the Fuel Technology Loop (FTL). Title I review of the loop handling equipment was completed.

The scheduled completion date for the loops is currently being revised. However, procurement of material and equipment is progressing adequately to meet the required dates for field installation.

Construction of the Component Development Test Loop (CDTL) was completed and operational shakedown of the loop started. Successful operation at 550°F was realized. Initial operation and testing of a single-stage Chempump in the CDTL showed a high mass transfer of the hot (up to 500°F) pumped fluid from the pump discharge, through the rotor chamber, and back to the pump suction. The necessary parts have been returned to the manufacturer for modification.

Initial testing of the ball valve has shown acceptable results.

A report, IDO-16675, containing complete details of the EOCR control rod latch reliability test has been issued.

A conceptual design of the FTL nuclear mockup was completed. This mockup will duplicate the nuclear characteristics of the in-pile tube containing a fuel-follower sample for the A-3 core loading.

Detailed design of the approach-to-power samples is nearing completion.

The eight driver elements being instrumented are D-4, D-6, D-9, D-10, D-11, D-12, D-16, and P-12. These elements were chosen on the basis of coolant flow, flux distribution, core symmetry, and rod programming.

A successful run was made demonstrating displacement of Santowax OMP with ethylene glycol from a small model fuel element.

Chemical cleaning procedures for the EOCR have been tested in a small circulating loop. Fouling tendency tests on Santowax contacting chemically cleaned surfaces will be run.

Screening tests have been run in the MTR gamma facility to study the role of free radicals in radiolytic degradation mechanisms.

Pyrolytic degradation screening tests have shown the need for impurity control.

Design of equipment to study film formation on heated surfaces was completed. Studies have been planned utilizing the MTR rabbit facility.

A calorimeter has been designed to differentiate gamma and fast neutron energy absorption in the EOCR.

Apparatus has been constructed to perform pyrolytic capsule fouling tests under irradiation.

The radiological hazards associated with the operation of the EOCR have been analyzed, and the estimated radiation dose rates are presented. It is concluded that operation of the EOCR appears to present no serious hazards.

A detailed study of the steady-state heat transfer and hydraulics of the first EOCR operational core has been made. The presentation records the calculational methods and the EOCR hot-spot and hot-channel factors, the recommended coolant flow distribution among the fuel assemblies and control rods,

and the calculated operating power levels as a function of the fuel-plate hot-spot temperature which is permitted.

A two-dimensional burnout study has been made on the proposed first EOCR operational core loading, and an operating life of 1200 Mwd or more is expected.

EOCR Operations Branch personnel continued to study and evaluate design and construction of the EOCR. This evaluation and study was directed toward efficient and safe operation of the facility.

Representatives of the branch witnessed plant equipment component tests performed by the construction contractor. Testing of an EOCR prototype control rod and check-out of reactor control circuitry continued.

Operational planning included the completion (in initial draft form) of portions of the final hazards report and the utilities section of the plant operating manual. Considerable effort was expended in forecasting anticipated needs and initiating design and procurement of various items which will be required for initial operation of the plant.

THIS PAGE

WAS INTENTIONALLY

LEFT BLANK

ORGANIC REACTOR TECHNOLOGY
1962 QUARTER 1
JANUARY 1 - MARCH 31, 1962

CONTENTS

FIGURES

TABLES

THIS PAGE

WAS INTENTIONALLY

LEFT BLANK

I. ORGANIC COOLANT RESEARCH

1. INTRODUCTION

The Research Division of Phillips Petroleum Co at Bartlesville, Okla, under Contract AT(10-1)-1080 with the Idaho Operations Office of the U. S. Atomic Energy Commission, as part of Phillips' program on technology of organic-cooled and moderated nuclear reactors, continued its study of the fundamentals of radiolytic breakdown of organic compounds, the deposition of film on fuel element surfaces, the selection of more resistant coolants, and the stabilization and reclamation of coolants.

Basic work in the radiolysis of terphenyls and on the mechanism and prevention of film formation continued to receive the major emphasis during this quarter. Work in the area of new coolants was extended and both this field and that of stabilization were closely correlated with the fundamental radiolytic studies. Studies on reclamation of damaged coolant by a hydrocracking process reached a point that a feasible, operable process appeared in hand. A preliminary economic evaluation was made and the final phases of the experimental work initiated.

2. RADIOLYTIC EXPERIMENTS

(P. S. Hudson, W. M. Hutchinson, A. J. Moffat, P. W. Soloman, R. A. Mengelkamp)

2.1 Introduction

During this quarter continuing emphasis was directed toward the understanding of the fundamentals of coolant breakdown to yield film. Together with other basic studies of mechanism of coolant radiolysis to high and low boilers, these have made up the bulk of the radiolytic studies. Due to extended operating difficulties with the Linac, however, the amount of time available for radiolytic experiments was severely limited.

2.2 Dosimetry for the Linear Electron Accelerator (Linac)

The high energy output of the Linac, together with the power fluctuations and the energy distribution in the beam, poses problems in dosimetry. A sampling calorimeter designed to handle the dosimetry was described in the previous quarterly report [1]. Due to the reduced time available on the Linac and especially due to erratic operation and limited available power during on-stream time, further tests with the calorimeter have been held in abeyance.

2.3 Film Deposition Under Irradiation

Tests were carried out in the large circulating loop using the irradiation cell which simulates the geometry of an OMRE fuel element channel, in the smaller loop using the thick-channel cell, and in the simple agitated cracking cell. One area receiving attention was the possible effect of a hydrogen atmosphere in reducing film deposition, a study which has been supplemented by extensive tests in the static pyrolysis apparatus.

2.31 Large Circulating Loop. Using the large out-of-pile circulating loop with the OMR replica cell, the effect of a hydrogen gas blanket as compared to a nitrogen gas blanket was studied.

Tests EPL-15 and 16 - Effect of Hydrogen Blanket

Test EPL-16 was conducted with a hydrogen blanket. It has been reported that hydrogen inhibits fouling in hydrocarbon heat exchangers under refinery conditions. The purpose of this study was to investigate the effect of hydrogen under electron irradiation conditions. Test EPL-15 was a control test conducted with a nitrogen blanket. In Table I conditions used for the tests are shown. These are standard conditions normally employed with the large loop. Test results are shown in Table II and photographs of the test cell plates and windows are shown in Figures 1 and 2.

Inspection of the test results in Table II shows no significant difference in film thickness on the windows and plates. However, there appears to be more weight of film on the window and plates after the hydrogen run. X-ray diffraction analyses indicate that magnetite is the primary form of iron found when nitrogen is used as a blanket, whereas the heavier alpha-iron and cementite are formed when a hydrogen blanket is used. This suggests that the magnetite in the coolant was reduced by the hydrogen. There is no significant difference in the amount of carbon, hydrogen, and ash between the two films. The appearance

TABLE I

CIRCULATING LOOP TEST CONDITIONS

Test No.	EPL-15	EPL-16	REPL-1	REPL-2
Coolant	OMP	OMP	OMP	Modified Core 2(a)
High boiler (%)	0	0	0	11
Ferrocene (%)	0.2	0.2	0	0
Total iron content (ppm)	600	600	0	14
Blanket gas	N_2	H_2	N_2	N_2
Blanket pressure (psig)	200	200	200	200
Electron window temp. (°F)	900	900	700	700
Bottom plate temp. (°F)	760	770	—	—
Bulk coolant temp. (°F)	730	732	650	640
Coolant velocity (ft/sec)	6.0	6.0	2.5	0.8
Test time (hr)	56	51	4	4

(a) This is a modified Core 2 coolant which contains 11% high boiler, 1.3% alkyl terphenyls, 15.8% o-terphenyl, 46.6% m-terphenyl, 23.2% p-terphenyl, 0.6% triphenylene, 1.5% quaterphenyls, and 14 ppm iron content.

TABLE II

CIRCULATING LOOP TEST RESULTS

Test No.	EPL-15	EPL-16	REPL-1	REPL-2
Film thickness on window (mils)	0.1	0.1	0.1	0
Film thickness on plates (mils)	0.1	0.1	—	—
Film thickness on cell walls (mils)	—	—	1.6	0
Film weight on window (mg)	7.4	9.0	—	—
Film weight on plates (mg)	46.8	94.8	—	—
Film composition				
%C	18.4	27.8	54.5	—
%H	1.4	1.6	2.6	—
C/H	1.1	1.9	1.8	—
% Ash	80.7	81.7	44.9	—
X-ray diffraction analysis	Fe_3O_4, α-Fe Austenite	α-Fe, Fe_3C Austenite, Fe_3O_4	Fe_3O_4, α-Fe	
Heater deposit	yes	no	no	no
Increase of HB in coolant (%)	3.6	3.8	1.1	—
Estimated dose (rads)	4.0×10^8	4.0×10^8	10^8	10^8
Blanket gas* mass spectrometer (mol%)				
H_2	13.15	80.2	—	—
N_2	81.58	11.3	—	—
CO_2	0.73	1.1	—	—
O_2	0.07	0.1	—	—
C_1 and heavier	4.47	7.3	—	—

* Gas samples taken at end of test.

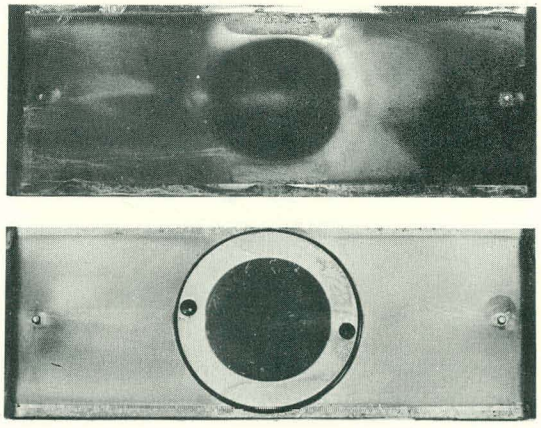

EPL – 15
SANTOWAX – OMP
+600 PPM IRON
6 FPS 12–15–61
FLOW ⟶

Fig. 1 Electron irradiation window and plates from test EPL-15.

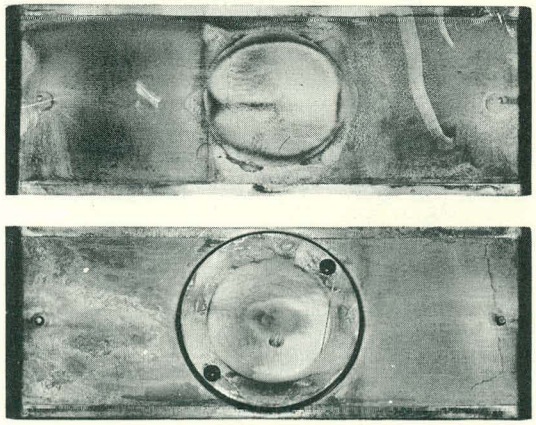

EPL – 16
SANTOWAX – OMP
+ 600 PPM IRON
6 FPS H_2 BLANKET
1–11–62
FLOW ⟶

Fig. 2 Electron irradiation window and plates from test EPL-16.

of the film produced with the hydrogen was more lustrous and shiny. A check of the 220-volt hairpin heater, which is, of course, not exposed to radiation, showed no deposit with hydrogen but a deposit was noted with the nitrogen blanket. This deposit was 88.1% carbon, 4.4% hydrogen, 1.67 C/H, and ash was 8.7%. This low ash was typical of films formed pyrolytically in the circulating loop.

Overall, there appeared to be no significant benefit from using a hydrogen blanket under electron irradiation conditions. This will be checked using Core 2 coolant at a later date. Pyrolytic capsule data have been obtained with hydrogen blankets. These results indicate better heat transfer with film formed with hydrogen. This is discussed later in this report under "Pyrolytic Experiments".

2.32 Small Circulating Loop. Two initial electron irradiation shakedown runs were conducted on the smaller loop (Research Electron Pumping Loop or REPL). This loop is now fitted with an irradiation cell with a channel 1.75 in. deep, and the whole system requires only three or four liters of coolant. The out-of-beam volume ratio is about 24:1 while in the large EPL loop it is of the order of 800:1.

Test REPL-1 and 2 - Test Procedure Development

The test conditions for REPL-1 are shown in Table I. The test was terminated at the end of 4 hr due to pump and cell leakage. Test results are shown in Table II. Film was noted on the window which was very adherent (See Figure 3). Film on the sides of the cell was not very adherent. The rapid film formation may have been caused by pump shaft galling which raised the ash content to about 538 ppm. Increasing the pump temperature will provide better lubrication and greatly reduce shaft wear and galling.

About 1.1% high boiler was generated in the test period which probably supplied binder for film formation.

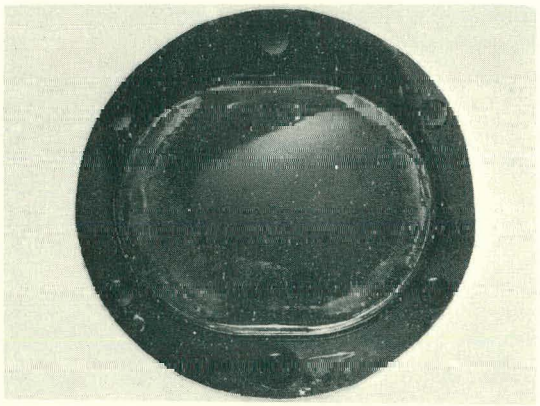

REPL-1
SANTOWAX-OMP
2.5 FPS
2-21-62
FLOW ⟶

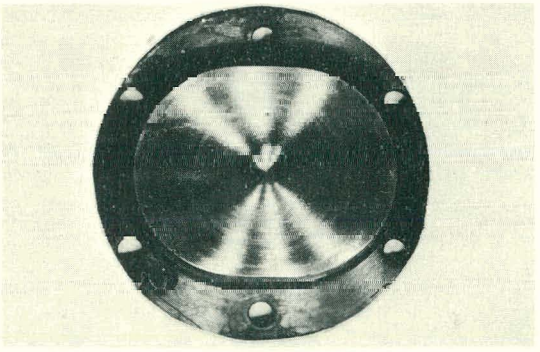

REPL-2
CORE II COOLANT
(CM-10235-64 H)
0.8 FPS
3-22-62
FLOW ⟶

Fig. 3 Electron irradiation windows from tests REPL-1 and REPL-2.

The test conditions for the second shakedown run, REPL-2, are shown in Table I. Again the test was terminated after 4 hr. The leakage this time was only at the window. Cell leakage was prevented by removing the trace heating from the cell as soon as coolant had begun to circulate. Pump wear was controlled by increasing operating temperature to above 300°F. Ash in the coolant was only 52 ppm at the end of the test. The window is being redesigned as a result of this test. It will be noted in Table II that no film was generated in this test. A photograph of the window is shown in Figure 3.

It appears that this small loop may produce significant test films in much less time than the larger EPL loop.

Effect of Beta Current on Film Formation

In order to study the effect of beta current on film formation, two stainless steel plates were located inside the REPL-2 irradiation cell about 0.8 in. below the window. One plate was grounded while the other plate was not. No significant film was developed on the plates or window during this short test. No measureable beta current was observed flowing from the plate, through a microammeter, to ground. The reason for no current flow to the grounded plate may be due to the one-half power operation of the Linac during the test or that the condenser plates were located too far from the window. This experiment will be repeated at full Linac power.

Summary of Loop Test Results

Based on the circulating loop tests run during this quarter, the following two items summarize results and conclusions of the work.

(1) A comparison of film formed under a hydrogen blanket with film formed under a nitrogen blanket shows no reduction in film thickness or film weight in the electron-irradiated circulating loop.

(2) The small electron irradiation circulating loop with the 1.75-in. coolant channel promises to be capable of producing significant films in much less time than the larger EPL loop.

2.33 Rocking Irradiation Cell. Several shakedown tests have been made with radiation rocker 3. The plans for this apparatus were given in the last quarterly report [2]. Table III summarizes the test conditions of the runs made during this quarter. Most of the runs were made to establish a base line for the tests. Irregular operation of the Linac made it difficult to obtain uniform test conditions.

In Run 1, Core 2 coolant with 0.2 wt% ferrocene was irradiated for 8 hr under 200-psig nitrogen pressure. The film deposited on the top part of the tube as a brittle cohesive coke.The appearance of the film suggested pyrolytic damage.

In Run 7 a leak developed and coolant was lost. Again, a brittle coke was formed on the top side of the tube. The loss of coolant may have caused the tubes to be less than liquid full, resulting in pyrolysis on the exposed surface.

Run 9 behaved satisfactorily; however, the film was coke-like.

TABLE III

CONDITIONS AND COOLANTS USED IN RADIATION ROCKER UNDER LINAC

Run No.	Irrad. Time (hr)	Coolant	Bulk Temp (°F)	Tube Temp(°F) Top	Bottom	Atmosphere or Additives
1	8.0	Core 2(a)	697	932	903	200 psig N_2; 0.2% ferrocene
7	8.0	Core 2(a)	689	—	902	200 psig N_2
9	8.0	Core 2(a)	689	—	897	200 psig N_2
11	8.0	Core 2(a)	696	850(b)	900	200 psig N_2
13	8.0	Core 2(a)	697	866(b)	902	200 psig N_2
15	8.0	OMP	692	875(b)	903	200 psig N_2
17	4.0	OMP	650	900	740	200 psig N_2
22	8.5	OMP	670	900(c)	850	200 psig N_2
24	8.0	OMP	486	901(c)	620	200 psig N_2; 0.136% Fe_3O_4; 0.25% (10899-12c)(d)
26	8.0	OMP	639	908(c)	760	20 wt% benzene + N_2 to give 200 psig
28	8.0	OMP	484	896(c)	607	240 psig ethane

(a) Core 2 coolant contains 23% HB

(b) Air jet used to cool top of tube

(c) Test section insulated with asbestos tape

(d) Benzene insoluble material from high boiler

In Runs 11, 13, and 15 the coolant was melted prior to irradiation. This procedure eliminated the stagnant pool of coolant in the tube during the initial phase of the test. However in Run 11, the Linac was shut down during the test and the coolant solidified. In this run a heavy coke formed again. Thus, it was necessary to keep the coolant molten before and during the test to avoid pyrolysis. In Run 13 the coolant remained molten and the film was deposited as a fine, carbon black type of material on the top surface of the tube. Run 15 was made with virgin Santowax OMP. The same type of film was formed as was found in Run 13.

In Run 13 the electron beam power was reduced so the thermocouple on the top of the tube read 900°F throughout the run. In this run the top of the stainless steel test section was blued where the electron beam impinged. Very little film was deposited. A similar result was obtained in Run 22, where the tube was insulated with asbestos tape to reduce heat loss from the test section and provide a more uniform temperature.

Run 24 was made with added particulate (Fe_3O_4) and benzene insoluble high boiler. These conditions give more film in the pyrolytic tests. However, the results, identical to those in Runs 17 and 22, showed a blued surface with little film.

Run 26 used a benzene atmosphere and Run 28 used an ethane atmosphere. Again, the test surface was blued with little film.

In summary, Runs 17, 22, 24, 26, and 28 gave similar results: a blued upper surface and a small amount of film. The failure of the apparatus to distinguish between various test conditions indicates a change in procedure is necessary. Future work will include higher test temperatures in an effort to lay down film.

2.34 Cells for Irradiation of Samples Under the Linac. Recent electron irradiation of a series of biphenyl and p-terphenyl samples under the Linac has shown the need for more sophisticated equipment than the simple rotator used presently. Analyses of the irradiated samples from this series gave highly erratic results. This was attributed to the fact that the irradiation tubes were in almost a horizontal position during the run and the electron beam struck only part of the sample.

To eliminate this problem, a horizontally oscillating table has been designed. This will hold eight samples which can be passed back and forth through the Linac beam at a preselected speed. Agitation will be by means of magnetic stirrers. Provision will be made for collecting gas samples when desired. This apparatus should be available soon.

2.35 Film Removal From Test Samples - Ultrasonic Removal with Hydrochloric Acid. Complete removal of carbonaceous films from the electron pumping loop test plates by ultrasonic treatment was not successful with organic solvents. The use of acid media with the ultrasonic treatment removed the film completely. However the use of acid undoubtedly would dissolve any exposed inorganic portions of the films. To verify this dissolving action, 11.4 mg of film which had been removed from the cell plates of EPL test 14 (Santowax OMP + 0.2% ferrocene irradiated for 6.5 hr) with water were subjected to ultrasonic treatment in 10% hydrochloric acid solution (10 ml 37% hydrochloric acid + 90 ml water) for 4 hr. Only 3 mg of material was recovered showing the acid treatment dissolved a considerable portion of the film. The analyses before and after acid treatment showed the following:

	°C	% H	C/H Ratio	% Ash	X-Ray Diffraction
Before acid treatment	12.3	0.7	1.4	87.7	α-Fe, Fe_3O_4
After acid treatment	33	3.0	0.9	58	α-Fe, Fe_3O_4

The sample after treatment was too small for an accurate analysis but it still contained both α-iron and magnetite indicating some of the inorganic portion was protected by organic film. An electron micrograph of the two materials, magnified 5000 times, showed essentially no difference.

From the above results, quantitative determinations of film weights would not be possible in acid media. Total organic film would be possible by this method, however.

2.4 Fundamental Studies

2.41 Partial Reaction Rates of Biphenyl. Biphenyl samples were irradiated at 80°C and at 300°C under a Linac (6-Mev pulsed electron beam). Analyses of the products of these irradiations was completed this quarter, using an improved procedure for evaluating the gas chromatograms. This procedure is described in some detail in a subsequent part of this report (See page 37). From the relative yields of quaterphenyls so determined, the partial reaction rates were calculated. Exposures to irradiation were limited to 12 min at 180-rep rate to keep conversion low. (0.5% and 1.0% at 80°C and 300°C, respectively.)

The samples were evaporated at 80 to 90°C at 1-mm Hg to leave a residue still containing about 90% biphenyl. The sublimate contained no material higher than biphenyl detectable by gas chromatography. The residues were then analyzed by gas chromatography, with the use of known mixtures of biphenyl and the six linear quaterphenyls, as described on page 37.

The results of these tests, with calculation methods shown, are given in Table IV. The composition of quaterphenyl isomers found was taken as equivalent to the relative yields from biphenyl. Partial reaction rates were calculated from these data.

The calculations were based on the following reaction model:

Event 1: Generation of reactive species by irradiation of a biphenyl molecule

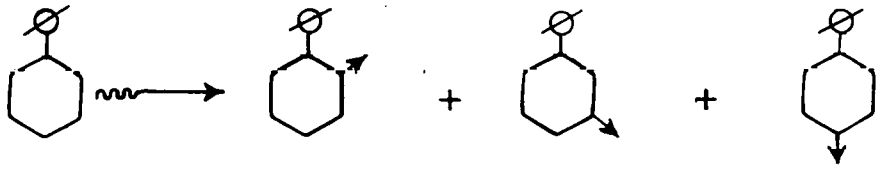

TABLE IV

ANALYSIS OF QUATERPHENYLS FROM IRRADIATION OF BIPHENYL WITH ELECTRONS (LINAC)

Sample	Analyses	Evaluation Method	Deviation of Sum From Unity (%)	Average Deviation (%)	Composition of ϕ_4 Isomers (%) (Relative Yield)					
					0,0	0,M	0,P	M,M	M,P	P,P
Irradiations at 80°C										
A-1	31-37	Ht x W	+0.09	2.7	12.98	23.42	21.78	11.21	22.24	8.37
A-1	31-38	Ht	-0.17	2.4	12.07	24.15	21.65	11.72	22.84	7.57
A-4	50-69	Ht x W	0.00	2.8	14.36	25.81	20.61	10.70	21.00	7.62
A-4	50-69	Ht	+0.85	1.0	12.59	26.43	19.87	11.42	21.78	7.91
Irradiations at 300°C										
V	70-75	Ht x W	+0.75	1.7	5.46	20.13	17.35	18.26	29.92	8.88
V	70-75	Ht	-0.72	1.3	5.26	16.70	15.92	20.06	32.35	9.71
VI	42-47	Ht x W	+0.38	4.1	3.99	19.03	17.13	19.33	31.28	9.27
VI	42-48	Ht	-0.98	3.0	4.21	18.02	15.82	20.29	32.14	9.28

The arrows indicate reactive sites at the ortho, meta, and para positions. These may be radicals, ions, molecule-ions, excited molecules that eventually react at the site indicated, etc. The kinds of reactive species are not differentiated. The conditional (or relative) probabilities of formation of the three isomeric types of reactive species are notated as Pr_o (ortho reactive species), Pr_m, and Pr_p. These probabilities apply only to those reactive species that attack and substitute a biphenyl molecule. If recombination or hydrogen abstraction occurs, the presence of that reactive species is not detected in the products of reaction.

Event 2: Reaction of reactive species to substitute a biphenyl molecule

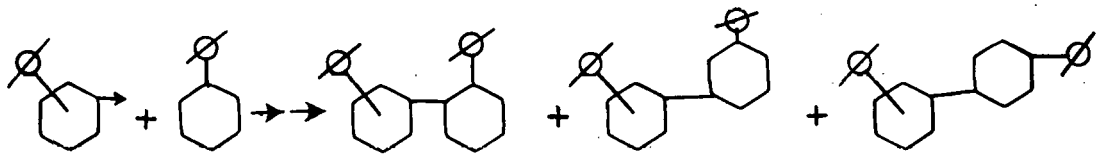

The conditional (or relative) probability for attack at the three different positions on a biphenyl molecule are notated Pa_o (attack at the ortho position), Pa_m, and Pa_p. Attack is equivalent to substitution. If no substitution occurs, the act is not detected in the products of reaction.

Both events are necessary for formation of a quaterphenyl from biphenyl. The probability of the complete reaction (both events) is the product of probability of event 1 times the probability of event 2. From these considerations the following equations are obtained:

$$\text{Rel. yield } 0,0\text{-}\phi_4 = Pr_o\, Pa_o \quad (1)$$

$$\text{Rel. yield } 0,m\text{-}\phi_4 = Pr_o\, Pa_m + Pr_m\, Pa_o \text{ (two reactions form same product)} \quad (2)$$

$$\text{Rel. yield } 0,p\text{-}\phi_4 = Pr_o\, Pa_p + Pr_p\, Pa_o \text{ (two reactions form same product)} \quad (3)$$

$$\text{Rel. yield } m,m\text{-}\phi_4 = Pr_m\, Pa_m \quad (4)$$

$$\text{Rel. yield } m,p\text{-}\phi_4 = Pr_m\, Pa_p + Pr_p\, Pa_m \text{ (two reactions form same product)} \quad (5)$$

$$\text{Rel. yield } p,p\text{-}\phi_4 = Pr_p\, Pa_p \quad (6)$$

$$Pr_o + Pr_m + Pr_p = \text{unity (1.00)} \quad (7)$$

$$Pa_o + Pa_m + Pa_p = \text{unity (1.00)} \quad (8)$$

Equations (7) and (8) are implied in the conditional (relative, fractional) probabilities in Equations (1) through (6) but demonstrate the conditions of these probabilities and are useful in calculations by hand. Solution of the equations is readily done by hand by solving for Pa in Equations (1), (4), and (6) in terms of yield/Pr and substituting into Equations (2), (3), and (5). This gives quadratics in Pr which simultaneously yield two solutions for each equation. These resolve into two symmetrical sets. One set solves for Pr and the other for

Pa. Also Pr can be converted into Pa (and vice versa) through Equations (1), (4), and (6).

In all cases the solutions were self-consistent but could not distinquish between the real Pr and Pa. This had to be assigned from results of experiments where event 1 was absent (eg, from the photolysis of 2-iodobiphenyl in biphenyl). This will be discussed later when the Pr and Pa are converted into the partial reaction rates r and k, respectively.

The partial reaction rates r and k are the same as the probabilities Pr and Pa, respectively, after adjustment is made for the number of ortho, meta, and para sites on biphenyl. Partial rates are usually given with respect to another molecule, such as benzene, obtained by competitive reactions. In the present case biphenyl alone was irradiated so the partial rates are relative. The meta position was chosen for reference. Thus the partial rates for the meta position were taken as unity (and not reported). Partial rates for ortho and para positions were obtained by:

$$k_o = \frac{Pa_{o/4}}{Pa_{m/4}} = \frac{Pa_o}{Pa_m}$$

$$k_p = \frac{Pa_{p/2}}{Pa_{m/4}} = \frac{2\,Pa_p}{Pa_m}$$

$$r_o = \frac{Pr_{o/4}}{Pr_{m/4}} = \frac{Pr_o}{Pr_m}$$

$$r_p = \frac{Pr_{p/2}}{Pr_{m/4}} = \frac{2\,Pr_p}{Pr_m}$$

Conversely, the reported sets of k and r can be converted into complete sets of Pa and Pr by normalizing the latter to make each set sum to unity.

Table V reports the partial rates of biphenyl calculated from the relative yields of quaterphenyl isomers presented in Table IV. Sample identification, analysis numbers, and methods used in evaluation of chromatograms are listed in the first three columns. The fourth column (heading labeled "Fit") gives the average percent deviation between experimental relative yields (Table IV) and yields calculated from the reported partial rates. This deviation is a measure of internal consistency of a set of analyses with the partial rate model. In all but one case this deviation is less than the scatter among analyses (column 5 Table IV). The major individual deviations between experimental and calculated yields (Fit) were usually those of o,m- and o,p-quaterphenyl. These often constituted one-half of the total deviation. While calculating deviations, algebraic sums were obtained to test for balance in the solutions. The difference between the + and - algebraic sums never exceeded 10% of either sum.

TABLE V

PARTIAL RATES OF BIPHENYL FROM RELATIVE YIELDS OF QUATERPHENYLS

Sample	Analyses	Evaluation Method	Fit (% Deviation)	Partial Reaction Rates r_o	r_p	k_o	k_p
Irradiations at 80°C							
A-1	31-37	Ht x W	2.9	0.96	1.0	1.2	3.0
A-1	31-38	Ht	1.7	1.06	0.9_1	0.9_7	2.8
A-4	50-69	Ht x W	1.6	0.86	0.96	1.6	3.0
A-4	50-69	Ht	0.5	0.64	0.98	1.7	2.9
Irradiations at 300°C							
V	70-75	Ht x W	0.2	0.61	0.78	0.49	2.5
V	70-75	Ht	1.0	0.57	0.83	0.49	2.4
VI	42-47	Ht x W	2.6	0.7_0	0.9_3	0.2_9	2.1
VI	42-48	Ht	1.4	0.49	0.75	0.42	2.4

As was mentioned in the discussion on solutions of the partial rate model, the Pr and Pa sets are not distinguished. This must be done by comparing the r and k values with k values obtained by experiments where only event 2 occurs. Fortunately such data were available from photolyses of 2-iodobiphenyl in biphenyl and 4-iodobiphenyl in biphenyl [3]. Products from these photolyses were exclusively o,o-, o,m-, and o,p-quaterphenyl from 2-iodobiphenyl-biphenyl; and o,p-, m,p-, and p,p-quaterphenyl from 4-iodobiphenyl-biphenyl. This showed that under the conditions of photolysis (80°C) no isomerization of free radicals or hydrogen abstraction occurred. The k values so obtained were sufficiently close to those from electron irradiation (Table V) that assignments could be made as to which solutions were r and which were k. The data from photolysis were:

$$k_o = 1.3_6 \qquad k_p = 2.0_6$$

The r and k values from electron irradiations at 80°C show that assignments of r and k could be made confidently. The data from electron irradiations at 300°C sufficiently resemble those obtained at 80°C so that assignments of r and k can also be made at 300°C.

Two types of conclusions about the nature of the radiolysis processes may be drawn from the r and k values. Deviation of r values from unity indicate either a selective process for generation of reactive species or some selective

process for destruction of some reactive species. The deviations from unity of r_o and r_p values from the 80°C irradiations are not a convincing demonstration of a non-random process. But both the r_o and r_p values at 300°C are definitely lower than unity. Whether this is due to a selective generative or destructive process cannot be obtained. Since the selective process is operative at 300°C and slightly, if at all, at 80°C, weakening of the C-H bonds at the meta positions suggests itself. Note also that the r_o values are consistently lower than the r_p values at 300°C.

Another kind of conclusion may be drawn from the k values. The k_p values obtained by electron irradiation at 80°C are definitely larger than those obtained by photolysis of iodobiphenyl in biphenyl at 80°C. The latter k value (2.06) is for substitution of biphenyl at the para positions by biphenyl radicals. Hence some reactive species more para-selective than free biphenyl radicals must be operative during the electron irradiation of biphenyl. Some ortho-hindrance at 300°C also appears to be present.

The partial reaction rate model was also applied to some data published by Hoigne and Gaumann [4] concerning the irradiation of toluene. Irradiation was from Van de Graaff electrons but the irradiation temperature was not mentioned in the article. Analysis was by gas chromatography. Reference samples were used but precision of analysis was not given. The radiation products from toluene were bibenzyl, benzyl toluenes, bitolyls, and several unknowns. The relative yield of isomers of bitolyl were given. From these were calculated r and k values using the partial rate model. The relative yields of the bitolyls were calculated from the r and k values to check for fit. The average deviation between experimental and calculated yields was 1.2%. It so happened that $r_o = k_o$ and $r_p = k_p$. These are given below with the experimental yields of isomeric bitolyls and yields calculated from the partial rates:

$$r_o = 0.73 = k_o$$

$$r_p = 1.17 = k_p$$

Isomer:	o,o′	o,m′	o,p′	m,m′	m,p′	p,p′
Experimental:	10	26	16	19	22	6.5
Calculated:	9.85	26.3	15.9	18.7	21.8	6.4

3. PYROLYTIC EXPERIMENTS

(P. S. Hudson, R. B. Regier, R. A. Mengelkamp, and P. W. Solomon)

3.1 Film Deposition

The pyrolytic studies continue to be directed largely to support of the film deposition problem. While it has still been necessary to defer the operation of the large pyrolytic loop, the limited time available on the Linac made possible a larger proportion of the effort for pyrolytic tests this quarter.

3.11 Static Pyrolytic Capsule Apparatus. Work continued on the study of pyrolytic parameters affecting film formation, using the 1200-g capsule described in a previous report [5]. During the current period a study of the effect of a hydrogen blanket on various coolants was made. A single test also was conducted to determine the effect of carbon black in the coolant. In order to reduce the amount of coolant required for a test, a new capsule requiring only 600 g of coolant was fabricated and is currently undergoing test procedure development.

Effect of a Hydrogen Gas Blanket on Various Coolants

There have been reports that a hydrogen gas blanket is capable of inhibiting film formation in hydrocarbon heat exchangers at normal refinery temperatures and pressures. In order to determine whether a hydrogen blanket would inhibit film formation using terphenyl type coolants a series of tests was conducted.

The test procedure involved maintaining an electrically heated tube at a nominal (maximum of the gradient along the tube) temperature of 950°F. Bulk coolant temperature was 620°F. As film was formed on the heated tube, the power required to maintain the 950°F maximum decreased. The fouling potential of the coolant was measured by (a) film weight deposited and (b) power reduction observed during a 24-hr test period.

Test results are shown in Table VI. Tests SF-36 and SF-39 were duplicate tests conducted with a hydrogen blanket. Good test repeatability is indicated. Film formation rate with the hydrogen blanket was almost twice that with a nitrogen blanket in the control test, SF-40. However, power reduction with

TABLE VI

TEST RESULTS OF EFFECT OF SUBSTITUTING HYDROGEN FOR NITROGEN IN THE GAS BLANKET

Test	Coolant	Iron (ppm)	Blanket Gas	Film Formation Rate (mg/hr)	Power Reduction (%)	X-Ray Diffraction	Ash (%)
SF-36	OMP	600(a)	H_2	1.17	5	α-Fe	91
SF-39	OMP	600(a)	H_2	1.13	5	α-Fe	—
SF-40	OMP	600(a)	N_2	0.61	76	Fe_3O_4	59
SF-38	Core 2	50	H_2	0.63	11	α-Fe, Fe_3C, Fe_3O_4	82
SF-6	Core 2	50	N_2	0.33	15	Fe_3O_4	—
SF-11	Core 2	50	N_2	0.33	18	Fe_3O_4	57
SF-41	OMP	100(b)	H_2	0.62	0	α-Fe, Fe_3C	>100(c)
SF-17	OMP	100(b)	N_2	0.23	0	Fe_3O_4	—

(a) 600-ppm iron was added in the form of ferrocene

(b) 100-ppm iron was added in the form of magnetite

(c) This film increased weight when ashed. Iron content was probably 90% in the film.

hydrogen was only 5% as compared to 76% with nitrogen. These differences were explained when X-ray diffraction analysis of the film showed α-iron as the inorganic component when hydrogen was used. The α-iron has a much better thermal conductivity than magnetite which is the usual inorganic component of the film. This effect is quite pronounced when the film has a high iron content. It would be much less in the OMRE where ash in the film is only 20 to 30%. Ash content of the fouling film appeared to be higher with hydrogen. However, as this determination was made on a very small sample, the significance of the analysis may be questionable.

Test SF-38 was conducted using Core 2 coolant with hydrogen. Tests SF-6 and SF-11 are duplicate control runs. This Core 2 coolant gave about twice as much film weight with hydrogen present as did the control runs. There was much less difference in power reduction between the hydrogen and nitrogen blankets than with Santowax OMP. Thus it appears that hydrogen has less effect on heat transfer properties when a coolant, such as Core 2, with 22% high boiler is used. X-ray diffraction analysis of the film showed cementite, magnetite, and α-iron as major compononts. Since not all of the magnetite in Core 2 coolant was reduced to α-iron, some of the magnetite may have been coated with polymer. X-ray diffraction of the iron in Core 2 coolant prior to testing shows it to be in the form of magnetite.

In tests SF-41 and SF-17 magnetite was added to Santowax OMP. In this case a very small amount of organic film binder was available as compared to the earlier tests where ferrocene and Core 2 high boiler were present. This is reflected in low film-formation rates and zero power loss. However, again, more weight of film was formed when the hydrogen blanket was used.

It appeared that all three coolants tested showed a consistently higher film-formation rate with a hydrogen blanket. This probably was due to reduction of magnetite to the more dense α-iron. However, the α-iron particulate has a better thermal conductivity than magnetite. This was indicated by less power reduction when a hydrogen blanket was used. In the OMRE, ash content of the films formed was in the range of 20 to 30%. Reduction of the particulate to α-iron in the OMRE with hydrogen would appear to be of questionable benefit because the heat transfer should not be much improved for largely organic films.

Effect of Carbon Black on Film Formation

In order to determine the effect of carbonaceous particles on film formation, 100 ppm of carbon black (Wyex, an EPC channel black) were added to a newly opened supply of Core 2 coolant. This batch of Core 2 coolant appears to give about the same film formation rate but the power reduction value was higher than with the former lot. These results may be seen in Table VII. There appeared to be no significant difference in film-formation rate when Wyex was added to the coolant. However, power reduction appeared to be higher. The film formed with the Wyex was about 1.5 mils thicker than the film formed in the control test SF-43. If these results can be extrapolated to nuclear reactor operation, it appears that coke and other forms of carbon would be detrimental to heat transfer surfaces. This suggests that high boiler can be absorbed on carbonaceous particles and subsequently be attached to a hot surface. This may partially explain how fouling films can form with coolants with low ash contents.

TABLE VII

TEST RESULTS SHOWING EFFECT OF WYEX CHANNEL BLACK ON FILM FORMATION

Test	Coolant	Wyex (ppm)	Film Formation Rate (mg/hr)	Power Reduction (%)	C/H	Ash (%)
SF-45	Core 2[a]	100	0.35	39	1.2	59
SF-43	Core 2[a]	None	0.37	29	1.6	60

[a] New 5-gal can of OMRE Core 2 coolant (CM 10235-50D)

New Capsules

In order to have a common test procedure for evaluating nuclear coolants an Atomics International Pyrolytic Capsule Fouling Test (PCFT) bomb was fabricated. This device will be employed soon.

Another capsule, which requires only 600 g of coolant, has been fabricated and is undergoing tests. The test procedure will be similar to Static Film (SF) tests being conducted in this laboratory at a constant heater temperature of 950°F and variable power input with the 1200-g capacity capsule.

Conclusions

The data obtained in the SF tests indicated:

(1) Film formation rate increased when a hydrogen blanket was used instead of a nitrogen blanket.

(2) Film thermal conductivity, as measured by power reduction, increased when the hydrogen blanket was used.

(3) Carbonaceous particles tended to decrease thermal conductivity of fouling film.

3.12 Film Deposition on Glass Surfaces. Results from the static film test apparatus indicated coolants which contained benzene insoluble components gave higher film-formation rates. Since benzene solutions of coolant deposit insoluble film on glass, the rate of deposition was studied. It was hoped this would lead to a rapid screening method for fouling potential of coolants.

A 1.13 wt% solution of Core 2 coolant (see Table VIII) in benzene was filtered and portions were placed in 12 colorimeter tubes. The tubes were allowed to stand at room temperature for various intervals of time. The solution was decanted and the deposited film was washed thoroughly with benzene. The optical density of the film was measured in a Klett-Summerson photoelectric colorimeter with three filters: red, green, and blue. These data are given in Table VIII.

A plot of the optical density vs time is shown in Figure 4. The optical density (arbitrary units) approached 160 as a limiting value. In Figure 5, a

TABLE VIII

OPTICAL DENSITY OF FILMS FROM BENZENE SOLUTIONS OF COOLANT

Core 2 coolant; removed November 22, 1960; 23% HB; 904 MWD.

Time (hr)	Optical Density(a)			Log $(OD_\infty - OD_t)$(b)
	Red	Green	Blue	
4.25	0.5	6	16	2.16
6.33	4.5	9	22	2.14
8.92	7.0	16	36	2.09
21.92	16.5	33	62	1.99
30.00	21.5	46	75	1.93
46.17	29.5	58	103	1.76
55.33	38	68	113	1.67
94.08	51	86	140	1.30
118.58	48	89	148	1.08
142.16	53	95	153	0.85

(a) Klett-Summerson photoelectric colorimeter, three color filters and optical density in arbitrary units.

(b) Data from blue filter; assume $OD_\infty = 160$; OD_t = optical density at given time; solution concentration, 1.13 wt%.

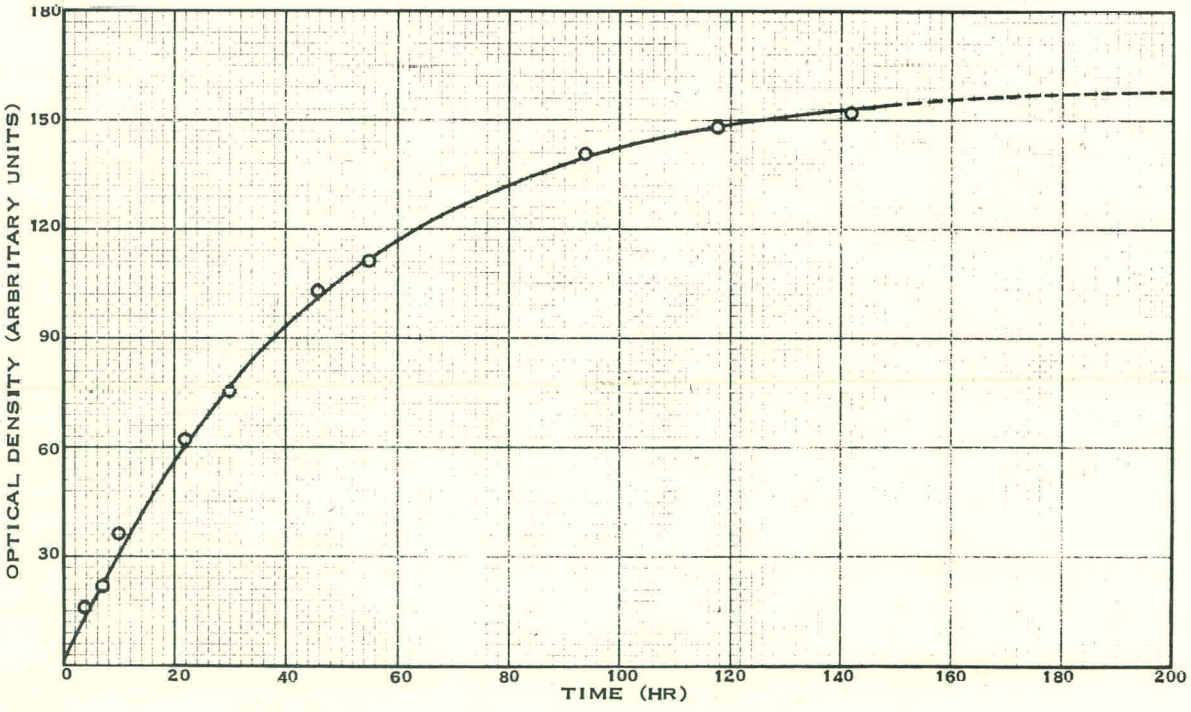

Fig. 4 Optical density of film vs time (data from Table I).

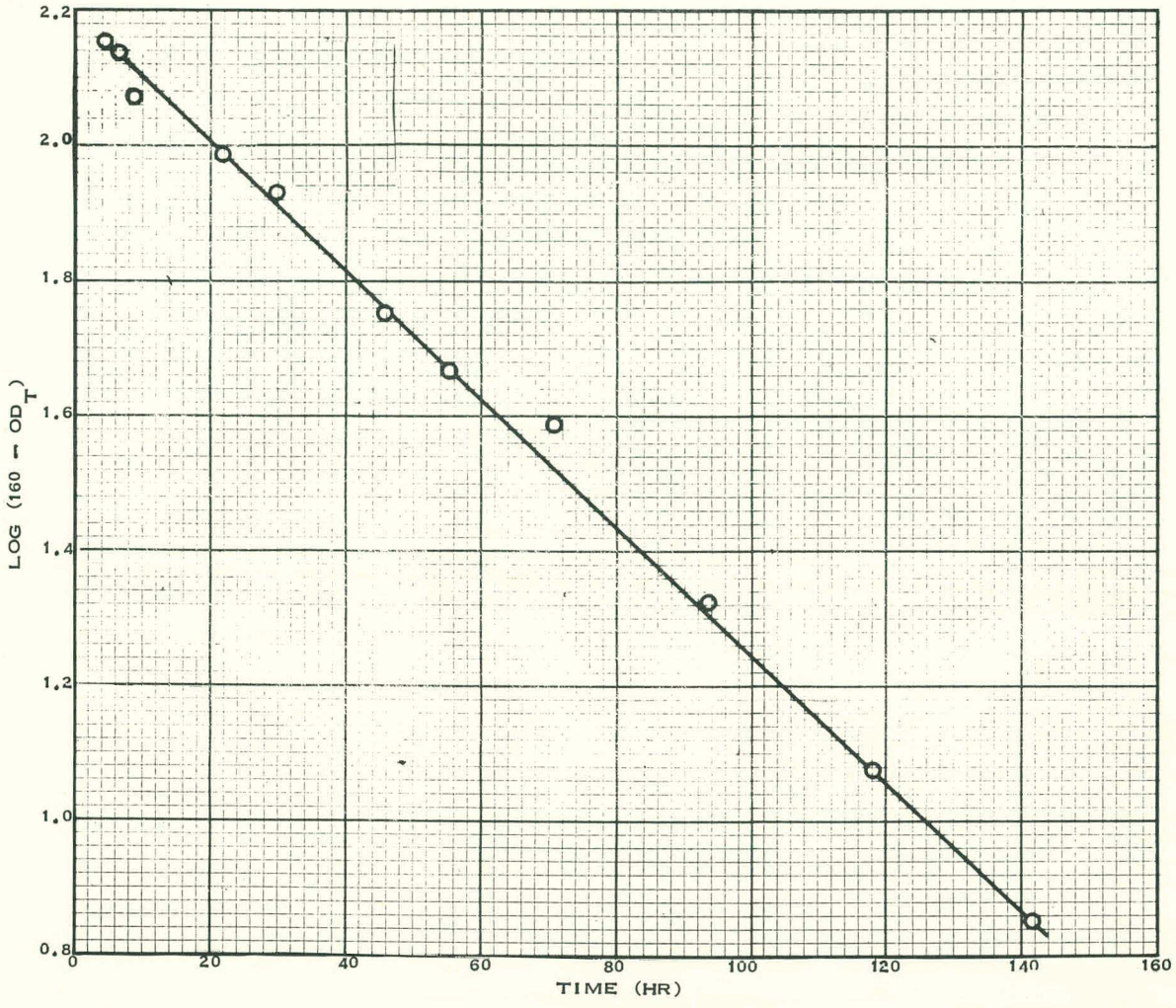

Fig. 5 Film formation on glass from benzene solution of Core 2 coolant (data from Table I).

first order plot was obtained by graphing log (160 - optical density) vs time. In static film tests, plotting the log (percent power loss) against log time gave a straight line. Similar plots with the benzene solution data gave a slightly sinusoidal curve. These different curves may be due to the isothermal nature of the benzene solution tests. It is likely that the benzene solution film rates may be governed by a different process such as diffusion. As more coolant samples become available they will be screened by this method.

Characterization of Deposits

Films were prepared from OMRE high boiler and from Core 2 coolant by allowing 5% solutions in benzene to stand 42 days in glass containers at 25°C. The solutions were decanted and the films washed with benzene. There was also some insoluble material suspended in both solutions. The films were removed from the containers by vigorous agitation with hot water followed by hot dilute caustic and collected on 0.45-μ Millipore filters. The solutions were allowed to stand an additional 15 days in glass flasks. The flasks were examined for

film at the end of this time. None had formed. The solutions were centrifuged to recover the suspended material.

The data in Table IX were obtained on the four insoluble fractions.

X-ray diffraction showed all the fractions were substantially amorphous. Both films from glass showed traces of α-Fe and austenite. The suspended particles from OMRE high boiler probably contained a trace of $Fe_{20}C_9$ and that from Core 2 coolant showed a pattern which may be that of carbon. Electron micrographs of the four materials appeared identical. They showed only translucent, flake-like particles with no evidence of inorganic nuclei. Infrared spectra of the two Core 2 coolant fractions were almost identical and contained a considerable carbonyl band as well as 11.2 to 11.4-μ and 12.1 to 12.2-μ bands indicative of 1,3,5- substituted benzene rings and consecutive para linkages. The spectra of the two OMRE high boiler fractions were considerably different. Neither showed more than a trace of carbonyl. A large band of unknown origin was present in the spectrum of the glass film which was very small in that of the suspended particles. The 11.2-μ meta and 12.1-μ para bands in the spectrum of the glass film were shifted to longer wavelengths in the spectrum of the suspended particles.

Conclusions

All of the insoluble fractions were mainly organic. The suspended materials were higher in ash than those on the glass. The large amount of suspended particles obtainable from Core 2 coolant was unusual since it contains only 23% "high boiler". The OMRE high boiler was recovered from Core 1 coolant which had a different composition from original Core 2 coolant. This may account for the difference between coolant and high boiler.

A correlation between suspended particles and fouling ability of a coolant may provide a quick lab test for reactor coolants.

TABLE IX

BENZENE INSOLUBLE MATTER FROM COOLANTS

Coolant	Amount Recovered (mg)	Coolant (wt%)	C (%)	H (%)	C/H Ratio	O (%)	Ash (%)
OMRE High Boiler							
On glass	8	0.03	88(a)	5(a)	1.6	—	0.4
Suspended particles	204	0.8	93.5	4.4	1.8	1.6	4.0
Core 2 Coolant							
On glass	5	0.02	88(a)	5(a)	1.6	—	0.2
Suspended particles	205	0.8	91.9	4.4	1.7	3.0	0.7

(a) Samples too small for accurate determination.

Benzene Insoluble Material in Core 2 Coolant

It has been observed that the benzene insoluble material slowly settles out of suspension. Centrifugation greatly accelerates the process. To study the behavior of the suspended material, it was centrifuged down after various intervals of time.

A 4.3% solution of Core 2 coolant in benzene was filtered through Whatman No. 1 filter paper. The solution was poured into 200-ml centrifuge jars and allowed to stand for various times. After centrifuging, the material was filtered off on a 0.45-μ Millipore filter. All solutions were centrifuged a second time.

Table X shows the amount of insoluble material obtained by centrifugation after the stated time interval.

These data show the suspension exists or forms within the first few minutes. Allowing the solution to stand longer times before centrifuging resulted in more precipitate. This may be due to agglomeration and is reflected in the amounts obtained in the second centrifugation. The suspended material was 0.8% of the Core 2 coolant.

Apparently the suspended material (insoluble) was not responsible for film formation on glass. After the suspended material was removed, the solution still deposited a heavy film on the glass walls of the jar. Mixing and melting the centrifuged material with Santowax OMP as a 1% solution appeared to solubilize or suspend it. A 1% solution of the mixture in benzene gave very little film on glass.

Filtration of Core 2 coolant through carbon black removed a large percentage of the benzene insoluble material by adsorption. Eighty-five grams of Core 2 coolant were filtered through 15 g of Wyex carbon black at 350 to 400°C. The effluent was dissolved in benzene (4.3% solution) and centrifuged. A 2.5-mg precipitate was obtained. Untreated Core 2 coolant gave 75 mg. Treatment of the coolant with carbon black also decreased its ability to form film on glass from benzene solution. However, the optical density was decreased by a factor of 3 while the benzene insoluble material was reduced by a factor of 30.

TABLE X

SEPARATION OF INSOLUBLE FRACTIONS

Time (hr)	First Crop (mg)	Time (hr)	Second Crop (mg)	Total Wt (mg)
0.5	41.3	19.0	2.9	44.2
20.3	51.0	91.5	2.3	53.3
91.5	58.3	117.0	1.3	59.6
117.0	59.2	139.5	0.8	60.0

These results indicate the suspended material in benzene may be a more insoluble form of the material which gives film on glass. Chemical analyses of both materials, reported previously, were quite similar in elemental analysis. Thus both the amount of benzene insoluble material and film formers on glass may be an index to the fouling potential of a coolant.

3.13 Corrosion of Iron by Polyphenyls. One of the advantages of aromatic hydrocarbons as coolant-moderators for nuclear reactors is their reported compatibility with mild steel, which is the material of construction for coolant containment. Although available information indicates that mild steel is satisfactorily resistant to attack by virgin polyphenyls, some complications arise when they are used in a nuclear reactor. The iron which invariably comprises a substantial part of the fouling film that has appeared on OMRE fuel plates presumably comes from the containment system. This has been attributed to the insoluble particles of iron that are known to be present in used coolant.

The possibility that dissolved iron rather than particulate iron is the harmful form with respect to film formation has not been studied very extensively. One reason for this is the difficult analytical problem of determining relatively small amounts of dissolved iron in the presence of iron that is present as fine--even colloidal--particles. A previous experiment [6] studied the corrosion of chemically pure iron wire by exposing it to different polyphenyl coolants for one week at 300°C. In this experiment a portion of virgin Santowax OMP and a portion of the same material that had been irradiated with electrons to a dosage of 5×10^9 rads were maintained under argon and similar portions of each under air. At the end of the experiment all of the iron that had been removed from the wire was determined by ashing the polyphenyls and acid washing their glass containers. Analysis of the residue showed that about six times as much iron had been dissolved by the irradiated coolant subsequently exposed to air as had been dissolved by the other three, which were all essentially the same. This experiment gave no information about the rate at which iron was dissolved, nor the final form of the iron that had been dissolved.

During this quarter a similar experiment was completed that provides additional information about the behavior of iron under these conditions. Again virgin and irradiated Santowax were taken as solvents for iron; the irradiated portion had received 2×10^9 rads under the Linac while it was under an inert (argon) atmosphere. Before the corrosion test started a portion of the irradiated material was preoxidized by holding it at 300°C for 34 hr in a very slow stream of air. This treatment changed its appearance from almost white to deep brown--almost black while fluid. Into each of four glass tubes 25-g portions of terphenyl were placed, identified as follows:

Sample A--virgin Santowax, under argon

Sample B--irradiated Santowax, under argon

Sample C--virgin Santowax, under air

Sample D--irradiated, pre-oxidized Santowax, under air

The source of iron for this solubility study was Baker's reagent grade wire that had been activated to a specific activity of about 20 microcuries

per mg by insertion in the VH-2 facility of the MTR for six days. Approximately 15-mg portions of this wire, accurately weighed, were wrapped around mushroom-headed stirring rods and inserted into the glass tubes containing the polyphenyl samples. Samples A and B were in tubes closed with ground joints so their atmosphere could be controlled during the experiment. They were deaerated and flushed with argon before the exposure to iron was started. Samples C and D were kept in loosely capped test tubes. These four samples were inserted in a well-insulated, thermostatically controlled aluminum block maintained at 300°C. Samples of polyphenyl from these containers were taken after one- and three-days exposure, and then twice weekly for six more weeks. The sampling procedure consisted of vigorously stirring the sample with the glass rod bearing the iron wire, then drawing an approximately 1-g sample with a syringe into a tared glass tube drawn to a capillary at one end. A recognized defect of this procedure is the fact that samples A and B were exposed briefly to air during mixing and sampling, but no convenient way could be devised for preventing this. After each sampling of A and B they were permitted to freeze, and were then evacuated and flushed with argon before returning to the heater. In this manner 16 samples were taken from each of the four tubes during the course of the experiment.

After all samples had been collected they were all counted during one day, to eliminate decay corrections and to increase the precision of measurement. At the time of counting, the iron-59 had decayed to about 18% of its initial activity. With one exception all samples were counted in pairs (taken consecutively) because preliminary examination showed that the contained activity was too low to warrant individual counts. They were placed directly on a 1-1/2-in.-diameter x 3/4-in.-long NaI(Tl) detector, and counted with a single-channel analyzer operated to accept all counts above 0.4 Mev. A known aliquot of the original iron, counted in the same geometry as the samples, served to relate counting rate to weight of iron. For this experiment the relation was 271 c/m-microgram iron.

Examination of the glass containers used for these samples during their exposure showed that no substantial amount of iron remained on the glass after it had been washed with benzene. Tubes A, C, and D may have had as much as one to two micrograms adsorbed, while tube B showed no evidence of iron activity. Upon reweighting the individual iron wires after the test, A and B had each gained 0.1 mg, C had gained 0.4 mg and D was unchanged. Except for C, none of these changes is significant.

Results of analyses of these polyphenyl samples are shown in Figure 6. In confirmation of the first experiment described above, it is seen that irradiated Santowax subsequently exposed to air (sample D) is a much better solvent for iron than the other three are. It dissolved more iron, and did so more rapidly, than any of the others did. Samples A, B, and C appear to have dissolved the iron at a reasonably uniform rate, but this is more apparent than real because the quantity of solvent became continually smaller during the experiment. This is illustrated in Figure 7, where the dissolution rate of iron in micrograms per day is plotted vs exposure time for the first 24 days of the test. After that time none of the samples showed a dissolution rate greater than 0.05 micrograms per day. Note that the ordinate scale for D is different from the others. Figure 7 clearly shows that for all the samples the dissolution rate was greatest during the first three days of the exposure. The anomalous behavior of sample A, which might reasonably have been expected to show

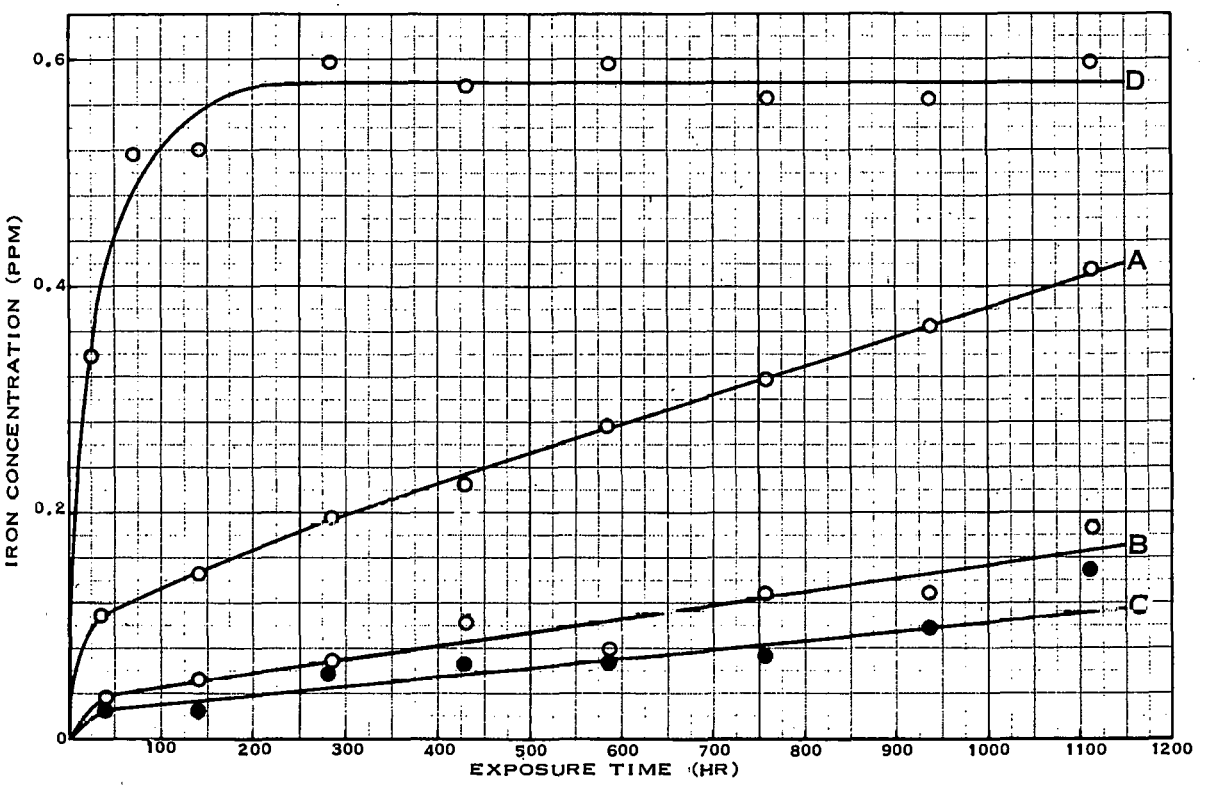

Fig. 6 Effect of time on concentration of iron in polyphenyls.

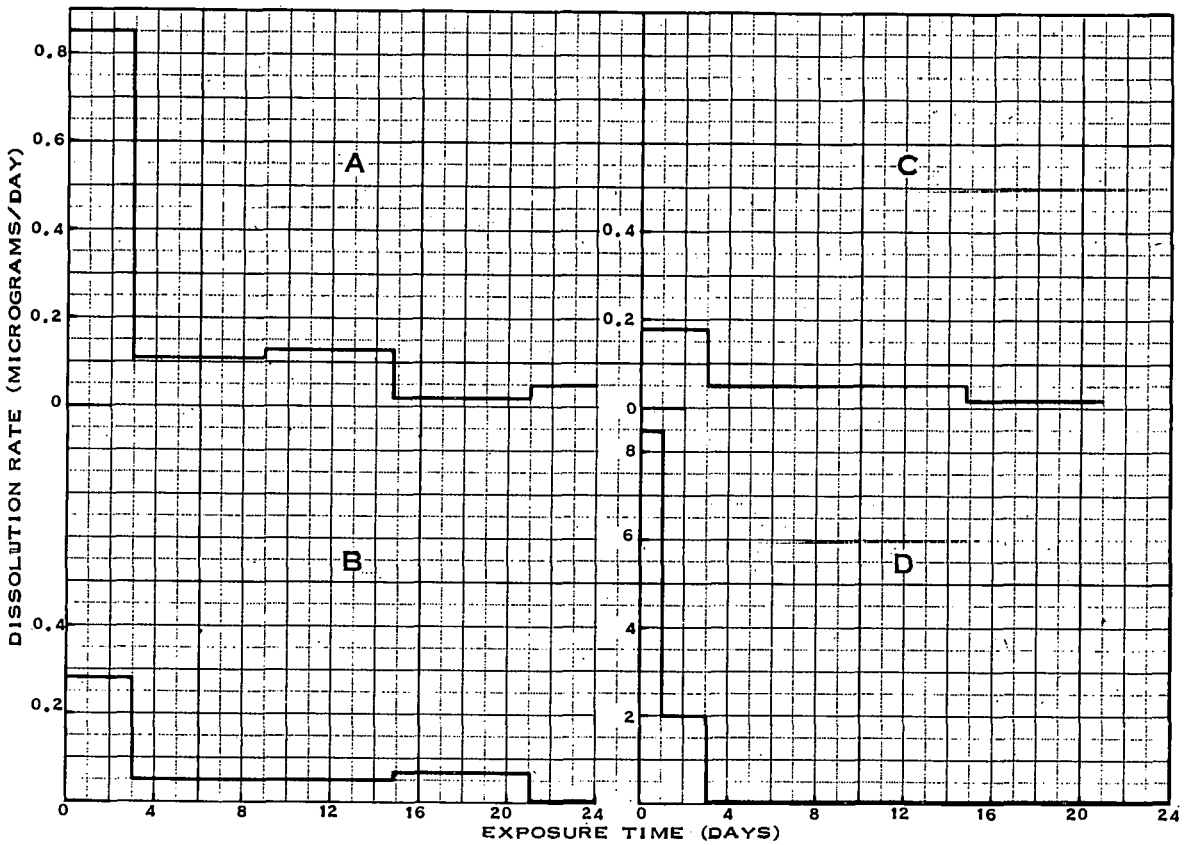

Fig. 7 Dissolution rate of iron in polyphenyls at 300°C.

the lowest solubility for iron, has not been explained. Even before the samples were counted it was noted that samples from A were progressively darker, indicating deterioration of the terphenyls. The dissolution observed with samples A, B, and C may have been caused by water, since no attempt was made to dry the samples before the experiment. The existence of a reactive form of iron on the surface of the wire that was used does not seem probable, because the wire was immersed in nearly boiling Santowax for an hour before it was cut and weighed just before the experiment was started.

The behavior of sample D (irradiated, oxidized Santowax) is of interest. This sample attained saturation with iron in one week, and for the remaining six weeks maintained the observed concentration within $\pm$ 0.02 ppm. This is strong evidence that the iron is in solution and not present as a suspension of insoluble particles which would be expected to show substantial variation in concentration as the particulate matter plates onto the glass. This evidence does not constitute proof of the solubility of iron, but does give rise to some interesting speculation.

Presumably, iron is dissolved by acidic compounds formed by oxidation of irradiated polyphenyls. This would be expected to produce iron salts, but Hückel [7] states "There are no genuine ferric salts of organic carboxylic acids . . . , generally triferric-hexacido-complexes occur if anionic complexes are not formed." In other words, iron in solution probably is present in coordination compounds. Functional groups capable of forming coordination compounds with iron, eg, hydroxyl, carbonyl, carboxyl, are known from infrared examination to be present in used terphenyl coolant. Iron may be held in solution in simple coordination compounds, but more probably it is incorporated into chelate structures. One of the most striking properties of chelate ring compounds is their unusual stability. In this report they resemble the aromatic rings of organic chemistry [8]. Ligands that can form chelate structures with ferric iron include salicylaldehyde, salicylic acid, pyrocatechol and their derivatives, 1,3-diketones such as acetylacetone, benzoylacetone, etc.

If the concentration of dissolved iron observed in the previously mentioned experiment (<1 ppm) is representative of actual reactor conditions, it is not surprising that it has escaped detection in the presence of substantially greater concentrations of particulate iron. It is obvious that not all oxygenated compounds are equally effective to corrode metallic iron. Table XI shows the oxygen content, determined by fast neutron activation, of the polyphenyl samples before and after their exposure in this solubility experiment.

TABLE XI

OXYGEN CONTENT OF CORROSION TEST SAMPLES

	Oxygen Content (wt%)	
Sample	Before	After
A	0.02	0.04
B	Not det'd	0.02
C	0.02	0.16
D	0.06	0.56

The oxygen picked up by sample C, which was exposed to the ambient atmosphere throughout the experiment, did not measurably affect the dissolution rate of iron. This probably explains the gain in weight of the iron wire immersed in this sample--simple oxidation.

Experiments are being planned to study the solubility and thermal stability of iron chelates that might reasonably be expected in irradiated, oxidized terphenyls. If the results of these experiments warrant further work, systems containing iron chelates will be studied in the dynamic irradiation loop in use in this project.

Pyrolysis of Ferrocene in M-terphenyl in Air and in Vacuum

To investigate the type of iron generated during pyrolysis, ferrocene was decomposed in presence and absence of air. In air, magnetite and austenite were the principle forms of iron. Only α-iron was found in the evacuated sample.

Four milligrams of ferrocene were heated 24 hrs at 400°C with 2 g of m-terphenyl. In one tube an air blanket was used. The second tube was degassed at 10^{-5} mm mercury. The pyrolyzed products were opened to the air, dissolved in benzene, filtered, and submitted for X-ray diffraction analysis. The air-blanketed sample contained austenite and magnetite while the evacuated sample showed only α-iron. Evidently when oxygen is present in a hot system where iron is being formed, the iron will be converted to oxide. Complete oxidation to hematite was not observed. Perhaps the organic material furnished a reducing atmosphere to give magnetite. Air exposure of finely divided iron at room temperature produced by the above procedure did not oxidize (at least not rapidly) to iron oxides.

3.14 Mechanism of Iron Carbide Formation in Fouling Films. There is evidence that radiolyzed coolant contains soluble iron. One possible mechanism of film formation in reactors would involve the decomposition of soluble iron compounds on the fuel elements. The radiolyzed coolant is known to contain organic acids. Iron salts or complexes of these acids could decarboxylate to form iron carbonate. Under reactor conditions, the iron carbonate may be reduced to carbide. The last step in the sequence was verified by reducing iron carbonate.

Fifty milligrams of ferrous carbonate were heated with 5 g of Santowax OMP in a stainless steel bomb at 360°C for six days under 100 psig of hydrogen. The bomb was evacuated daily and repressurized with hydrogen. After the test, the Santowax OMP was dissolved in benzene and the solids filtered off. X-ray diffraction showed that the iron carbonate had been converted to α-iron, cementite and austenite. The cementite (Fe_3C) is indirect evidence for the percarbide (Fe_2C) since it is known that the percarbide reacts with iron to form cementite at low temperature.

While these results are not conclusive, they indicate film formation from soluble iron may be possible. The corrosion of iron by organic acids emphasizes the need to exclude oxygen from the reactor.

3.2 Benzene in Polyphenyl Coolants for Nuclear Reactors

There are several possible benefits in using a small percentage of benzene in terphenyl coolants. First, benzene in the coolant may provide surface agitation via subnucleate boiling to reduce the film-formation rate. Secondly, coolant makeup with benzene rather than terphenyl may be possible. The main radiolysis products of benzene would be diphenyl and terphenyl. Thus the

bulk of the terphenyl coolant would be synthesized in the reactor. This would result in lowered makeup cost. The third benefit in using a polyphenyl coolant containing benzene would be the possibility of a direct-cycle organic-cooled reactor.

To test the possibility of using benzene in polyphenyl coolants, the vapor pressure of benzene in several polyphenyl mixtures was determined over a temperature range. All coolants were tested with 17 wt% benzene in the coolant. Table XII lists the results.

TABLE XII

VAPOR PRESSURE OF POLYPHENYL MIXTURES CONTAINING 17 WT% BENZENE

Santowax OMP		Core 2 Coolant(a)		OMRE High Boiler	
Temperature (°C)	Pressure (psig)	Temperature (°C)	Pressure (psig)	Temperature (°C)	Pressure (psig)
203	37	135	30	165	23
204	37	202	43	173	27
221	48	229	76	230	65
247	71	241	81	235	68
263	88	253	101	252	85
268	91	270	121		
309	129	274	122		
327	146	283	133		
		289	141		
		306	166		
		312	177		

(a) Contains 22% high boiler

The data in Table XII show that the vapor pressure of the coolants is less than 200 psig at reactor temperature. Also the vapor pressure of the coolants was somewhat lower than calculated for ideal solutions. Thus it appears possible to operate a reactor under normal temperature and pressure conditions with as much as 15 wt% benzene in the coolant.

It may be possible to design a direct cycle organic cooled reactor. The benzene in the coolant would be flashed through a turbine. The following schematic diagram represents the process.

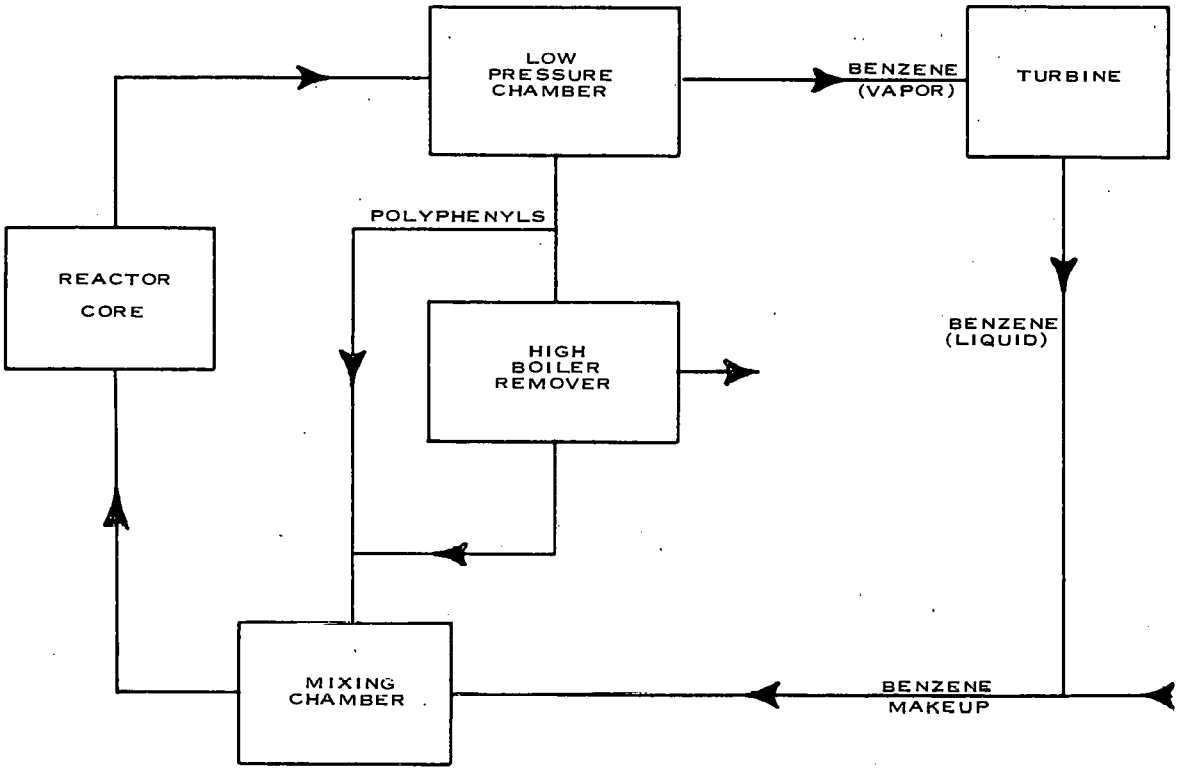

4. COMPOSITION AND ANALYSIS OF COOLANTS

(P. S. Hudson, W. M. Hutchinson, R. B. Rogier, A. J. Moffat, P. W. Solomon and R. C. Doss)

4.1 Characterization of Polyphenyl High Boiler

4.11 Sublimation Procedure. A series of known mixtures of OMRE high boiler and Santowax OMP was prepared which varied from 5 to 100% in high boiler. Duplicate samples, approximately 200 mg, were sublimed at 220°C and 0.1 mm of mercury for 30 min. The results in Table XIII were obtained.

The duplicate samples were in good agreement with one another. Up to approximately 20 wt% high boiler, the analysis agreed well with the known samples. From 20 to 80 wt% the results diverged from the known amounts in a linear fashion. The effect of intermediate boiler on sublimation analyses will be studied later. Presently these samples are being used to develop a gas chromatographic analysis for high boiler.

4.12 Characterization of Benzene Insoluble Fraction. A fraction (A) was isolated from an OMRE high boiler benzene solution by precipitation with cyclohexane (see Table XIV). The precipitate was extracted with benzene and the insoluble residue was treated in various ways in an attempt to characterize the material.

The fraction (A) was hydrogenated under the following conditions: Three grams of A were suspended with 3 g of stabilized nickel-alumina catalyst in

TABLE XIII

SUBLIMATION SAMPLES

Sample No.	Known High Boiler (wt%)	Duplicate Analysis of High Boiler (wt%)	
1	5.05	5.30	5.03
2	10.78	10.75	10.61
3	14.99	15.60	15.42
4	19.95	21.16	21.02
5	25.05	26.2	27.6
6	29.98	33.6	33.8
7	35.06	38.9	38.9
8	40.02	45.0	45.2
9	45.06	49.9	51.0
10	50.00	53.9	55.5
11	59.98	67.0	68.0
12	69.98	80.0	81.2
13	79.99	86.3	88.2
14	89.97	96.4	97.5
15	95.10	99.5	99.6
16	100.00	99.9	99.9

TABLE XIV

HYDROGENATED BENZENE INSOLUBLES

Fraction	Melting Point (°C)	Mol Wt	Wt%	Ash (%)	C (%)	H (%)	C/H	O (%)	NMR Analysis(a) Aromatic Protons (%)	NMR Analysis(a) Aliphatic Protons (%)
Original A	> 570	Not possible	—	0.77	94.1	5.0	1.57	0.41	Not obtainable	Not obtainable
Hydrogenated A (benzene soluble)										
Insoluble 90/10 n-pentane/ØH	300-570	2630	16	None	93.4	6.5	1.20	—	41.3	58.7(b)
Insoluble 90/1 n-pentane/ØH	230-350	1430	3	None	92.2	7.1	1.08	—	27.7	72.3(b)
Soluble n-pentane	55-75	497	25	0.54	89.9	9.4	0.80	—	16.2	83.8
Hydrogenated A (tetralin soluble)										
Boiling tetralin soluble	> 510	Not possible	56	9.8	83.1	4.5	1.54	3.0	Not run	Not run

(a) All samples contain para magnetic species.

(b) About half were cyclic methylene structure.

15 ml of decalin at 350°F and 1000 psig hydrogen pressure for 15 hr in a stainless steel bomb. The resulting mixture was extracted with benzene and then boiling tetralin. The benzene soluble material was fractionated further with n-pentane. Physical and chemical properties indicated considerable hydrogenation occurred.

In addition, NMR data, shown in Table XV, were obtained for the n-pentane soluble fraction.

TABLE XV

NMR ANALYSES

Protons (%)	Description of Protons
5.0	Adjacent to aromatic rings
33.9	On cyclic methylene groups
21.2	On alkyl methylene groups
14.2	On methyl groups
9.5	Bridge protons in condensed cyclics or cycloalkanes adjacent to aromatic rings

Infrared confirmed the NMR results qualitatively: very few methyl groups could be seen and aliphatic/aromatic band ratios increased as solubility in n-pentane increased. Polyphenyl structures were still evident in all the spectra.

Two more intense hydrogenations were conducted on A in an attempt to completely saturate the material. The conditions shown in Table XVI were used with the same catalyst as before.

The products were extracted with warm benzene several times on Run B and exhaustively Soxhlet-extracted with benzene on Run C. The solutions were filtered through 0.45-μ Millipore filters and the solvents evaporated. A final drying at 100°C in vacuo yielded a brown solid in both cases. The properties shown in Table XVII were determined. The average data obtained in the first hydrogenation, designated Run A, are given for comparison.

NMR indicated paramagnetic species were present even after vigorous hydrogenation. Perhaps colloidal nickel catalyst got through the Millipore filters. Infrared indicated the high oxygen content in Run C was due to aliphatic carbonyl. Infrared in conjunction with NMR data suggests the carbonyl group is the benzyl ketone type. Also, infrared supports the NMR data concerning aromatic structure. In Runs B and C, infrared spectra showed aromatic bands

TABLE XVI

HYDROGENATION CONDITIONS

	Run B	Run C
Solvent	Decalin	Cyclohexane
Reaction time (hr)	16	40
Reaction temperature (°C)	230-43	220-45
Total pressure (psig)	2660	3060

TABLE XVII

HYDROGENATED BENZENE INSOLUBLES

	Run A	Run B	Run C
Benzene soluble (wt%)	44	58	49
Number average (mol wt)	720	776	705
C (%)	91.5	90.5	88.2
H (%)	8.2	9.0	9.7
O (%)	Not run	0.28	1.5
Ash (%)	< 0.5	< 0.1	0.7
C/H Ratio	0.93	0.84	0.76
NMR Analysis			
Total aromatic H (%)	27.1	12.3	8.1
Total aliphatic H[a] (%)	72.9	87.7	91.9

(a) Protons adjacent to aromatic rings and protons on bridge carbons, Run B 17.4%, Run C 10.3%; protons not adjacent to aromatic (mainly naphthenic), Run B 70.3%, Run C 76.9%; unidentified (may be due to 9,10-dihydroanthracene or phenanthrene structure or methylene adjacent to keto group), Run C 4.7%.

due to various polyphenyl type structures. Thus, hydrogenation did not completely eliminate the aromatic rings.

The benzene insoluble fraction (A) was treated with five reagents: (a) concentrated sulfuric acid, (b) nitric acid, (c) 1:1 sulfuric-nitric acid mixture (all run with 0.5-g sample of A for 3 hr at 120°C), (d) excess bromine in carbon tetrachloride at 25°C, (e) ozone (used when fraction was in the solid, dry state). The products obtained from these treatments analyzed as shown in Table XVIII.

Infrared indicated sulfuric acid reacted by two paths: (a) formation of sulfonic acids and (b) formation of sulfones or sulfoxides. The second band could also be interpreted as fused-ring structures containing one or two adjacent protons (no more than two protons, the 13.3-μ and 14.3-μ bands are missing). Some aliphatic hydroxyl groups also may be present.

With nitric acid or the mixture of sulfuric and nitric acids, aromatic nitro groups were formed. In addition, a large amount of carbonyl was present. The carbonyl was not of the quinoid or carboxyl type but mainly aliphatic ketone. Polyphenyl structures were present after nitration.

With the bromine treatment, infrared found no carbon-bromine bonds. However, elemental analysis gave 44% bromine. This may indicate adsorption of bromine by fraction A rather than true chemical bonding. However, evacuating the brominated material for 2 hr at 80°C gave no loss in weight.

TABLE XVIII

ANALYSES OF TREATED SAMPLES

Treatment	Wt. Product (g)	Melting Point (°C)	C (%)	H (%)	O (%)	N (%)	S (%)	Br (%)
H_2SO_4	0.9	> 510	38.9	4.0	43.4	—	13.7	—
HNO_3	0.7	~ 510	58.7	2.6	30.4	8.3	—	—
1:1 H_2SO_4:HNO_3	0.8	160-200(d)	47.2	2.2	45	4.4	1.4	—
Br_2	0.8	180(d)	55.2	2.5	—	—	—	44.2
Ozone	—	—	92.2	4.9	2.2	—	—	—

Ozonolysis resulted in slight oxidation. A small carbonyl band appeared at 5.8 μ after ozonolysis.

Assuming all nitrogen is present as nitro groups, the oxygen is present as carbonyl and the sulfur is in the form of sulfuric acid (with the remaining oxygen as hydroxyl), empirical structures for fraction A can be written: for sulfuric acid treatment, $C_{7.5}H_{5.3}$ (SO_3H) $(OH)_3$; for nitric acid treatment, $C_{7.3}H_{4.4}$ (NO_2) (CO); and for bromination, $C_{8.4}H_{4.5}$ Br. The empirical formula of Fraction A was $C_{7.8}H_5$.

Certain deductions can be made from the above data (and other facts) concerning the structure of the benzene insoluble material:

(1) The polyphenyl structure which is present contained large amounts of consecutive para and 1,3,5 substituted phenyl linkages. Fused ring structure also was present. This accounts for the insoluble nature of the fraction.

(2) The amount of aliphatic structure is unknown. However, aliphatic ketones were found upon oxidation. Excess oxygen in the sulfonated product could be attributed to aliphatic double bonds which have sulfated and subsequently hydrolyzed. These double bonds are not readily detected by infrared.

(3) Extremely stable free radicals exist in the insoluble fraction since hydrogenation did not eliminate paramagnetic species. The ESR signals were similar to those from carbon black. Possibly the nickel catalyst may be carried into the product.

(4) The insolubility of the fraction must be due to structural features rather than high molecular weight. Mild hydrogenation caused about half the material to become benzene soluble. However, even under drastic hydrogenation a portion remains insoluble.

4.13 Characterization of Components by Oxidation - Model Compounds. In an effort to characterize the high boiler formed from irradiated terphenyls, several model compounds have been subjected to potassium permanganate-pyridine oxidation. Model compounds may give information about the type of material which form acids when OMRE high boiler is oxidized.

Neither acenaphthene or tetralin were oxidized by the reagent. Thus single cycloaliphatic structures are not oxidized under these conditions. Previously, alkyl groups were not oxidized with this system. 9,10-Dihydroanthracene and tetraphenylethylene gave anthraquinone and benzophenone almost quantitatively. No acids were obtained here. It does appear that with certain activated methylene groups, permanganate-pyridine oxidation might yield acids. Also, certain types of double bonds which I.R., NMR and Bromine Number do not detect may be attacked by permanganate-pyridine. Such structures might be responsible for the acids obtained.

OMRE High Boiler and Benzene Insoluble OMRE High Boiler

OMRE high boiler was oxidized under two conditions noted in Table XIX: (a) with mild, selective conditions; potassium permanganate-pyridine containing 0.5% water and (b) a more severe condition; potassium permanganate containing 5% of a 2% aqueous sodium hydroxide solution. Also the benzene insoluble high boiler was oxidized under the mild conditions [1].

Infrared indicated the acids were quite similar. Molecular weights were in the range 160 to 180 as calculated from neutralization equivalents. The acids solubility in ether indicated monoacids.

The addition of alkali during the oxidation greatly increased the amount of acids obtained. A considerably greater amount of acid precursor was present in the benzene insoluble OMRE high boiler than in the total OMRE high boiler. The nature of these precursors is unknown as yet.

TABLE XIX

OXIDIZED FRACTIONS

			Analysis of Acid Products			
Material	Oxidation System	Acid Yield (mg)	C (%)	H (%)	O[a] (%)	Neutral Equivalent[b]
OMRE high boiler	(2)Severe	122	70.9	5.4	23.7	310
OMRE high boiler	(1)Mild	80	76.2	4.8	19.0	348
Benzene insoluble high boiler	(1)Mild	137	72.7	4.8	22.5	355

(a) By difference

(b) mg KOH/gram of sample

4.2 Identification of Polyphenyls Produced by Irradiation of Terphenyls

Work is continuing on the isolation and identification of the various isomeric hexaphenyls and lower polyphenyls produced when pure samples of ortho, meta, and para terphenyls are electron irradiated. In each series, the hexaphenyls have been separated and trapped on a preparation column scale using gas-solid chromatography. In the last quarterly report [9] identification of many of the hexaphenyls produced from p-terphenyl irradiation was discussed.

The remaining unidentified peaks in this series are being examined. A few of the peaks obtained from irradiated o-terphenyl have been studied. Two of the peaks have been positively identified as triphenylene and o,p,p,o-hexaphenyl (theoretically the highest isomeric hexaphenyl possible from o-terphenyl). A third peak eluting just ahead of triphenylene was apparently a partially hydrogenated triphenylene. Two other peaks eluting in the hexaphenyl range have been tentatively identified as impure o,m,p,o-hexaphenyl and o,m,m,o-hexaphenyl. Almost all of the fractions trapped chromatographically from irradiated o-terphenyl were oils. Recrystallization of the oils from cyclohexane or ethanol and water gave solids. The melting points in most cases were quite broad, indicating further separation work.

In the near future, work will be initiated on characterizing the hexaphenyl fractions from m-terphenyl.

4.3 Analytical and Calculation Techniques

4.31 Spot Tests for Polyphenyls and Fused Ring Aromatics. The results of two color reactions, investigated for use in detecting aromatic hydrocarbons eluted from liquid/solid chromatographic columns, are tabulated in Table XX. This technique will be used for separations of hydrocarbon types and isomers from irradiated polyphenyls. Unsaturates, fused-ring hydrocarbons and polyphenyls were examined in the tests.

Method A was the procedure used by Silverman and Bradshaw [10],

First 0.2 ml 37% formaldehyde was added to 10 ml H_2SO_4 and mixed. Ten drops of this solution were added to ~ 0.5 ml of cyclohexane in which a trace of the desired compound was suspended or dissolved. The sample was shaken well and examined after 20 min.

Method B was according to Altschuller and Sleva [11],

A trace of the desired compound was placed in a tube, ten drops of H_2SO_4 were added, the sample was mixed, and the color noted. Two drops of 10% p-dimethylaminobenzaldehyde were mixed in acetic acid, and the color was again observed.

Polyphenyls almost without exception gave colors with sulfuric acid-formaldehyde reagent but not with sulfuric acid alone or the dimethylaminobenzaldehyde reagent. The color was brown with quaterphenyls or higher molecular polyphenyls in the formaldehyde test. Therefore the formaldehyde test would be useful in detection but not in identification of compounds eluted from the chromatographic column.

TABLE XX

COLOR TESTS FOR AROMATICS

Compound	Source(a)	Color		
		Sulfuric Acid	Formaldehyde (Method A)	Dimethylamino-benzaldehyde (Method B)
None	—	none	light yellow	light salmon
Biphenyl	Eastman	none	brown	lavender
O-terphenyl	Eastman	none	green	red
M-terphenyl	Eastman	none	violet	rose
P-terphenyl	Eastman	none	purple	blue
O-quaterphenyl	PPCo	none	brown	none
O,m-quaterphenyl	PPCo	none	brown	none
O,p-quaterphenyl	PPCo	none	brown	none
M-quaterphenyl	PPCo	none	brown	none
M,p-quaterphenyl	PPCo	none	brown	none
P-quaterphenyl	Eastman	none	brown	none
1,2,4-triphenylbenzene	PPCo	none	brown	none
1,3,5-triphenylbenzene	Aldrich	none	blue	none
M-quinquephenyl	NBS	none	brown	none
M,p,m-quinquephenyl	PPCo	none	brown (green ring at interface)	none
P-quinquephenyl	PPCo	none	yellow	none
1,2,3,4-tetraphenylbenzene	PPCo	none	brown	none
M-hexaphenyl	NBS	none	purple	none
M,o,p,m-hexaphenyl	PPCo	none	brown	none
M,p,m,m-hexaphenyl	PPCo	none	brown	none
O,p,p,o-hexaphenyl	PPCo	none	brown	none
M,p,p,m-hexaphenyl	PPCo	none	brown (purple ring at interface)	light pink
P,p,m,p-hexaphenyl	PPCo	none	brown	none
P,p,o,p-hexaphenyl	PPCo	none	brown (purple ring at interface)	none
P,m,m,p-hexaphenyl	PPCo	none	brown	none
P-hexaphenyl	PPCo	none	yellow	none
Pentaphenylbenzene	PPCo	none	brown	none
2,4-diphenyl-3'-(3-xenyl)biphenyl	PPCo	yellow	brown	yellow
3,5-diphenyl-4'-(3-xenyl)biphenyl	PPCo	none	brown	none
Hexaphenylbenzene	PPCo	none	brown	none
M-octaphenyl	NBS	none	brown	none
1,6-diphenyl-1,3,5-hexatriene	Matheson	rose	brown	brown
Diphenylacetylene	Aldrich	yellow	none	yellow-green
Cis-stilbene	K & K	none	brown	blue-green

(Continued)

TABLE XX (Continued)

Compound	Source(a)	Color		
		Sulfuric Acid	Formaldehyde (Method A)	Dimethylamino-benzaldehyde (Method B)
Trans-stilbene	Eastman	none	orange-brown	none
Tetraphenylethylene	Aldrich	none	brown	none
Triphenylethylene	Aldrich	yellow	yellow-brown	green
1,1-diphenylethylene	Eastman	yellow	yellow-brown	yellow-green
1-phenyl-3-(4-xenyl)-1,3-cyclohexadiene	PPCo	violet	violet	violet
1,1,4,4-tetraphenyl-1,3-butadiene	Light's	none	none	blue
1,4-diphenyl-1,3-butadiene	Aldrich	none	orange-brown	blue-green
Benzene	Merck	none	red	yellow
Phenylcyclohexane	Eastman	none	orange	purple
Bicyclohexyl	Bios	none	red	yellow-orange
Tetralin	Fisher	none	brown	orange-red
60/40 cis/trans-decalin	Matheson	none	none	yellow
Bibenzyl	Eastman	none	red	yellow
4-benzylbiphenyl	Aldrich	yellow-orange	violet	violet
P-dicyclohexylbenzene	Eastman	none	brown	none
O-tercyclohexyl(mp, 44.5-5.50)	PPCo	none	none	light purple
M-tercyclohexyl(mp, 61-20)	PPCo	none	none	none
P-tercyclohexyl(mp, 162-30)	PPCo	none	none	light pink
Diphenylmethane	Matheson	yellow	red-brown	yellow
Triphenylmethane	Eastman	none	orange-brown	none
1,1,2-triphenylethane	Eastman	none	red-brown	yellow
Triphenylene	Aldrich	none	blue-green	none
Anthracene	Aldrich	yellow	yellow	yellow-green
Octahydroanthracene	Terra	none	brown	red
1,2-2',1'-anthracenoanthracene	Light's	yellow	light orange	yellow
Naphthacene	Eastman	green	light red	green
Anthanthrene	Light's	brown	red-brown	brown
1,2,7,8-dibenzanthracene	Terra	none	blue-green	none
1,2-benzanthracene	Light's	rose	purple	rose
9,10-dihydroanthracene	Light's	yellow	brown	yellow
9,10-diphenylanthracene	Light's	none	orange	none
1,2,3,4-dibenzanthracene	Aldrich	none	blue	none
Acenaphthene	Eastman	yellow	purple	blue-green
Acenaphthylene	Aldrich	none	blue	none
Tetrahydroacenaphthene	Aldrich	yellow	brown	yellow
1,1-binaphthyl	Eastman	none	violet	none
Naphthalene	Eastman	none	brown	none

(Continued)

TABLE XX (Continued)

Compound	Source(a)	Color		
		Sulfuric Acid	Formaldehyde (Method A)	Dimethylamino-benzaldehyde (Method B)
1-phenylnaphthalene	Aldrich	yellow	brown	purple
2-phenylnaphthalene	Aldrich	none	purple	none
Tetrabenznaphthalene	Terra	none	purple	none
Phenanthrene	Aldrich	none	blue	none
9,10-dihydrophenanthrene	Aldrich	yellow	blue-green	lavender
Octahydrophenanthrene	Aldrich	yellow	red-brown	red
Pyrene	Terra	yellow-green	violet	blue
1,2,4,5,8,9-tribenzopyrene	Aldrich	none	blue-green	none
1,2,4,5-dibenzopyrene	Aldrich	none	none	none
1,2,3,4-dibenzopyrene	Light's	red	lavender	red
1,2-benzpyrene	Aldrich	none	none	red
0-phenylenepyrene	Aldrich	yellow	blue	blue-green
Dihydropyrene	Aldrich	none	violet	blue
Tetrahydropyrene	Aldrich	yellow	blue	lavender
1,2,3,6,7,8-hexahydropyrene	Eastman	none	brown	none
Perhydropyrene	Aldrich	yellow-orange	brown	orange-brown
Fluorene	Aldrich	none	blue-green	violet
Difluorenyl	Aldrich	none	blue	none
3,4-benzofluorene	Aldrich	none	brown	blue
2,3-benzofluorene	Aldrich	none	violet	none
1,2-benzofluorene	Aldrich	none	violet	none
Indene	Aldrich	yellow-(red solid)	red-brown	orange
Indane	Aldrich	yellow	brown	orange
4,5-benzoindane	Aldrich	red-brown	brown	purple
Fluoranthene	Aldrich	none	blue	violet
11,12-benzofluoranthene	Aldrich	none	purple	none
3,4-benzofluoranthene	Aldrich	none	blue	lavender
Benzo-(m,n,o)-fluoranthene	Aldrich	pink	blue-green	red
Pentacene	Aldrich	lavender	purple	lavender
3,4-benzotetraphane	Aldrich	red	red	red
1,2,8,9-dibenzpentacene	Aldrich	green	blue	green
5,12-dihydrotetracene	Aldrich	none	brown	none
1,2-benzpentacene	Light's	purple	purple	purple
Chrysene	Eastman	none	violet	none
α-truxene	Aldrich	none	blue	none
β-truxene	K & K	none	blue	blue-green
Perylene	Aldrich	purple	purple	purple
1,12-benzoperylene	Aldrich	none	none	none

(a)All commercial samples were the highest grade available. They were used as received for the tests. All samples prepared at Phillips were 99+% purity by gas chromatographic analysis.

Both aldehyde reagents gave excellent tests with many fused ring aromatics and olefinic compounds. No correlations were found between the compound structure type and the color. However, colors obtained were distinctive and should provide a convenient spot test for various individual compounds.

If a compound gave a color with the dimethylaminobenzaldehyde reagent, a non-polyphenyl structure would be indicated (except biphenyl and terphenyls).

4.32 Nuclear Magnetic Resonance Analysis of Acids. During the NMR analysis for organic acids in oxidation samples in perdeuteroacetone solvent, a hydrogen-deuterium exchange reaction was noted. The perdeuteroacetone was used as a solvent which would not give signals. Analysis showed that the carboxyl hydrogen decreased while a band indicating methyl-group protons appeared. These observations indicated an acid-solvent interaction:

$$RCOOH + CD_3COCD_3 \rightarrow RCOOD + CHD_2COCD_3$$

The relationship was quantitative. Thus NMR may be an excellent method for studying many types of exchange reactions kinetically.

4.33 Analyses for Oxygen in Polyphenyls. Because the presence of oxygenated compounds in polyphenyl coolant is considered to be deleterious to its optimum performance, methods for their analysis were studied during this quarter. This has included an evaluation of the fast neutron activation method for oxygen as applied specifically to terphenyls, and the application of paper chromatography to used reactor coolants.

To evaluate the precision and accuracy of analyses for oxygen by fast neutron activation when the method is applied to polyphenyl samples, six known samples were submitted to the Analytical Branch. These samples, containing 0.01 to 0.30 wt% oxygen, were prepared from diphenylphenyl ether and m-terphenyl. Each sample was activated and counted at least four times; estimates of errors are based solely on uncertainties in counting the induced activity. The results of this work indicate that in this concentration range the standard error of the measurement is $\pm$ 0.015 wt% absolute, or $\pm$ 10% relative, whichever is larger.

The technique of paper chromatography was applied to various polyphenyls to see if unique separations in samples known to contain oxygenated species could be found. Four different samples were studied. They were (a) Santowax OMP, (b) polymer from Santowax, formed in the absence of oxygen, (c) OMRE high boiler (0.08 wt% oxygen), and (d) biphenyl irradiated with oxygen (0.6 wt% oxygen). Initially, descending chromatography was used, but the ascending method was found to be faster and was used for most of the tests.

Conditions reported in the literature to separate successfully polycyclic aromatics or mixtures of steroids were applied to these samples but in no case were isolated spots, characteristic of successful chromatograms, observed. Solvents examined included toluene-ethanol-water and toluene-methanol-water on acetylated paper, and chloroform, toluene, normal and iso-octane, or cyclohexane as mobile phases on paper previously impregnated with formamide or propylene glycol as stationary phases. Chromatograms were examined under a 2537 A ultra-violet light to observe the results of the chromatographic processes.

For all systems studied, samples either remained at the point of application, or moved with the solvent front ($R_f \cong 1$), and with some a long tail connected these two points. The nearest approach to success was the observation that with certain solvents, solutes known to contain oxygen produced strong quenching of the fluorescene at the point of application while solutes known to be oxygen-free exhibited typical aromatic fluorescence. No additional work is planned using this technique.

4.34 Measurement and Calculation of Chromatograms. As was discussed in a previous section of this report, analyses of biphenyl samples irradiated at 80°C and 300°C under a Linac were completed and the partial reaction rates were calculated from the relative yields of isomeric quaterphenyls formed. The samples were evaporated at 80 to 90°C/1 mm Hg to leave residues containing about 90% biphenyl.

The residues were analyzed by gas chromatography using the techniques and calculations indicated below, which were developed to give the best information from these samples. Known mixtures of biphenyl and the six linear quaterphenyls were used with the unknowns. Knowns and unknowns were run consecutively in the same chromatograph. It was found that only runs made on the same day could be compared accurately, since deviations between days were about three times as great as among runs. After the second approximation, the two known mixtures matched the two sets of unknowns within two percent of each isomeric quaterphenyl. Chromatograms of unknowns and knowns were compared by peak area and by peak height.

Peak areas (x2) were obtained as the products of peak heights times peak width at one-half height. This method is similar to triangulation but eliminates the drawing of lines other than baselines. The heights were measured with a ruler and the widths with a low-power microscopic scale. The precision of the latter was about one-third that of the former. The peaks were greatly elongated with straight sides, the larger peaks occupying full chart width. With the charge used (about 0.5 microliters of quaterphenyls), the response of the instrument was proportional. The ratio of peak area (%) to concentration (%) of the knowns departed little from unity (0.97% - 1.04%) and was not dependent on charge within a two-fold range. The peak areas (%) of each quaterphenyl in the chromatograms were averaged. The deviations of individual chromatograms from this were averaged to give average percent deviation, a measure of scatter between chromatograms. The larger of the average percent deviations of the unknown and known samples was taken as the measure of scatter. In all but one case the average deviations of the unknowns were larger. The composition of unknowns were calculated from each chromatogram by:

$$\text{Wt\% of i-th}\phi_4 \text{ in unknown} = \frac{\text{\% Peak area of i-th}\phi_4 \text{ in unknown} \times \text{wt\% i-th}\phi_4 \text{ in known}}{\text{\% Averaged peak area of i-th}\phi_4 \text{ in known}}$$

Compositions were calculated individually from each chromatogram of unknowns. The sum of the quaterphenyls should equal unity (100%) if corrections made with the averaged peak areas from chromatograms of knowns were valid. These corrections were quite small and deviations of sum from unity did not exceed 0.75%.

The evaluation of chromatograms by peak height alone was complicated by a considerable difference in response of the chromatograph to the various quaterphenyls. The ratio of peak height (%) to concentration (%) from chromatograms of knowns also depended on size of charge to the chromatograph. These observations were made from plots of peak height (%) to concentration (%) ratios vs size of charge of knowns. Because actual values of the latter could not be determined accurately, the sum of peak heights of the quaterphenyls (mm) was substituted for them. The plot dramatized the dependence on specific quaterphenyl and charge size mentioned before. A handier method used for all reported calculations from peak heights was to plot peak heights (%) vs sum of peak heights (mm) for each quaterphenyl from both known and unknown chromatograms. Lines were drawn through the points from chromatograms of the known. Each peak height (%) of the unknown could then be compared with that of the known by interpolating the known line to make the charge of the known equal to that of the unknown. This procedure resulted in averaging the known chromatograms but minimized the real scatter of the known points. Average percent deviations were obtained from the calculated compositions of the unknowns. For these reasons, and perhaps because of better precision, the deviations (scatter) among chromatograms obtained by the height method were always lower than those obtained by the area method.

The results of analyses of two samples irradiated at 80°C and two at 300°C were given in Table IV. The first heading is identification of the radiation sample. The second heading lists the number of the chromatograms. The third heading gives the method used in evaluating the chromatograms; by peak area (height x width) or by peak height alone. The fourth heading lists the average deviation of the sum of the quaterphenyls from unity (or 100%). Note the superiority of evaluation by peak area here. The fifth heading gives the deviation of individual chromatograms from the mean divided by the mean, and averaged over all six quaterphenyls to give one value for scatter. (The deviations of the minor components tended to be slightly larger than the majors but not enough to invalidate the average.) The last columns list the relative concentrations (or yields) of the six isomeric quaterphenyls.

Deviations between the compositions listed in Table IV were examined with respect to method of evaluation of chromatograms and duplicate samples, and compared with scatter among analyses. Average percent deviation among analyses (column 5) ranged from 1.0 to 4.1 with means of 2.8 and 1.9% for the peak area (ht x w) and peak height (ht) methods of evalution, respectively. Deviations between methods of evaluation (ht x w vs ht for A-1, A-4, V, and VI) ranged from 2.2 to 5.3% with a mean of 3.2%. Deviations between samples (A-1, A-4, V, and VI) averaged 2.4%. Thus differences between the methods of evaluation were larger than differences between samples and differences among analyses (scatter). For this reason, partial reaction rates were calculated from compositions obtained by both methods used for evaluation of chromatograms.

4.35 The LGP-30 Digital Computer in the Solution of Radiolysis Problems. The LGP-30 digital computer was used to calculate the concentration of the isomeric quaterphenyls in radiolysis products. The peak altitude and peak width at half height from the chromatogram were used to calculate peak areas. The computer was programmed to calculate individual peak areas, individual peak percentage of total area, average peak area (when several chromatograms are used), percentage average peak area, and average individual quaterphenyl concentrations. The LGP-30 computer is used for these simple calculations

only when numerous chromatograms are to be averaged. Also for numerous calculations the LGP-30 offers a high degree of confidence in the values obtained.

A program was developed by T. A. Matthews, Computing Department, Phillips Petroleum Co, Bartlesville, Okla. for the solution of nonlinear, simultaneous, algebraic equations. The analog simulator is used and the method of steepest ascents employed. This procedure was applied successfully to the calculation of partial reaction rates from the six isomeric quaterphenyls formed by the radiolysis of biphenyl. Determination of the partial rates involved only six nonlinear equations with six unknowns. The rates could be calculated by hand but the analog simulator extends the calculation to include a larger number of simultaneous equations. Also the machine calculations should be valuable for complicated systems which include more than six unknowns.

4.4 Synthesis of Reference Polyphenyls

The synthetic program to produce pure samples of polyphenyls, particularly the more important hexaphenyls, was continued. It is hoped that these reference compounds will in part identify high boiler fragments formed from the irradiation of polyphenyls which in turn may lead to a better understanding of the chemistry of terphenyls.

An earlier report from Phillips Petroleum [12] presented calculations whereby the relative yields of hexaphenyls formed from the electron irradiation of m-terphenyl at 500 to 600°F were predicted. Nine were expected to constitute about 85% of the total yield of hexaphenyls. To date, seven of these nine have been made available. Efforts to synthesize the remaining two will continue, but are somewhat curtailed due to realignment of objectives with emphasis upon establishing a synthetic program to produce new ideal coolants.

During the current period two ketonic precursors of desired polyphenyls were obtained. In addition, one hexaphenyl (m,o,m,m-ϕ_6) was prepared which was predicted to form from the irradiation of m-terphenyl and two other hexaphenyls (p,o,p,p-ϕ_6 and p,m,p,p-ϕ_6) were prepared which were predicted to form from the irradiation of p-terphenyl.

The first substituted aromatic ketone obtained was 3-(4-biphenylyl)cyclohex-2-ene-1-one which was prepared in a 40% yield from 4-lithio biphenyl and 3-ethoxycyclohex-2-ene-1-one according to the method of G. F. Woods and I. W. Tucker [13]. This material was prepared in order to introduce an end meta-para linkage. The other substituted aromatic ketone synthesized was 2-(4-biphenylyl)cyclohexanone prepared according to the method of G. F. Woods and F. Scotti [14] in which 4-biphenylyl magnesium bromide is allowed to react with 2-chlorocyclohexanone in refluxing benzene to give a 50% yield of the desired material.

The first hexaphenyl prepared during this period was 2,3'-di(3-biphenylyl)-biphenyl referred to as m,o,m,m-ϕ_6. This material was obtained with great difficulty from the reaction of 3-lithium-m-terphenyl and 2-(3-biphenylyl)-cyclohexanone followed by aromatization. The coupling step proceeded smoothly; however, attempts to aromatize the coupled precursor with bromine in chloroform failed. Treatment with 10% palladium on charcoal or with red phosphorus at 300°C also failed to aromatize the material completely. Analysis of the precursor after aromatization with bromine indicated a large amount of bromide

ions present, obviously from over-bromination. Only after treatment with butyl lithium was it possible to completely remove all traces of bromine. Subsequent aromatization with red phosphorous and purification led smoothly to the desired hexaphenyl.

The other two hexaphenyls, namely p,o,p,p-ϕ_6 and p,m,p,p-ϕ_6 were readily obtained from 4-lithium-p-terphenyl and their corresponding substituted aromatic ketones. The ketone used in the preparation of p,o,p,p-ϕ_6 was 2-(4-biphenylyl)-cyclohexanone and that used in the preparation of p,m,p,p-ϕ_6 was 3-(4-biphenylyl)-cyclohexanone. Both of these hexaphenyls were obtained as benzene insoluble materials and were analyzed for identification of structure. Progress in the synthesis and separation of intermediates and polyphenyls is given in the following paragraphs.

3-(4-Biphenylyl)cyclohex-2-ene-1-one. 4-Lithium biphenyl was prepared from 69.9 g (0.3 mole) 4-bromobiphenyl and 21 g (0.33 mole) butyl lithium dissolved in 300 ml of n-heptane. A solution was slowly added at 10 to 15°C which contained 25 g (0.18 mole) 3-ethoxycyclohex-2-ene-1-one dissolved in 300 ml ether. The mixture was refluxed for 1 hr at 45 to 50°C, cooled and hydrolyzed with 500 ml of 5% aqueous sulfuric acid. The total mixture was steam distilled until all traces of biphenyl had disappeared. The residue was extracted with 600 ml benzene. The benzene solution was washed with dilute aqueous sodium bicarbonate and water and then concentrated to near dryness. To the concentrate was added a small amount of methanol. The crystalline product which formed was filtered and recrystallized from ethanol to give 18 g (40% yield) of a pale yellow crystalline material which had a melting point of 158 to 160°C.

2-(4-Biphenylyl)cyclohexanone. 4-Biphenyl magnesium bromide was prepared from 46.6 g (0.2 mole) 4-biphenyl bromide and 5.0 g (0.206 mole) magnesium turnings in 150 ml tetrahydrofuran. While the temperature was maintained near 25°C, a solution was slowly added which contained 26.4 g (0.2 mole) 2-chlorocyclohexanone dissolved in 60 ml ether. After the addition, the tetrahydrofuran and ether were removed by distillation and simultaneously replaced with 200 ml of benzene and the mixture refluxed for 8 hr after which time the complex was hydrolyzed with cold ammonium chloride. The organic layer was separated and the aqueous layer extracted twice with ether. The combined organic layers were dried over anhydrous magnesium sulfate, filtered, and the filtrate distilled. There was obtained a material which distilled at 180 to 230°C/0.3 mm and quickly solidified. Recrystallization from ether gave 25 g (50% yield) of a material which melted at 93 to 96°C.

2,3′-Di(3-biphenylyl)biphenyl or m,o,m,m,-ϕ_6. 3-Lithium-m-terphenyl was prepared from 3.09 g (0.010 mole) 3-bromo-m-terphenyl dissolved in 100 ml ether and 10 ml of an n-heptane solution which contained 0.7 g (0.011 mole) butyl lithium. A solution was then added which contained 2.49 g (0.010 mole) of 2-(3-xenyl)cyclohexanone dissolved in 50 ml ether. After the addition, the mixture was stirred 1 hr and the complex was hydrolyzed with cold dilute aqueous sulfuric acid. The ether layer was separated, washed with aqueous sodium carbonate and dried over anhydrous magnesium sulfate. After removing the desiccant, the filtrate was concentrated on a steam bath to give 5.1 g of a syrupy residue. The residue was treated with a small amount of red phosphorus and the mixture heated to 300°C for 3 hr. The mixture was extracted with benzene and filtered. The benzene filtrate was evaporated to dryness and the

residue which remained was dissolved in a 90-10 mixture of n-hexane and benzene and passed through a 12- x 700-mm glass tube packed half full with F-20 Alcoa activated alumina. Several fractions were obtained by washing the column with varying concentrations of benzene in n-hexane. The desired material was eluted when the column was washed with a 60-40 mixture of n-hexane and benzene. The elutant was evaporated and the heavy film which formed was crystallized from a 90-10 mixture of ethanol and benzene. The material melted at 58 to 60°C. Chromatography indicated a 100% pure hexaphenyl. The calculated analyses for $C_{36}H_{26}$ is: C, 94.3; H, 5.7. Experimental analyses found: C, 94.4; H, 5.8.

3,4′-Di(4-biphenylyl)biphenyl or p,m,p,p-ϕ_6. 4-Lithium-p-terphenyl was prepared from 3.09 g (0.010 mole) 4-bromo-p-terphenyl in 50-ml ether and 10 ml of a n-heptane solution which contained 0.7 g (0.011 mole) butyl lithium. After stirring for 30 min, a solution was added which contained 2.48 g (0.010 mole) 3-(4-xenyl)cyclohex-2-ene-1-one dissolved in a 100-ml solution of a 50-50 mixture of benzene-ether. After the addition, the mixture was stirred for 1 hr at 10 to 20°C and then poured into cold 5% aqueous sulfuric acid. A steam distillation was carried out for a short period to insure dehydration. The residue was treated with benzene. The benzene insoluble portion was removed, washed with ether and air dried. This material (2.0 g, mp 280 to 290°C) was heated at 320°C for 2 hr with a catalytic amount of 10% palladium/charcoal. The residue was extracted with boiling chloroform. Analysis of the chloroform extract indicated it to contain mostly p-terphenyl. The residue was extracted a second time with boiling p-xylene. Analysis of this fraction indicated pure hexaphenyl. Final purification of this fraction was carried out by sublimation at 360°C/0.05 mm. A white crystalline material was obtained which had a melting point of 321 to 323°C. Chromatography indicated a 100% pure hexaphenyl. The calculated analysis for $C_{36}H_{26}$ is: C, 94.3; H, 5.7. Experimental analysis found: C, 94.2; H, 5.7.

2,4′-Di(4-biphenylyl)biphenyl or p,o,p,p-ϕ_6. 4-Lithium-p-terphenyl was prepared from 3.09 g (0.010 mole) 4-bromo-p-terphenyl slurried in 150 ml ether and 10 ml of an n-heptane solution which contained 0.7 g (0.011 mole) butyl lithium. To this slurry was added a solution which contained 2.49 g (0.010 mole) 2-(4-xenyl)cyclohexanone dissolved in 70 ml of benzene. The mixture was stirred for 1 hr at ambient temperature. The complex was hydrolyzed with cold dilute aqueous sulfuric acid. The organic layer was separated, dried over anhydrous magnesium sulfate, filtered and the filtrate evaporated to near dryness. The crystalline material which formed was heated with 10% palladium/charcoal at 310°C for 1 hr. The mixture was extracted with boiling benzene and the benzene filtrate concentrated. Upon cooling, the concentrate contained a crystalline material which was filtered, washed with methanol and air dried. The material which analyzed as 100% pure hexaphenyl by chromatography had a melting point of 231 to 232°C. The calculated analysis for $C_{36}H_{26}$ is: C, 94.3; H, 5.7. Experimental analysis found: C, 94.3; H, 5.7.

5. NEW ORGANIC COOLANTS FOR NUCLEAR REACTORS
(R. C. Doss, L. V. Wilson, Jr., and W. M. Hutchinson)

5.1 Ideal Coolants

During this period, more emphasis was placed on establishing a synthetic program to produce new coolants. A brief review of the literature quickly revealed that polyphenyls, fused-ring aromatics, and heterocyclics are probably the only organic materials which appear to hold promise as coolants. Since the polyphenyl series has been extensively studied, attention has been directed towards the two remaining type compounds, the fused rings, and heterocyclics.

A limited study of the fused ring compounds was made. Data are given in Table XXI. The study revealed that materials which possess the phenanthrene type structure give less polymer than other fused 3-ring compounds as noted

TABLE XXI

IRRADIATION OF IDEAL COOLANT CANDIDATES

Conditions: Temperature, 600-650°F; time, 8 hr

Irr. No.	Compound	Dosage (rads x 10^9)	Relative Polymer	Relative Gas
D-2	Santowax-OMP(control)	6.5	1.00(20.7%)	1.00(0.10 ml/watt-hr)
	Tetraphenylethylene		0.71	1.00
	Triphenylamine		0.91	3.33
D-3	Santowax-OMP(control)	8.7	1.00(25.3%)	1.00(0.11 ml/watt-hr)
	Anthracene		0.94	1.80
	Phenanthrene		0.77	0.73
	Pyrene		0.89	0.22
	1,2-bis(4-pyridyl)ethylene		2.94	2.90
D-4	Santowax-OMP(control)	4.4	1.00(16.2%)	1.00(0.09 ml/watt-hr)
	Acridine		1.22	0.79
	Naphthalene		0.41	—
	Anthracene		0.99	2.10
	9,10-dihydroanthracene		0.39	11.00
	Phenanthrene		0.79	0.83
	9,10-dihydrophenanthrene		0.17	5.00
D-5	Santowax-OMP(control)	4.7	1.00(16.4%)	1.00(0.08 ml/watt-hr)
	Phenanthridine		0.71	0.54
	1,10-phenanthroline		4.62	1.48
	Quinoline		1.05	0.90
	7,8-benzoquinoline		0.76	1.17
	Benzimidazole		1.47	8.10

by the relative polymer formation of anthracene (0.94) and pyrene (0.89) vs the relative polymer formation in phenanthrene (0.77). It was then thought that a hydrogen donor compound would contribute even more to lessening of the polymer formation, particularly one which would not be likely to polymerize readily. For this reason 9,10-dihydroanthracene and 9,10-dihydrophenenthrene were irradiated and found to reduce polymer formation by as much as 85% as compared to their corresponding parent aromatics. For example, phenanthrene had a relative polymer value of 0.79 while its 9,10-dihydro- derivative had a relative polymer value of 0.17. The polymer value of 9,10-dihydrophenanthrene gave the lowest relative polymer of any compound or mixture of compounds tested to date. It was thought that one possible explanation why dihydrophenanthrene was better than dihydroanthracene was because the former is a substituted biphenyl and the latter has a diphenyl methane type of structure.

Attention was then turned to heterocyclic compounds of the pyridine and quinoline series particularly those compounds which possess the phenanthrene configuration. Materials of this type which appear to have some promise as determined by polymer formation during electron irradiation were phenanthridine (0.71 relative polymer) and 7,8-benzoquinoline (0.76 relative polymer). Although the compound 1,10-phenanthroline has the phenanthrene type structure, it gave a poor relative polymer value (4.62). Other materials evaluated were quinoline (1.05 relative polymer), napthalene (0.41 relative polymer) and acridine (1.22 relative polymer). These were tested also for the purpose of correlation of structure. The imidazoles also are interesting from the standpoint of aromaticity. The only one tested this period was benzimidazole which in itself was not too promising.

Other structures which were investigated were tetraphenyl-ethylene, triphenylamine, and 1,2-bis(4-pyridyl)ethylene. The pyridyl compound gave high relative polymer (2.94). The tetraphenylethylene gave good relative polymer values (0.71); however this material melts above 200°C. Triphenylamine gave a relative polymer value of 0.91. Gas chromatographic analysis of the sublimate after irradiation indicated that a large fraction was fragmented by radiolysis and damage measured by high boiler content was misleading.

Other fused-ring compounds that are candidate coolants are certain hydroquinolines and some pyrazines. One such compound not commercially available was prepared for future examination. This material, 2,3,5,6-tetraphenyl pyrazine, was prepared in a 41% yield by heating benzoin and ammonium acetate in glacial acetic acid at 135°C [15]. The material had a melting point of 250°C which is unacceptable as a coolant but should contribute some information from a structural standpoint.

One useful aim of the ideal coolant program is to find a material that will not form film when pyrolyzed or radiolyzed. One working hypothesis, postulated by R. O. Bolt of California Research Corp, is that a precursor of the organic "glue" of film is partially hydrogenated polyphenyls that contain arylated cyclohexadiene rings. It is reasonably postulated that these rings may polymerize with G values much higher than those for completely aromatic hydrocarbons. Examination of the high molecular weight ends (benzene insolubles) of high boiler from OMRE Core II coolant suggests that they may be polymers of arylated cyclohexadienes[16] A suitable aromatic ring system might be found

that either did not accept hydrogen in the radiolysis process or did not polymerize in the hydroaromatic state.

To this end efforts to eliminate benzene rings in coolants should be made. Non-benzenoid ring systems of interest are pyridine, s-triazine, imidazole, and thiazole. To obtain sufficient molecular weight such rings would have to be connected as in biphenyl or fused as in napthalene. With the possible exception of pyridine the former connection is expected to be superior. A series of tests has been started to determine at what position each of these ring systems can best be connected. Linkages to various positions on the pyridine ring are to be tested with s-triazine as the central ring. One of these, tri-(2-pyridyl)- s-triazine, has been prepared in small quantity. Linkages to the other ring systems are to be tested with phenyl groups. The phenyl group is symmetrical and only three mono-phenyl derivatives each of imidazole and thiazole will have to be prepared.

Pyrolytic and radiolytic tests on these compounds should enable a preliminary evaluation of these ring systems as a type as well as to show at what positions they can best be linked. It is expected that linkages at different positions on these heterocycles will exhibit different stabilities. The optimum ring system can then be linked at the optimum position into a biphenyl analog. The non-benzenoid coolant then can be synthesized and tested for stability and film-forming tendency.

5.2 Coolants from Industrial Stocks

As mentioned in the previous quarterly report [17], the thermal instability of industrial stocks seems to be the most difficult problem in developing a material which would perform satisfactorily as an organic moderator-coolant. During this quarter industrial stocks which had exhibited good radiolytic stability were tested for thermal stability. Results of these tests are shown in Table XXII.

Tests were carried out for 48 hr at 650°F, 675°F, and 700°F. Large aluminum blocks described in an earlier report [18] were used to hold constant temperatures. Samples were tested in small steel sample holders which also were described in the earlier report [18]. Earlier tests using these sample holders noted problems with leaks and with the threads galling badly when the holders were dismantled after completion of a test. The leak problem was solved by using Fel-Pro, a copper-base pipe dope designed for high-temperature operation. This pipe dope did not eliminate the galling problem, since the lubricating properties were destroyed at the high temperature. However, it was found that the sample holders would come apart without galling if a small amount of penetrating oil was used on the threads as they were taken apart.

As can be seen in Table XXII, all of the industrial stocks show poor thermal stability when tested under these conditions. The phenol extract of heavy cycle oil had been distilled to remove heavy ends. Radiation of this sample at 600 to 650°F at a dosage of 5.6×10^9 rads gave a radiolytic polymer yield of 1.21 relative to a Santowax OMP control. Thermal polymer increased rapidly with temperature up to 27.4% polymer when tested at 700°F. The dimethyl sulfoxide extract of an SO_2 plant extract gave a relative radiolytic stability of 0.95, but gave 18.4% polymer when held 48 hr at 700°F.

TABLE XXII

THERMAL STABILITY

Industrial Stocks	Boiling Point (°F)	Before Test (% HB)	After 48 hr Test (°F) 650	675	700
Phenol extract of heavy cycle oil	610-862	0.5			
Gas (cc/gm)			7.4	14.3	23.0
% high boiler[a]			11.1	18.9	27.4
DMSO extract of SO_2 plant extract	562-869	0			
Gas (cc/gm)			7.3	8.5	21.9
% high boiler[a]			6.6	12.9	18.4
Humble NRC fraction	673-836	0			
Gas (cc/gm)			6.9	14.9	21.4
% high boiler[a]			1.7	2.3	4.4
Hydrodealkylated decant oil		2.6			
Gas (cc/gm)			—	—	—
% high boiler[a]			4.3	5.0	6.2
Pittsburgh coal tar	512-871	0			
Gas (cc/gm)			1.3	5.7	6.8
% high boiler[a]			17.6	18.3	23.7
Pittsburgh coal tar	512-955	5.3			
Gas (cc/gm)			4.7	5.8	6.9
% high boiler[a]			19.4	21.5	24.4
Pure Compounds					
Anthracene: Gas (cc/gm)			3.6	—	4.3
% high boiler[a]			1.0	2.2	5.9
Phenanthrene: Gas (cc/gm)			1.6	1.6	—
% high boiler[a]			0.1	0.1	—
Pyrene: Gas (cc/gm)			1.5	2.2	2.6
% high boiler[a]			0	0.5	0.6
Naphthalene: Gas (cc/gm)			1.5	2.2	2.7
% high boiler[a]			0	0	0

(a) Percent residue after sample is placed under 0.1-mm pressure and held for 30 min at 220°C.

The Humble Nuclear Reactor Coolant had been distilled to remove heavy ends. This improved the radiolytic stability from a relative polymer yield of 1.50 to a relative radiolytic polymer of 1.11 when compared with Santowax OMP. This Humble stock showed better thermal stability, but still gave 4.4% polymer when held 48 hr at 700°F. The hydrodealkylated decant oil, described in an earlier report, had a relative radiolytic polymer yield of 0.82. This stock showed improved thermal stability, with a change in high boiler of 3.5% when held 48 hr at 700°F.

Heavy fractions from Pittsburgh coal tar showed the most promise when tested at 600 to 650°F for radiolytic stability, giving relative polymer of 0.91 with radiolytic gas produced approximately the same as terphenyls. When tested for thermal stability, however, these fractions gave polymer yields as high as 24.4% when held 48 hr at 700°F. An attempt was made to find some particular part of the coal tar which seemed to be thermally unstable. Chromatograms were made of the coal tar before irradiation, after irradiation, and after thermal degradation. The relative peak areas remained essentially constant; no peaks showed increases or decreases. An attempt was made to dehydrogenate this coal tar by reacting the sample for 2 hr at 300°C using palladium on charcoal as a catalyst. Chromatograms of the coal tar before and after the attempted dehydrogenation show no apparent differences.

Of the stocks which showed good radiolytic stability when tested at 600 to 650°F, only the Humble NRC fraction and the hydrodealkylated decant oil show promising thermal stability. Future work will include additional hydrodealkylation runs on several stocks at varying conditions. Since many of these industrial stocks contain sulfur, future work also will include a study of the effect of catalystic desulfurization on radiolytic and thermal stability.

As seen in Table XXII, several pure condensed aromatics were tested for thermal stability under the same conditions used for the industrial stocks. All of these were stable under these test conditions. Anthracene gave the highest polymer yield of 5.9% when held 48 hr at 700°F. This high boiler after the unpolymerized anthracene was removed looked quite different from any others tested. The high boiler from anthracene had a granular, coke-like appearance, while the high boiler from industrial stocks seemed to be very viscous liquid. Chromatograms were made on the sublimates after thermal testing on the anthracene, phenanthrene, pyrene, and naphthalene. These sublimates all showed high purity, which means that the products of thermal decomposition were gas and high boilers, with little hydrogenation, isomerization, or ring breakage occurring.

6. RADIATION STABILIZERS

(R. B. Regier and H. A. Hartzfeld)

The study of radiation stabilizers has had for its objective the discovery of materials which, at reasonable cost, will reduce appreciably the damage to organic moderator-coolants under ionizing irradiation. Thus far this investigation has been limited to the stabilization of terphenyls. The testing of 74 individual additives, as well as several combinations of effective stabilizers, was reported previously [19]. With certain exceptions the best stabilizers comprised two types of substances: (a) compounds structurally related to

anthracene, and (b) sulfur in an elemental, divalent, or tetravalent state. The protection provided by such effective stabilizers as anthracene, phenothiazine, and 2-mercaptobenzothiazole was only slightly dependent on concentration over a wide range; in contrast, stabilization by elemental sulfur was greatly influenced by concentration. Combinations of effective stabilizers exhibited no synergism in protective action. Anthracene as an additive disappeared quite rapidly under irradiation, but its beneficial effect remained.

The current experimental program for studying stabilization of Santowax OMP under high temperature electron irradiation has been a continuation of the work described previously. With the exception of irradiation 40, Table XXIII,

TABLE XXIII

EFFECT OF ADDITIVES IN RADIOLYSIS OF SANTOWAX OMP

Irr. No.	Additive	Dosage (rads x 10^{-8})	Relative Polymer	Relative Gas
39	Control (9 hr)	6.5	1.00 (21.0%)	1.00 (0.076 ml/watt-hr)
	S_8, 0.7 mol% (1 hr)		— (2.3%)	—
	S_8, 0.7 mol% (2 hr)		— (3.9%)	—
	S_8, 0.7 mol% (3 hr)		— (6.4%)	—
	S_8, 0.7 mol% (5 hr)		— (10.1%)	—
	S_8, 0.7 mol% (9 hr)		0.78 (16.4%)	5.00
40	Control	5.4	1.00 (18.2%)	1.00 (0.062 ml/watt-hr)
	S_8, 0.4 mol%		0.81	3.36
	S_8, 0.7 mol%		0.76	4.74
	S_8, 1.0 mol%		0.74	5.76
	Anthracene, 3 mol%		0.87	0.94
	9,10-dihydroanthracene, 3 mol%		0.79	1.07
	Phenazine, 3 mol%		0.78	0.86
41	Control	5.8	1.00 (19.5%)	1.00 (0.093 ml/watt-hr)
	9,10-dihydroanthracene, 6 mol%		0.68	0.96
	9,10-dihydroanthracene, 12 mol%		0.57	1.17
	9,10-dihydroanthracene, 24 mol%		0.50	1.70
	Xanthone, 3 mol%		0.96	0.84
	Xanthydrol, 3 mol%		0.89	0.90
	Anthrone, 3 mol%		0.89	0.76
42	Control	5.0	1.00 (17.9%)	1.00 (0.104 ml/watt-hr)
	9,10-dihydroanthracene, 36 mol%		0.40	2.23
	9,10-dihydroanthracene, 50 mol%		0.36	3.18
	HB-40 (hydrogenated terphenyls), 3 mol%		0.97	1.33
	9,10-dihydrophenanthrene, 3 mol%		0.93	1.21
	1,2,3,4,5,6,7,8-octahydroanthracene, 3 mol%		0.80	1.22
	1,2,3,4,5,6,7,8-octahydrophenanthrene, 3 mol%		0.84	1.32
43	Control	7.9	1.00 (24.3%)	1.00 (0.113 ml/watt-hr)
	Benz(a)anthracene, 3 mol%		0.92	0.93
	Dibenz(a,h)anthracene, 3 mol%		0.99	0.95
	Benzo(a)pyrene, 3 mol%		0.99	1.02
	Dihydropyrene, 3 mol%		0.92	1.24
	Tetrahydropyrene, 3 mol%		0.87	1.24
	1,2,3,6,7,8-hexahydropyrene, 3 mol%		0.81	1.08

irradiations were carried out in aluminum cells at 580 to 650°F (304 to 343°C) for 8 to 9 hr. Irradiation 40 was conducted at 460 to 480°F (238 to 249°C) for 10 hr. Determinations of polymer in the irradiated samples were made by sublimation (in a closed system) at 220°C for 30 min at an initial pressure of 0.10 mm; gas analyses were carried out by mass spectrometry.

In previous attempts to determine the fate of elemental sulfur in Santowax OMP subjected to varying radiation doses, poor material balances for sulfur were obtained. However, a subsequent experiment demonstrated that very significant amounts of hydrogen sulfide, a product of the irradiation, were not released from the solid irradiation product in the usual method of collecting and measuring radiolytic gas. Consequently, this hydrogen sulfide had the opportunity to weather away prior to and during analysis of the solid. Irradiation 39 (Table XXIII) was designed to overcome this difficulty. Following irradiation, at varying total doses, of Santowax OMP containing 0.7 mol% (0.78 wt%) sulfur, the radiolytic gas was collected and measured with the aid of a Toepler pump. To provide essentially complete removal of gas, the solid was melted several times with alternate evacuations of the cooled cells. Hydrogen sulfide in the gas was determined by mass spectrometry, and the solid was analyzed for sulfur by the Leco method. The sublimate collected during determination of polymer content in the solid was analyzed for sulfur by the Wickbold turbidimetric method. These analytical results are summarized in Table XXIV.

This time the material balance for sulfur in each of the samples was quite good, compared to the result on the unirradiated blend of only 96.7% of the sulfur theoretically present. (The Leco method of analysis for sulfur does not readily lend itself to more precise results.) Most of the hydrogen sulfide was formed during the first 2 hr of irradiation. At the higher doses the amount of hydrogen sulfide approached two-thirds of that which would be formed by total conversion of the sulfur to this product; there was no evidence that this amount would be reduced by further irradiation. As the radiation dose was increased, a progressively smaller fraction of that sulfur which was not converted to hydrogen sulfide sublimed under the conditions of polymer measurement. It appeared that the amount of sulfur incorporated in the polymer reached a minimum after about 2 hr of irradiation, thereafter increasing until 18% of the initial sulfur content was non-sublimable after

TABLE XXIV

IRRADIATION OF SANTOWAX OMP-0.7 MOL% S_8

Irradiation time (hr)	1	2	3	5	9
Polymer (wt%)	2.3	3.9	6.4	10.1	16.4
Conversion of S to H_2S (%)	24.5	54.7	60.3	63.2	64.6
S remaining in irradiated solid (%)	68.5	41.6	33.3	35.2	35.2
Total S accounted for (%)	93.0	96.3	93.6	98.4	99.8
S in irradiated solid which sublimed from polymer (%)	83	82	71	67	48
Original S retained by polymer (%)	12	7.5	9.7	12	18

a dose of 6.5 x 10^9 rads. That elemental sulfur as such did not constitute a part of the polymeric residue was demonstrated by the complete sublimation of sulfur from a known mixture of sulfur and irradiated Santowax OMP.

Irradiation 40 (Table XXIII) was made at the relatively low temperature of 460 to 480°F (238 to 249°C), in contrast to the usual temperature of about 630°F (323°C), to study temperature effects on protective action provided by some of the more promising stabilizers. Table XXV gives the relative polymer values obtained from use of the same additives in previous irradiations carried out at 600 to 670°F (316 to 354°C). Any comparison of the two sets of values must be made with the realization that total radiation dose at the lower temperature was somewhat less than that used at the higher temperature. However, the results do indicate that the stabilizing action of sulfur, especially at higher concentrations, was greater at the lower temperature. In contrast, the beneficial action of the additives having the anthracene-like structure remained essentially constant. As expected, the radiolytic gas from the control was considerably less at the lower temperature. A comparison of relative gas values from stabilized Santowax at the two different temperatures would be misleading as some of these values are known to be greatly dependent on radiation dose.

Stabilization by 9,10-dihydroanthracene, unlike that by anthracene, was very dependent on concentration, progressively improving as the concentration of additive was increased (irradiations 41 and 42). At a concentration of 24 mol% the dihydroanthracene reduced polymer formation by 50%, with further reduction occurring at higher concentrations (64% reduction at 50 mol% concentration). Gas chromatography indicated the presence of anthracene as well as 9,10-dihydroanthracene in the irradiated product from the 24 mol% blend. Of the oxygen-containing compounds structurally related to anthracene, xanthydrol and anthrone exhibited significant protective action whereas xanthone had little effect. Unlike anthracene itself, additives [benz(a)anthracene, dibenz(a,h) anthracene, and benzo(a)pyrene] possessing the anthracene structure but modified by non-linear benzenoid substituents provided little or no stabilizing

TABLE XXV

STABILIZATION OF SANTOWAX OMP UNDER IRRADIATION AT 600-670°F (316-354°C)

Sample	Dosage (rads x 10^{-9})	Relative Polymer
Control	7.2	1.00 (23.0%)
S_8, 0.4 mol%	9.4	0.86 (23.5%)
S_8, 0.7 mol%	9.4	0.81 (22.1%)
S_8, 1.0 mol%(a)	10.1	0.94 (27.2%)
Anthracene, 3 mol%	7.2	0.85 (19.6%)
9,10-dihydroanthracene, 3 mol%	7.2	0.77 (17.8%)
Phenazine, 3 mol%	7.2	0.75 (17.2%)

(a) Temperature may have exceeded 670°F (354°C).

action (irradiation 43). This was in contrast with the beneficial effect observed previously when the benzenoid substituent was present in a linear arrangement (naphthacene).

Of considerable interest was the finding that the skeletal structure of stabilizers having condensed-ring systems was much less critical when partially hydrogenated (irradiations 42 and 43). Furthermore, to the extent that such additives were studied, protective action usually increased as the degree of hydrogenation increased. Thus, in contrast with phenanthrene itself, 9,10-dihydrophenanthrene was somewhat beneficial, and the much-more-effective 1,2,3,4,5,6,7,8-octahydro derivatives of anthracene and phenanthrene were nearly equivalent, each providing a degree of stabilization comparable to that of 9,10-dihydroanthracene. Similarly, each of the hydrogenated pyrenes (dihydropyrene, tetrahydropyrene, and 1,2,3,6,7,8-hexahydropyrene) was effective, with a progressive increase in stabilizing action with increased degree of hydrogenation. On the other hand, HB-40 (terphenyls hydrogenated to 40% of complete saturation) gave no significant stabilization. It appears that hydrogenated fused-ring systems, carbocyclic and heterocyclic, merit further study.

7. RECLAMATION OF RADIOLYZED ORGANIC NUCLEAR REACTOR COOLANT

(W. M. Hutchinson, L. E. Gardner and L. V. Wilson, Jr.)

7.1 Introduction

Research was continued on the use of catalytic hydrocracking for reclamation of damaged nuclear reactor coolant. During this quarter experimental work was directed toward completion of necessary data for a preliminary economic evaluation of hydrocracking techniques. Although several phases of the overall hydrocracking program were incomplete, immediate attention was given to the development of a set of process conditions which could be used in plant scale operation. The most feasible route for commercial application appeared to be a low conversion, long process cycle operation with recycle of unconverted material. Thus, data were obtained for product yields and coke formation rates at "steady-state" activity in catalytic hydrocracking of both raw high boiler and recycle stock. This information was used along with previous cost estimation data on residual oil hydrocracking to obtain a reliable evaluation for coolant reclamation. Other experiments carried out this quarter included hydrocracking of OMRE Core II coolant and OMRE Core III-A high boiler. Also, further evaluations and analyses were made on distilled reclaimed coolant. The incomplete areas of research should be concluded at the end of the next quarter.

7.2 Catalytic Hydrocracking of High Boiler

7.21 Low Conversion Hydrocracking Process. In the last quarterly report[20] the use of low conversion, long process cycles was mentioned as a potential method of coolant reclamation. The main advantage of this type of operation lies in the elimination of frequent regenerations required by rapid coke deposition. All short runs (2 to 4 hr) at high conversion have resulted in extremely high coke yields which in turn gave low selectivities and product recoveries. In commercial operation, short process cycles are quite expensive

due to the cost of pressurizing, depressurizing, flushing, etc. Also, three reactors might be required. Consequently, runs longer than 2 hr have been made to obtain the required data for estimation of the economics of longer process cycle operation with recycling of unconverted material.

Catalyst Selection

Data on hydrocracking both model compounds (biphenyl and terphenyls) and OMRE high boiler indicated that the following catalyst compositions possessed good activity for selective polyphenyl conversion:

$NiO-Al_2O_3$	(low Ni content, low surface area)
$Pt-Al_2O_3$	(low surface area)
$CoMoO_4-Al_2O_3$	(high metals, low surface area)
$CoO-V_2O_5-Al_2O_3$	(low surface area)

Since it was desirable to develop data immediately for a preliminary economic study, no further testing was carried out on these catalysts to differentiate between them. These catalysts were all prepared in this laboratory, and the same alumina support was used in each preparation. Thus any differences in activity were due to the active ingredient of the preparation. Both nickel and platinum catalysts gave higher conversion at the same temperature than did the other two catalysts. However, the latter two had lower coke-formation characteristics at similar levels of conversion. Cobalt-vanadia-alumina showed lower hydrocracking activity than cobalt molybdate-alumina. Thus, it appeared that cobalt molybdate had a slight edge over the other three, and it was chosen for immediate testing to obtain information for the economic evaluation. Another point in favor of using this catalyst is that it is less susceptible to poisoning than catalysts from materials such as sulfur, nitrogen, or oxygen-containing compounds. This may prove to be quite important in future selection of a catalyst since stabilizers for terphenyl coolant may contain these well-known catalyst poisons. In particular, nickel or platinum-containing catalysts would be readily poisoned if these additives were present. Also, cobalt molybdate is quite stable toward effects of repeated regeneration.

Longer Runs

Runs of 2, 4, 6, and 24 hr were made on $CoMoO_4Al_2O_3$ catalyst using the following reaction conditions:

Temperature	900°F
Total pressure	1000 psig
Charge rate	1.0 vol liquid/vol catalyst/hr
Charge	40 wt% high boiler in p-xylene
Hydrogen flow	30 mol hydrogen per mol HB

The same catalyst sample was used for all runs with air regeneration between each run at 900°F. The air rate was controlled to prevent the hot zone from exceeding 1050°F. After the initial run some activity was lost, but succeeding runs indicated no further loss in activity. Product samples were taken periodically and analyzed. Analytical procedure was to distill off the solvent at atmospheric conditions, remove last traces of solvent and alkylbenzenes under a low-temperature vacuum, and finally carry out analytical tests on the solvent-free product. Material boiling between biphenyl and triphenylene was determined by the combination of sublimation at 240°C and 0.1 mm with subsequent analysis by chromatography. After these tests were performed the remaining products were combined and distilled at 4.0 mm to an end point of 225 to 250°C. The resulting distillate was considered reclaimed coolant and was subjected to various evaluation tests. The atmospheric distillate also was analyzed by chromatography. Reactor effluent gas was measured and analyzed by mass spectrometry. By calibration of the flow controller it was possible to calculate a hydrogen consumption value for any given time on stream.

Data from these runs are plotted in Figures 8 and 9 where on-stream time is plotted against conversion, product recovery, selectivity, coke formation, and molecular weight of solvent-free product. These plots indicated that "steady state" of catalyst activity was obtained after the first 6 hr on stream. No attempt was made to increase conversion by increasing temperature or contact time. Average catalyst temperature was 899°F during the run, and the maximum temperature recorded was 921°F. Conversion of high boiler leveled out slightly above 20% at a product recovery of about 95wt%. Selectivity to biphenyl

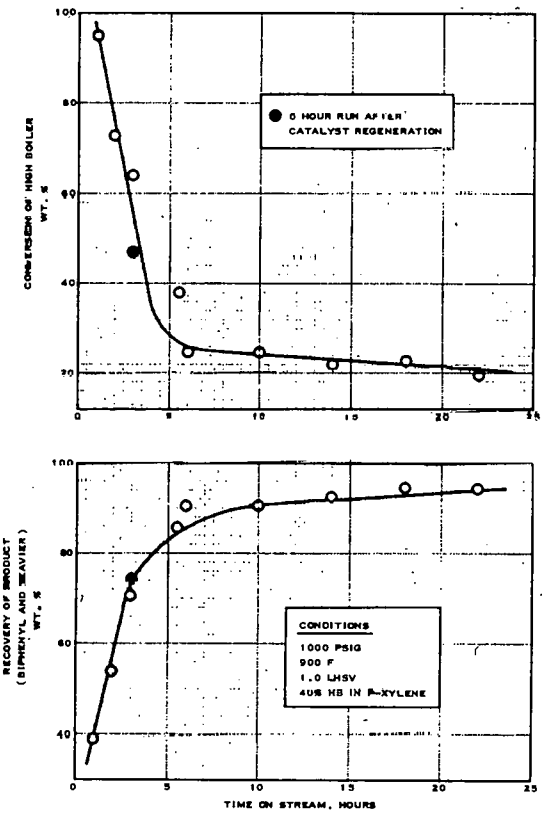

Fig. 8 Hydrocracking OMRE Core II high boiler over low-surface cobalt molybdate catalyst.

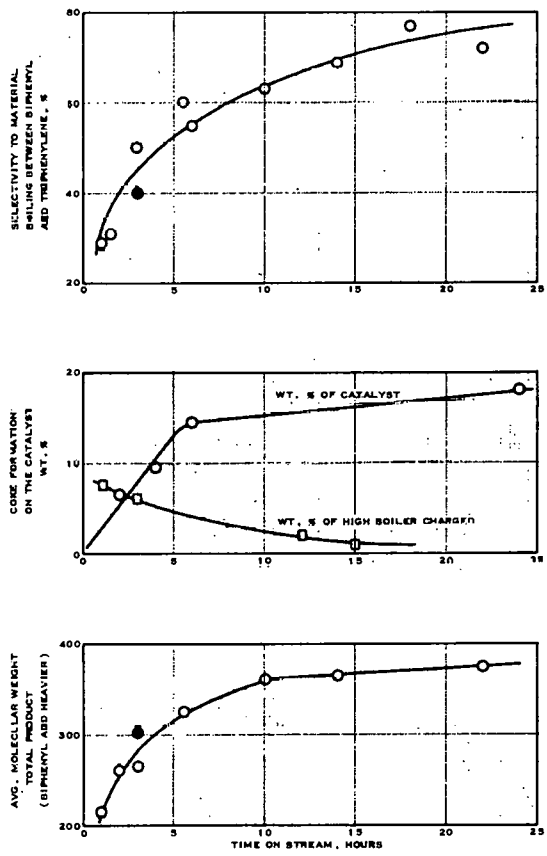

Fig. 9 Hydrocracking OMRE high boiler.

through triphenylene range product was still increasing at the end of the 24-hr run. Table XXVI summarizes the data from the 24-hr run. Yields, product

TABLE XXVI

24-HR HYDROCRACKING RUN ON OMRE CORE II HIGH BOILER OVER COBALT MOLYBDATE CATALYST

Conditions: 1000 psig, 900°F, 1.0 LHSV, 40% high boiler in p-xylene, 30 mol H_2/mol high boiler.

	Hr on Stream					
	0-4	4-8	8-12	12-16	16-20	20-24
High boiler conversion(a) (wt%)	73	25	25	22	23	20
Selectivity(b) (%)	31	55	63	69	77	72
Product recovery(c) (wt%)	54	91	91	93	95	95
Distilled coolant yield (wt%)	29	21	21	23	24	21
Hydrogen consumption (mol/mol)	530		(340)(d)		150	
Coke yield (wt% of high boiler charged)			(1.9)(d)			
Coke yield (wt% of catalyst)			(18.2)(d)			
Yields (wt% of high boiler charged)						
Lights (< biphenyl)+coke	46	9	9	7	5	5
Reclaimed coolant	29	21	23	24	25	22
Unconverted high boiler	25	70	68	69	70	73
Product analysis(c)						
Sublimate(e) (wt%)	53	23	23	24	26	23
Average molecular weight	261		360	366		374
C/H atomic ratio	1.19		1.31	1.27		1.33
Sublimate analysis(f) (wt%)						
Alkylbiphenyls	13	15	9	10	11	8
Alkylterphenyls	20	14	11	10	11	12
Biphenyl	14	16	9	10	14	8
Phenanthrene	7	6	4	4	2	4
O-terphenyl	6	9	8	8	10	8
M-terphenyl	20	23	31	30	27	30
P-terphenyl	9	11	19	17	15	18
Triphenylene	4	4	7	8	8	9
Quaterphenyls	7	2	2	3	2	3

(a) Disappearance of high boiler.

(b) Selectivity to material boiling between biphenyl and triphenylene.

(c) Includes biphenyl and heavier.

(d) Data for complete 24-hr run.

(e) Sublimate material at 240°C, 0.2 mm, 30 min.

(f) Chromatographic analysis using LiCl-chromosorb-P column programmed 150-350°C at 15°/min. This material is considered reclaimed coolant.

analysis, and reclaimed coolant composition (sublimate at 240°C and 0.2 mm) are shown. Coke yields were 18.2 wt% of catalyst or 1.9 wt% of high boiler charged. From these data it was possible to calculate coke formation rates for the 6- to 24-hr period. These were 0.20 wt% of catalyst per hour and 0.5 wt% of high boiler charged. Since these figures were calculated using a constant rate between 6 and 24 hr they are maximum expected values since the coking rate apparently decreases in the increasing on-stream time. Using the above coking rates an on-stream cycle period in excess of 100 hr can be estimated for this low conversion process. Obviously longer experimental runs are required to definitely establish the ultimate cycle length. The present thought is that about 30 wt% coke on the catalyst can be tolerated for a low conversion process.

Hydrogen consumption was calculated for the above run. This was done by recording inlet hydrogen flow on the chart of the calibrated flow controller and measurement of reactor effluent gas of known hydrogen concentration (by mass analysis). Other factors in the overall calculation included excess gas produced due to product accumulation in the high pressure receiver which reduced the gaseous volume in the pressurized system. Also a correction was made for the gas dissolved in the hot liquid product using the expression:

$$\text{Log } S = \log (10.0 + 0.026\ P) - \frac{450}{T}$$

where S = solubility of hydrogen in cc/cc of liquid

P = pressure in psi

and T = liquid temperature, °C + 273

Hydrogen consumption values were calculated for portions of the run in which inlet flow was constant as shown by the flow recorder. During the "steady-state" part of the run, net hydrogen consumed was 1.6 moles hydrogen per mol high boiler (or 150 std ft^3/bbl). The low value was reasonable since very little ring saturation was expected at the reaction conditions used. In the first 4 hr of the run, net consumption was found to be 6.0 moles per mol (530 std ft^3/bbl). These data were consistent with the high initial activity of the freshly regenerated catalyst.

Plots of product data on the molecular weight-conversion correlation along with lower biphenyl yields indicated that some composition changes occurred in the unconverted residue fraction of the products. For example, at 20 to 25% conversion the average molecular weights of the recovered products from the 24-hr run (360 to 375) were low compared to the established curve at the same conversion level (400 to 450). Thus it was indicated that the recycle stock might be more amenable to hydrocracking than the virgin high boiler.

A 6-hr run following the 24-hr run after regeneration of catalyst indicated no change in activity. The data from this run are plotted on Figures 8 and 9; a midpoint was plotted (at 3 hr) since the complete 6-hr product was batched together and analyzed.

An incidental observation after these long runs was that upon removal from the reactor both catalyst particles and α-alumina preheat section particles

were stained with iron rust. This was obtained presumably by deposition of particulate from the high boiler. Thus, an additional benefit might be realized by utilization of a fixed bed, catalytic hydrocracking process.

7.22 Recycle of Unconverted High Boiler. In order to support the idea of a low conversion process, it was desirable to study the effects of recycling the unconverted material. Product properties and appearance indicated that the unconverted residue might be less refractory toward hydrocracking than the original high boiler. Recycle stock was prepared by combining several samples of once-through hydrocracked OMRE high boiler. Vacuum distillation on the solvent-free material gave a distillate (or reclaimed coolant) fraction and a residue which could be used for recycle material. A typical example of this was a product from 30% conversion (avg) of OMRE high boiler which had an average molecular weight of 357 and a carbon/hydrogen atomic ratio of 1.32. Sublimable material at 240°C, 0.2 mm, and 30 min was 26 wt% which was quite similar to the products obtained in the 24-hr run. The distillation was carried out at 4.0 mm to an end point of 246°C. Maximum kettle temperature was 338°C. Properties of charge and product are shown in Table XXVII.

The residues from these distillations were dissolved in p-xylene to give a 40 wt% solution of high boiler. All samples were slightly different in solution from the original high boiler in that they were not completely black but had a dark brown color.

For each recycle run the catalyst was pre-conditioned by a 4-hr run on virgin high boiler which deposited coke and saturated the catalyst bed with oil. This was followed by a 2-hr run using the diluted recycle stock. In all recycle runs the sixth-hour (total time) product was worked up and analyzed for comparison with the sixth-hour product from a standard run on OMRE high boiler. Three runs were made, two of which were equivalent to a first recycle operation. The third run was recycling the combined unconverted material recovered from the first two recycle runs. The data from these runs are summarized in Table XXVIII along with comparable data on virgin OMRE high boiler. Conversions varied from 28 to 41% for the recycle runs. In all three runs coke yields were lower than for the standard run. Coolant yield (per pass) was higher for the standard run. This was due mainly to the method of calculation which is determined by multiplying product yield times percent sublimate. In the first pass the sublimate is larger since the original high boiler contains 11% sublimable material. Product properties were all

TABLE XXVII

PROPERTIES OF PRODUCTS

	Average Mol. Wt.	C/H Ratio	Sublimate at 240°C, 0.2 mm (wt%)
Hydrocracked product	357	1.32	26
Distilled reclaimed coolant	222	1.22	96
Residue (recycle stock)	584	1.45	0

very similar as shown by analyses of sublimates in Table XXVIII. Thus it can be concluded that results from these recycle runs were favorable in that coke yields were low at about the same conversion level as in tests on virgin OMRE high boiler. Data from these runs indicate an ultimate yield value of about 80%. Several recycle runs would be required to definitely establish this value, preferably on mixtures of fresh high boiler and recycle stock.

7.23 Product Evaluation - Radiation Stability. Four electron irradiations under a Linac were carried out on six different samples of reclaimed coolant.

TABLE XXVIII

HYDROCRACKING OF RECYCLED RESIDUE FROM LOW CONVERSION OF OMRE HIGH BOILER

Conditions: 1000 psig, 900°F, 1.0 LHSV, 40% high boiler in p-xylene, 30 mol H_2/mol high boiler, 6-hr runs.

	Standard Test		Recycle Tests					
	Virgin High Boiler	First Pass	Stock A[a]	First Run	Stock B[a]	First Run	Stock C[b]	Second Run
High boiler conversion[c] (wt%)		38		28		35		41
Selectivity[d] (%)		60		64		60		56
Product recovery[e] (wt%)		86		90		87		80
Distilled coolant yield per pass (wt%)		29		16		19		19
Coke yield (wt% of high boiler charged)		6.0		4.5		3.8		4.6
Coke yield (wt% of catalyst)		14		10		10		10
Yields (wt% of high boiler charged)								
Lights (< biphenyl) + coke		14		10		14		20
Reclaimed coolant	9	29		18		21		21
Unconverted high boilor	91	57	100	72	100	65	100	59
Product analysis[e]								
Sublimate[f] (wt%)	11	34	0.0	17	0.0	22	0.0	24
Average molecular weight	545	325	588	390	584	352	566	362
C/H atomic ratio	1.49	1.30	1.42	1.35	1.45	1.26	1.41	1.30
Sublimate analysis[g] (wt%)								
Alkylbiphenyls		13		17		9		10
Alkylterphenyls		15		21		11		10
Biphenyl		18		15		11		9
Phenanthrene		4		4		4		4
O-terphenyl		12		7		7		9
M-terphenyl		20		19		26		29
P-terphenyl		12		9		15		16
Triphenylene		2		4		8		9
Quaterphenyls		4		4		9		4

(a) Residues from vacuum distillation of hydrocracked high boiler products.

(b) Residues from vacuum distillation of products from first recycle runs.

(c) Disappearance of high boiler.

(d) Selectivity to material boiling between biphenyl and triphenylene.

(e) Includes biphenyl and heavier.

(f) Sublimable material at 240°C, 0.2 mm, and 30 min.

(g) Chromatographic analysis using LiCl-Chromosorb-P column programmed 150-350°C at 15°/min.

Three samples were distilled reclaimed coolants from OMRE high boiler hydrocracking runs. The remainder were hydrocracked products which contained some material higher boiling than quaterphenyls. Some of the samples were run simultaneously, and all samples were run along with Santowax OMP as the control for relative comparisons. Dosages varied from 5.3 to 8.8 x 10^9 rads at 600 to 650°F for 8 hr.

Complete analytical data were obtained for these irradiations including molecular weights, carbon to hydrogen atomic ratios, and compositions before and after irradiation. Polymer determinations were made using the micro-sublimation technique at 220°C, 0.10 mm, and 30 min. Some values were also obtained at more severe conditions of 240°C and 0.2 mm. All available data from radiolytic stability tests are summaried in Table XXIX. In all tests products from hydrocracking gave polymer yields lower than the control. In some cases decreases in quaterphenyl content as shown in the table may be misleading since sublimation conditions may not have been severe enough to sublime all the quaterphenyls present. However, this is in a favorable direction, and some of the polymer values for irradiated, distilled coolant may be high. Sublimations at higher temperatures on the residue from the standard sublimation should result in more accurate determinations on quaterphenyl content. No attempt was made to analyze the irradiated products for predictions of comparative reaction rates of alkylpolyphenyls and polyphenyls. In general, the alkyl concentration decreased after irradiation. The concentrations of terphenyls in reclaimed coolant indicated much slower rate (net) of disappearance than did the terphenyls in Santowax OMP.

Nuclear Magnetic Resonance Analysis

A sample of distilled, reclaimed coolant was analyzed by nuclear magnetic resonance for hydrogen distribution, and the information tabulated in Table XXX was obtained. This analysis suggested that alkyl chains longer than methyl, but probably not longer than propyl, were present. The presence of isopropyl groups appeared likely. Also the spectra indicated condensed aromatics which were most likely triphenylene and phenanthrene.

Viscosity, Density

Low temperature viscosity and density determinations were made on distilled reclaimed coolant. These values are compared with m-terphenyl values in Table XXXI.

7.24 Hydrocracking OMRE Core III - A High Boiler. In initial OMRE Core III operation high distillation throughput maintained high boiler content in the coolant at 4 to 5%. Thus high boiler molecular weight was lower than with Core II operation, and it was of interest to obtain hydrocracking data with the two samples for comparison. The lower molecular weight material would be expected to have lower coke-forming characteristics.

A sample of Core III-A high boiler was obtained and characterized. Inspection data are shown in Table XXXII and compared with properties of Core II material. Chromatographic analysis on these sublimate fractions and the molecular weight values indicated a large concentration of hexaphenyls in Core III-A high boiler. The terphenyl content of Core III-A was 4.7%

TABLE XXIX

RADIOLYTIC STABILITY OF HYDROCRACKED OMRE HIGH BOILER AND DISTILLED RECLAIMED COOLANT SAMPLES

	Irradiation 1[a]				Irradiation 2[a]							
Sample	Santowax-OMP		30 wt% Hydrocracked Product D in Santowax-OMP		Santowax-OMP		Distilled Reclaimed Coolant A		Distilled Reclaimed Coolant C		Hydrocracked Product F	
Dosage (rads x 10^9)	5.3		5.3		6.5		6.5		6.5		6.5	
Radiolytic polymer (wt%)[b]	0.0	19.8	9.6	22.1	0.0	20.7	0.0	18.5	0.0	18.0	21.4	33.6
Radiolytic gas (cc/watt-hr)		0.10		0.18		0.10		0.35		0.32		0.29
Relative polymer		1.0		—		1.0		0.89		0.87		—
Relative gas production		1.0		1.8		1.0		3.5		3.2		2.9
Analytical Data												
Average molecular weight	230	253	250	260	230	255	225	241	217	232	232	255
C/H atomic ratio	1.29	1.30	1.25	1.28	1.29	1.29	1.19	1.22	1.20	1.18		
Composition (wt%)												
Alkylbiphenyls	0.0	0.0	1.9	0.5			4.7	3.6	11.7	7.2		5.7
Alkylterphenyls	0.0	0.2	2.2	0.8			9.3	7.8	13.9	8.7		6.4
Biphenyl	0.4	0.3	3.2	1.2			6.3	4.9	10.8	7.9		8.4
Phenanthrene	0.0	0.0	0.0	0.0			1.7	2.0	4.1	3.5		2.5
O-terphenyl	11.9	8.2	10.3	9.7			4.5	4.3	4.2	4.0		3.6
M-terphenyl	55.0	45.0	44.6	41.9			21.6	20.2	19.1	18.5		14.2
P-terphenyl	32.5	32.8	25.7	21.9			12.8	11.9	10.2	11.4		8.4
Triphenylene	0.2	0.2	2.5	1.7			13.6	9.8	9.8	9.3		5.7
Quaterphenyls	0.0	0.0	0.2	0.2			25.5	14.0	16.2	11.5		11.0
Residue	0.0	19.8	9.4	22.1				21.5		18.0	21.4	33.6
Dosage (rads x 10^9)	8.7		8.7		8.8		8.8		8.8		8.8	
Radiolytic polymer (wt%)	0.0	25.3	0.0	20.8	0.0	26.3	0.0	19.3	25.1	39.6	73.8	73.4
Radiolytic gas (cc/watt-hr)		0.11		0.27		0.12		0.29		0.29		0.17
Relative polymer		1.0		0.82		1.0		0.73		—		—
Relative gas production		1.0		2.5		1.0		2.4		2.4		1.4
Analytical Data												
Average molecular weight	230	261	222	243	230	261	225	248	250	276	337	388
C/H atomic ratio	1.29	1.31	1.22	1.26	1.29	1.29	1.19	1.22	1.24	1.25	1.33	1.35
Composition (wt%)												
Alkylbiphenyls	0.0	0.0	7.8	5.7	0.0	0.0	9.2	5.3	8.4	6.4	2.4	1.5
Alkylterphenyls	0.0	0.3	9.9	8.6	0.0	0.1	13.2	7.0	8.2	8.0	2.9	2.7
Biphenyl	0.4	0.4	8.1	5.8	0.4	0.4	7.0	4.8	4.2	4.8	3.0	2.1
Phenanthrene	0.0	0.0	3.2	2.1	0.0	0.0	1.6	1.3	2.7	2.7	1.1	0.8
O-terphenyl	11.9	8.6	4.7	3.5	11.9	7.4	6.2	5.3	5.5	4.0	1.8	1.4
M-terphonyl	55.0	39.5	21.3	18.7	55.0	36.0	22.6	20.0	18.9	13.2	6.7	7.7
P-terphenyl	32.5	24.6	14.2	11.1	32.5	29.1	11.4	11.7	10.1	6.2	3.9	4.7
Triphenylene	0.2	1.3	14.9	14.3	0.2	0.7	10.4	9.4	8.0	6.3	2.0	2.8
Quaterphenyls	0.0	0.0	15.9	9.4	0.0	0.0	18.8	15.9	8.9	8.8	2.4	2.9
Residue	0.0	25.3	0.0	20.8	0.0	26.3	0.0	19.3	25.1	39.6	73.8	73.4

(a) Electron irradiations under the Linac at 600-650°F for 8 hr on 12-g samples in rotating tube apparatus. Data in right hand columns are after irradiation.

(b) Polymer was determined by sublimation at 220°C and 0.1 mm in Irradiation 1 and 240°C and 0.2 mm in Irradiation 2.

compared to 8.7% for Core II high boiler. Solubilities of the two samples have not been determined.

Two hydrocracking runs were carried out on Core III-A high boiler over cobalt molybdate-alumina catalyst. The runs were 2 hr and 6 hr in length,

TABLE XXX

NMR ANALYSIS DATA

Hydrogen Type	Hydrogen Distribution (%)
Aromatic ring	81.9
Adjacent CH_3	4.2
CH_3 beta to aromatic ring	3.0
Other CH_3	2.2
CH and CH_2 adjacent to aromatic ring	4.1
CH_2 not adjacent	3.4
Unidentified (possibly naphthenic)	1.2

TABLE XXXI

VISCOSITY AND DENSITY

	210°F		260°F	
	Coolant	m-ϕ_3	Coolant	m-ϕ_3
Viscosity (centistokes)	3.6	3.5	2.1	2.1
Density (g/ml)	1.037	1.040	1.014	1.020

and complete data are summaried in Table XXXIII along with comparable data obtained in runs on Core II high boiler. These initial hydrocracking tests indicated greatly reduced coke yields, similar conversions, higher recoveries, and higher selectivities. Thus the improved efficiency of hydrocracking the lower molecular weight high boiler was quite apparent. The low coke-formation rates should increase on-stream cycle time at least threefold for the low conversion process discussed above. Also, higher conversions could be predicted without excessive coke formation. Similar observations have been made in hydrocracking-modified OMRE high boiler. Other workers [21] have shown that removal of the very high molecular weight material resulted in coke reduction at a given conversion level.

7.25 Hydrocracking Core II Coolant. A series of hydrocracking tests on OMRE Core II coolant was quite promising in that yellow solid products were obtained in good yields at nearly complete conversion of the 23% high boiler in the coolant. In general, reaction conditions were as follows: 1000 psig, 850 to 950°F, 1.0 to 2.0 LHSV, 50% coolant in p-xylene and 25 to 50 moles hydrogen per mole coolant. Run times were 4, 6, and 12 hr, and the same cobalt-molybdate-on-alumina catalyst was used after many air regenerations.

TABLE XXXII

COMPARISON OF CORE II AND III-A SAMPLES

	Core II High Boiler	Core III-A High Boiler
Appearance	black	reddish-brown
Average molecular weight (M_n)	545	449
$C/_H$ Atomic Ratio	1.42	1.35
Sublimate (wt% of sample)		
At 240°C, 0.2 mm	9.2	9.2
At 314°C, 0.1 mm(a)	20.7	26.9
At 347°C, 0.1 mm(b)	14.0	38.8
Total sublimate	43.9	74.9
Residue remaining	56.1	25.1

(a) Sublimation of 240°C residue.

(b) Sublimation of 314°C residue.

Contrary to previous runs on high boiler, product appearance improved with increasing on-stream time.

Data from four of the runs at different reaction temperatures and run times are summarized in Table XXXIV. At the highest temperature, 930°F, overcracking occurred and production of low boiling material was quite high. During this run temperature rises in the catalyst bed of 100°F were observed, and some dealkylation of the xylene solvent occurred. At 900°F product recoveries were 95 to 97 wt% and the yield pattern indicated no net loss of terphenyls. Material in the product higher boiling than quaterphenyls appeared to be mainly hexaphenyls. The yields are shown in Table XXXIV and compared with the original composition of Core II coolant. Operation at 850°F appeared to be slightly more selective in terphenyl production, but more material heavier than quaterphenyl was in the product. In general, product molecular weights were in the 220 to 225 range compared to 270°F for Core II coolant. These data indicate that the higher boiling polyphenyls hydrocrack at a faster rate than the terphenyls. This was consistent with previous hydrocracking data on the series benzene-biphenyl-terphenyl. Para-terphenyl content was decreased in all runs (except 850°F), and the ortho and meta isomers changed very little (based on yields). These products had higher total terphenyl contents than products from hydrocracking 100% high boiler. At the present time, the net result of hydrocracking the total coolant appears to be conversion of the

TABLE XXXIII

COMPARISON OF HYDROCRACKING CORE II AND CORE III HIGH BOILERS OVER COBALT MOLYBDATE

Conditions: 1000 psig, 900°F, 1.0 LHSV, 40% high boiler in p-xylene, and 30 mol H_2 per mol high boiler.

	Core III-A			Core II		
	2-hr Run	6-hr Run		2-hr Run	6-hr Run	
Hours sampled	1-2	2-4	5-6	1-2	2-3	5-6
High boiler conversion[a] (wt%)	94	39	32	95	64	38
Selectivity[b] (%)	48	78	91	29	50	60
Product recovery[c] (wt%)	54	92	97	39	71	86
Reclaimed coolant yield (wt%)	48	34	33	33	38	29
Coke yield (wt% of HB charged)	1.8	—	2.4	7.5	—	6.0
Coke yield (wt% of catalyst)	1.3	—	5.4	6.3	—	15
Yields (wt% of high boiler charged)						
Lights(< biphenyl) + coke	46	8	3	61	29	14
Reclaimed coolant	48	34	32	34	38	29
Unconverted high boiler	6	58	65	5	33	57
Product analysis[c]						
Sublimate[d] (wt%)	89	37	34	86	53	34
Average molecular weight	218	291	292	215	266	325
$C/_H$ atomic ratio	1.18	1.21	1.22	1.20	1.24	1.30
Sublimate analysis[e] (wt%)						
Alkylbiphenyls	13	19	16	18	16	13
Alkylterphenyls	11	12	12	12	13	15
Biphenyl	17	18	16	16	14	18
Phenanthrene	2	4	3	6	7	4
O-terphenyl	8	6	4	4	7	11
M-terphenyl	24	20	20	19	22	20
P-terphenyl	19	16	18	9	12	12
Triphenylene	4	3	5	6	7	2
Quaterphenyls	2	2	6	10	2	5

(a) Disappearance of high boiler.

(b) Selectivity to material boiling between biphenyl and triphenylene.

(c) Includes biphenyl and heavier.

(d) Sublimable material at 240°C, 0.2 mm, and 30 min.

(e) Chromatographic analysis using LiCl-Chromosorb-P column programmed 150-350°C at 15°/min.

TABLE XXXIV

HYDROCRACKING OMRE CORE II COOLANT

Conditions: 1000 psig, 850-930°F, 1.0 LHSV, 50 wt% coolant in p-xylene, 25 mol H_2/mol coolant, $CoMoO_4$-Al_2O_3.

	Run 4	Run 20	Run 22	Run 19	Core II Coolant
Run time (hr)(a)	6	4	6	6	
Average temperature (°F)	850	900	900	930(b)	
Product recovery(c) (wt%)	93	97	95	77	
Coke yield (wt% of coolant charged)	2.1	4.5	2.7	3.7	
Coke yield (wt% of catalyst)	6.2	7.9	7.7	10.5	
Yields (wt% of coolant charged)					
Alkylbiphenyls	1	2	2	7	0.2
Alkylterphonyls	7	8	6	6	1.2
Biphenyl	2	6	5	9	0.5
Phenanthrene	2	1	1	2	
O-terphenyl	20	21	22	16	20.5
M-terphenyl	39	38	39	27	37.3
P-terphenyl	15	12	13	6	15.0
Triphenylene	2	3	3	2	2.6
Quaterphenyls	1	1	3	2	0.2
Heavier than ϕ_4's	5	3	1	2	22.5
Lights + coke	6	5	5	22	
Product analysis(c)					
Average molecular weight	235	225	223	206	270
C/H atomic ratio	1.20	1.22	1.22	1.18	
Color	yellow to yellow-brown				

(a) Sample taken in last hour of run.

(b) Temperature rise in catalyst bed to 990-1000°F.

(c) Solvent-free product.

high boiler in the coolant to alkylbiphenyls, alkylterphenyls, and biphenyl with little loss in terphenyls. Runs are in progress to optimize terphenyl yields, determine cycle length, and further evaluate this method of reclamation. A typical chromatogram of hydrocracked Core II coolant is shown in Figure 10.

This method of high boiler conversion might prove to be quite efficient since a high boiler distillation step would be eliminated. Only an atmospheric flash would be required to remove light products up through alkylbenzenes.

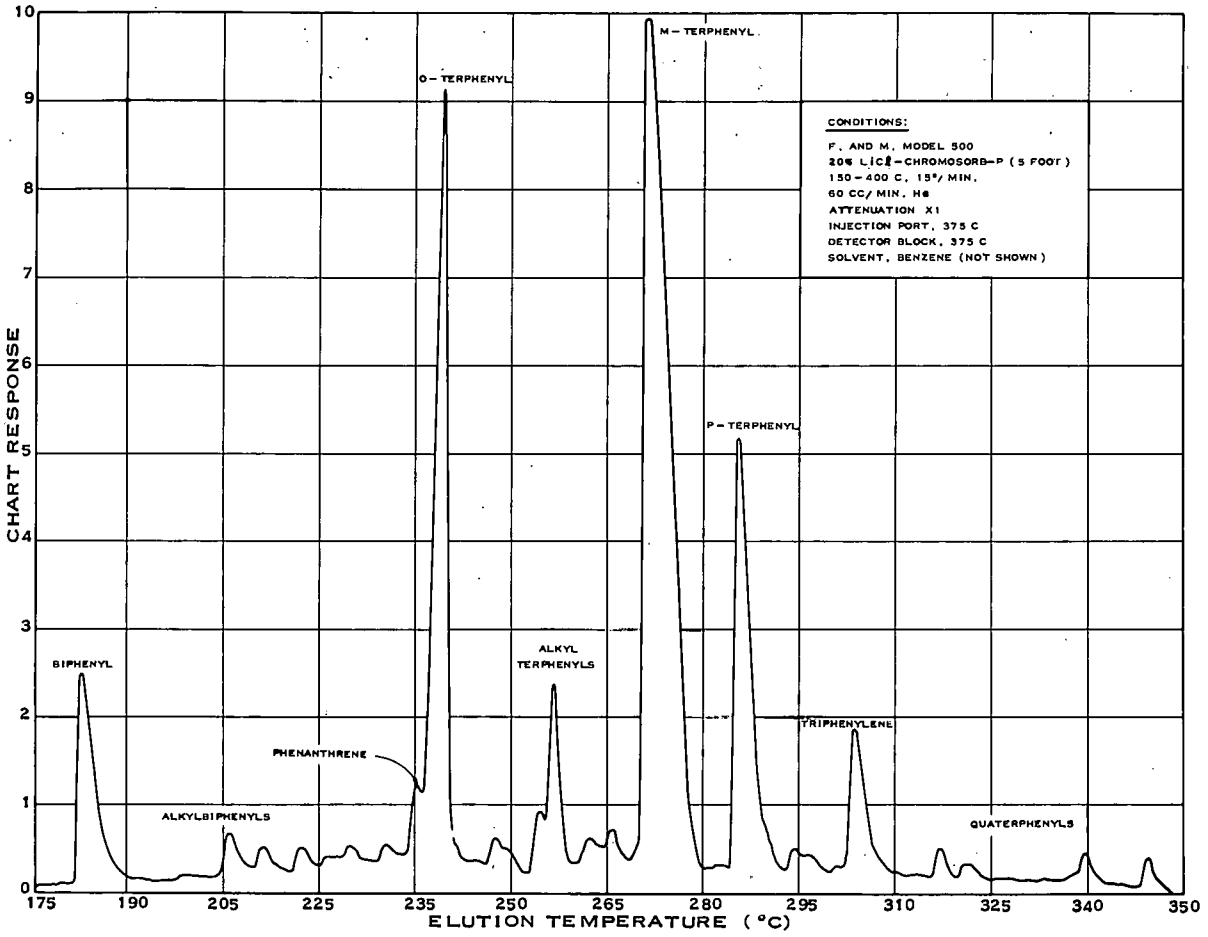

Fig. 10 Chromatogram of hydrocracked Core II coolant.

Conversion of hydromatics to aromatics in the terphenyl range might be an important benefit.

Conclusions and Present Status

Data included in this report were used in preparing the economic evaluation discussed in the following section. The evaluation is made for a long process cycle, low conversion operation. At the present time more data are needed for such an evaluation on coolant hydrocracking or Core III-A high boiler hydrocracking.

Experimental work is now designed to complete several phases of hydrocracking studies which have been initiated during this project. Thus, a complete evaluation of reclamation by hydrocracking should be available by the end of the next quarter.

7.3 Economic Evaluation of Hydrocracking Process

A process design and economic analysis for a plant to produce usable coolant by hydrocracking the high boiling polymers in used coolant is being developed and is nearly completed. As a basis for this evaluation it is being assumed that the hydrocracking plant would be built large enough to convert

50,000 lb per day of high boiler. This amount of high boiler would be expected to be produced in a 1000-Mw thermal reactor if it is assumed that high boiler is formed at a rate of 50 lb of high boiler per Mwd. Operation directly on coolant from the reactor without previous separation of high boilers according to Section 5 above will also be evaluated for comparison.

II. EOCR EXPERIMENTAL PROJECTS

1. LOOPS

1.1 Coolant Technology Loop and Fuel Technology Loop (R. S. Kern, F. K. Clements, L. L. Porter)

Close liaison continued with AEC-IDO and Fluor Corp. on the Title II design of the Coolant Technology Loop (CTL) and the Fuel Technology Loop (FTL). Procurement and construction of the loops by C. F. Braun continued during the quarter. Vendor drawings and data for most of the loop equipment were received and reviewed. Title I review of the Loop Handling Equipment and Procedures was completed.

1.11 CTL and FTL Design Liason. Phillips Petroleum was represented at two EOCR loop design review conferences with AEC-IDO and Fluor Corp. during this quarter. During the conference held January 23-26, 1962, the discussions centered around the following areas of the Title II design:

(1) Final review of drawings and specifications issued to date.

(2) Deficient areas of design, such as in-pile tube insertion and removal procedures, in-pile tube instrumentation leadout, subpile room study, piping and supports design analysis, operating manuals, and steady-state analysis.

(3) Subpile room shielding concept for FTL.

(4) In-pile tube design revisions and shop test specifications.

(5) Sampling equipment design.

Due to the questionable concept of supporting the FTL shielding directly on the piping, AEC-IDO was requested to defer procurement of this shielding pending further review and analysis by Phillips. Since the FTL can be decontaminated, the lack of this shielding will not restrict initial FTL tests. If shielding is warranted in the future, Phillips will design and procure it.

The next design conference was held March 6-8, 1962, with discussion of the following major items:

Title I Review of Loop Handling Equipment. This review resulted in extensive changes to Fluor's concept, which had an estimated cost of $275,000. Phillips recommended suitable alternate approaches which reduced the cost by an estimated $80,000.

Operating Manual for Loops. The scope and format used by Fluor in preparing the first section of the CTL manual was deemed unsatisfactory to Phillips. Phillips submitted an outline and two example sections to Fluor to be used as a guide in preparing these manuals.

Design Information for Hazards Analyses. Fluor and AEC-IDO agreed to provide, with few exceptions, the information requested by Phillips. Several

significant problem areas were uncovered by this request; among them were the design of the piston-operated block valves during failure of the air supply, and an inadequate reserve supply of instrument air upon compressor failure. Fluor is currently resolving these problems.

1.12 CTL and FTL Construction. At the end of this quarter, construction progress on the loops was 7% complete. Procurement of material and equipment was progressing adequately to meet the required dates for field installation. The major construction efforts during the quarter were:

(1) Demolition and forming for extension of the FTL pipe corridor.

(2) Escavation and forming for the tank storage annex.

(3) Phenoline painting of cubicle walls.

(4) Rerouting of certain reactor piping.

(5) Placement of cubicle shielding doors.

The scheduled completion date for the loops is currently being revised.

Fabrication of the CTL and FTL in-pile assemblies was resumed in late March, after revised drawings were issued to the vendor. Delivery of these assemblies is scheduled for late August 1962.

A vendor's alternate proposal of using capacitance probes for liquid level indication was adopted, resulting in a cost saving of $30,000.

The design criteria for the loops, issued by Phillips on January 3, 1961, required that all loop vessels be designed and tested in accordance with the ASME Unfired Pressure Vessel Code. Since these vessels contain reactor coolant, they are designated as primary nuclear vessels and, as such, their design and fabrication also must be in accordance with applicable ASME Code nuclear case interpretations. At the start of loop design, Code Cases 1270 N-2 and 1273 N-3 were in effect with respect to primary nuclear vessels. In February 1961, Code Case 1273 N-4 was issued, and in April 1961, Code Cases 1270 N-3 and 1273 N-5 were issued. Due to an apparent oversight, the vessel drawings and specifications were issued in April 1961, requiring compliance with Cases 1270 N-2 and 1273 N-3. Though it was pointed out in August 1961, that these cases have been superseded, AEC-IDO decided not to upgrade the drawings and specifications to the more recent cases. As a consequence, one vendor has been unable, as yet, to obtain ASME Code certification and stamping for approximately 20 loop vessels.

1.2 Component Development Test Loop (E. R. Oetken, R. G. Young, S. Cohen, R. S. Kern)

1.21 Construction and Operation. During the present quarter the construction of the CDTL was completed, with the exception of installation of the primary circulating pump and automatic fire protection system. A flow

sheet of the system is contained in the previous quarterly report [23]. Figures 11 and 12 show the CDTL control panel and the interior of the CDTL cubicle. The operational shakedown of the CDTL has been started, using the single-stage Chempump and an eutectic mixture of biphenyl, ortho- and meta-terphenyl which freezes at approximately 50°F. The eutectic, which is being used to prevent organic freeze-up in case of heater failure during the loop check-out, will be replaced with Santowax OMP after installation and check-out of the main coolant pump. Initial loop operation at temperatures up to 550°F at 200 psig has had only two malfunctions:

(1) The turbine-type flowmeter functioned erratically for the first several hours of loop operation and then failed completely. A high pressure drop across the section of the loop containing the instrument indicates that the turbine may have been blocked by foreign material not removed by the preoperational loop cleanup.

(2) The surge tank heaters shorted after several hours of operation. A preliminary examination indicated that the heater leads may have burned out.

The cause of these failures will be determined and corrected at the time the primary coolant pump is installed. The CDTL will not be operated at its design temperature of 800°F until the results of pyrolytic degradation tests, now being made, are available.

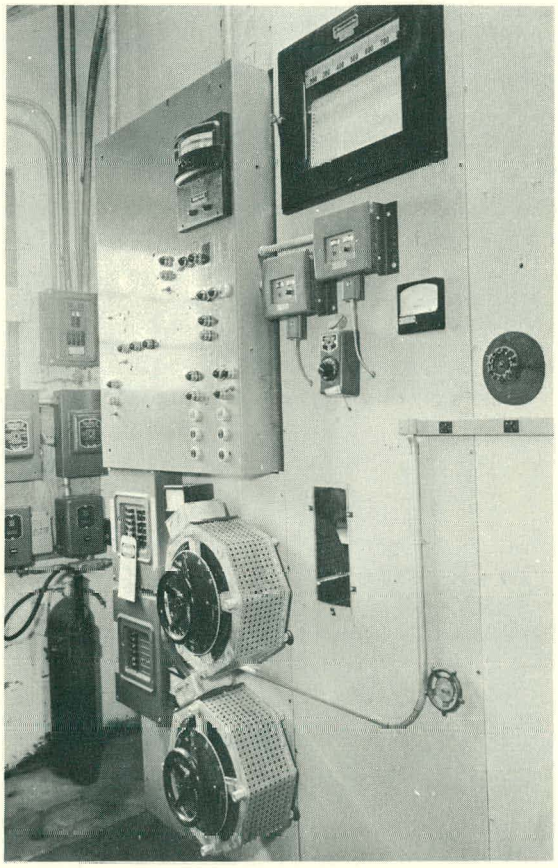

Fig. 11 CDTL control panel.

The design requirements for the CDTL (circulation of Santowax at 800°F,

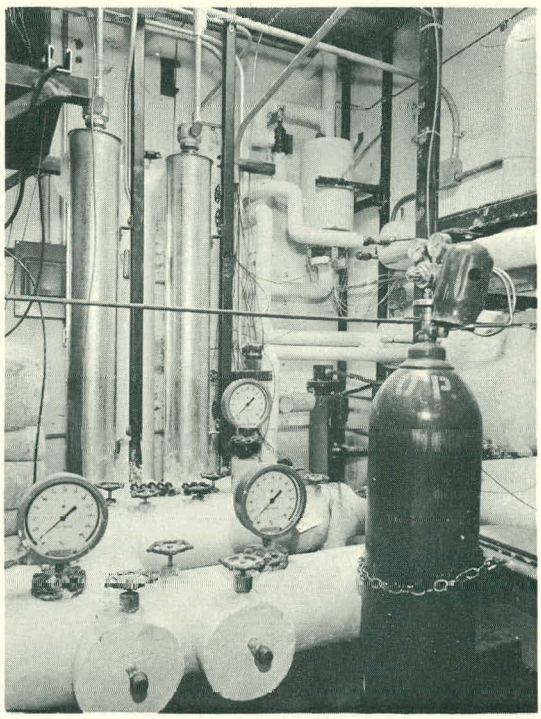

Fig. 12 Interior of CDTL cubicle.

with 10 to 15 kw of heat input) resulted in several features which will be useful in the design of future test loops.

Circulation Heater Design. The CDTL contains two 5-kw loop heaters to make up the high heat losses during thermocouple calibration experiments. The heaters were constructed by inserting a bundle of three hairpin immersion elements into a 2-in. pipe. The resulting flow area, approximately 0.017 ft^2, gives reasonably high heat transfer coefficients. At a 10-gpm flow rate and a heater power density of 12 watts/$in.^2$, the resulting film temperature drop is less than 100°F. It is expected that this will prevent heater failure at the design operating temperature of 800°F.

Rotameter Design. A rotameter with a magnetic follower was installed in the CDTL to give a direct reading of flow. To keep the organic in the magnetic follower from freezing, an oven with a viewing port (shown in Figure 13) was built around the magnetic follower. Infrared lamps controlled by a thermostat provide both heat and illumination. This method may prove to be a simple and direct means of measuring hot organic flow rates.

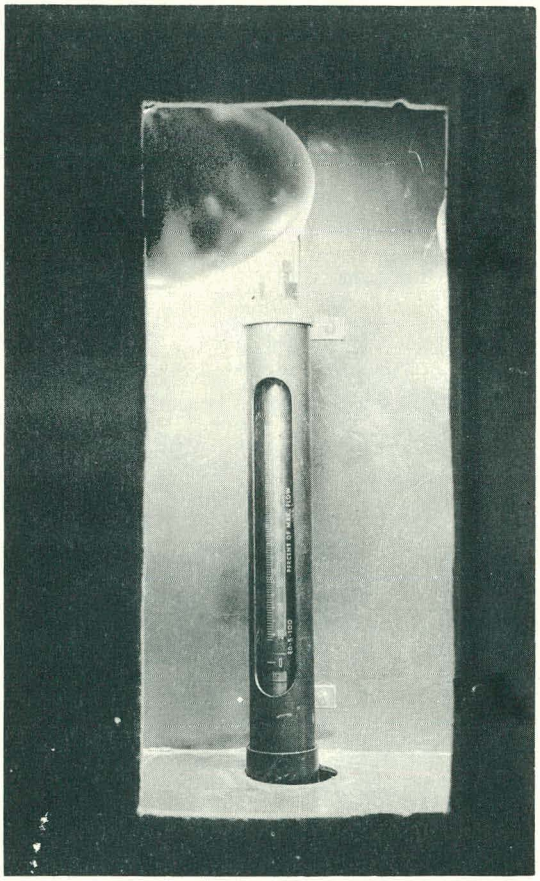

Fig. 13 Rotameter oven.

Loop Tracing Heaters. Loop piping and valves were traced with high-temperature-resistance heater tape (Chromolox TWM-20). To increase the effectiveness of the tracing, high-temperature-conducting cement (Thermon T-63) was applied over the tape. Previous experience was that this water-base cement would short out the tape. To prevent this, the tape was coated with high temperature aluminum paint, followed by a coat of ordinary floor wax. This treatment gave a high resistance to ground and prevented heater failure.

1.22 Experimental Program - EOCR Fuel Plate Thermocouples - Design. Ceramic-insulated stainless-steel-sheathed thermocouples with spade tips have been selected for measuring EOCR fuel plate surface temperatures. This type of thermocouple has been selected on the basis of being the best compromise available between mechanical reliability of thermocouple attachment, influence of cooling flow on indicated temperature, and fouling characteristics. Thermocouples between 0.025 and 0.062 in. in diameter (Figure 14) are presently being considered.

Attachment. Resistance welding and brazing are being considered for attaching thermocouples to EOCR fuel plates. Test sections using both methods will be constructed and tested to determine the better method.

Test Section Design. A test section has been designed for installation into the CDTL to evaluate and calibrate the thermocouples. The general scheme is to flow Santowax at EOCR operating conditions through a hydraulic mockup of EOCR coolant channels and remove heat across dummy EOCR fuel plates into a cold water heat sink. Figure 15 illustrates this design and Figure 16 shows the orientation of the thermocouple tips. This particular orientation has been selected to minimize fouling at the thermocouple tips.

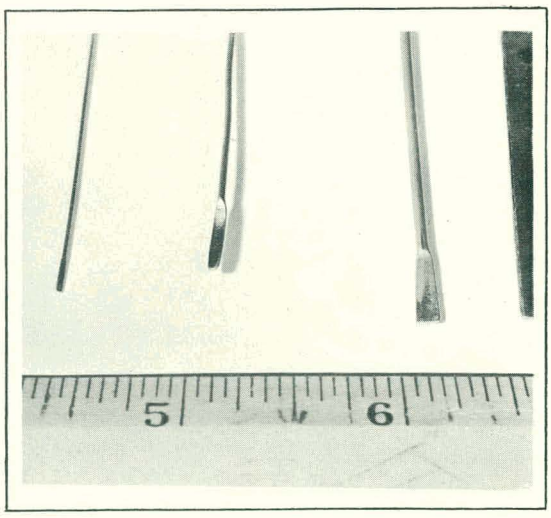

Fig. 14 Spade tip thermocouples.

A full-scale mockup of the test section has been pressure tested to 600 psig to determine the deformation characteristics of the coolant channel. A maximum of 0.010-in. increase in channel thickness was measured at 100 psig. Instrumented test sections will be tested similarly to determine correction factors for channel thickness at test pressure. Figure 17 shows the test section after being tested to 600 psig, which resulted in a permanent 0.050-in. deformation of the plate.

1.23 Experimental Program - Chempump Test (D. R. Conkling, R. G. Young) No-leakage requirements for the EOCR test loops resulted in design selection of canned-type pumps wherever practical. Because of the lack of operating experience and difficulties encountered at other facilities using canned-type pumps for high temperature Santowax, it was considered advisable to evaluate a single-stage canned pump prior to EOCR loop operation. A single-stage Chempump (Model CFHT 1-1/2 to 3/4S), similar to those being furnished for the CTL and FTL, has been installed in the EOCR Component Development Test Loop to evaluate its performance and reliability. Figure 18 is a drawing of the pump showing its design.

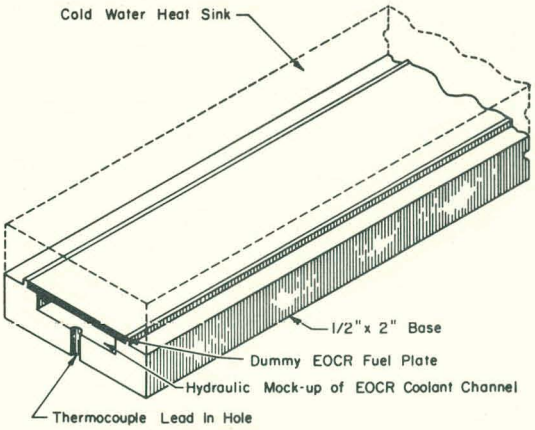

Fig. 15 CDTL test section for calibrating EOCR fuel plate thermocouples.

The pump is designed to handle fluids at temperatures up to 1000°F and has only one moving part, a rotor-impeller assembly which is driven by

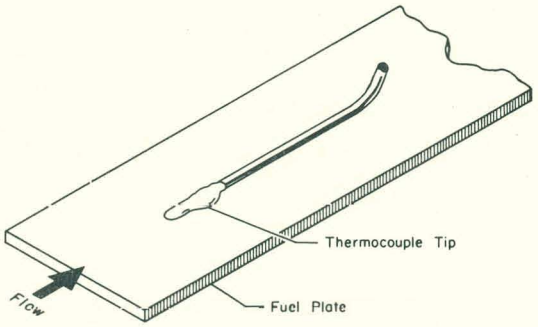

Fig. 16 EOCR fuel plate thermocouple orientation.

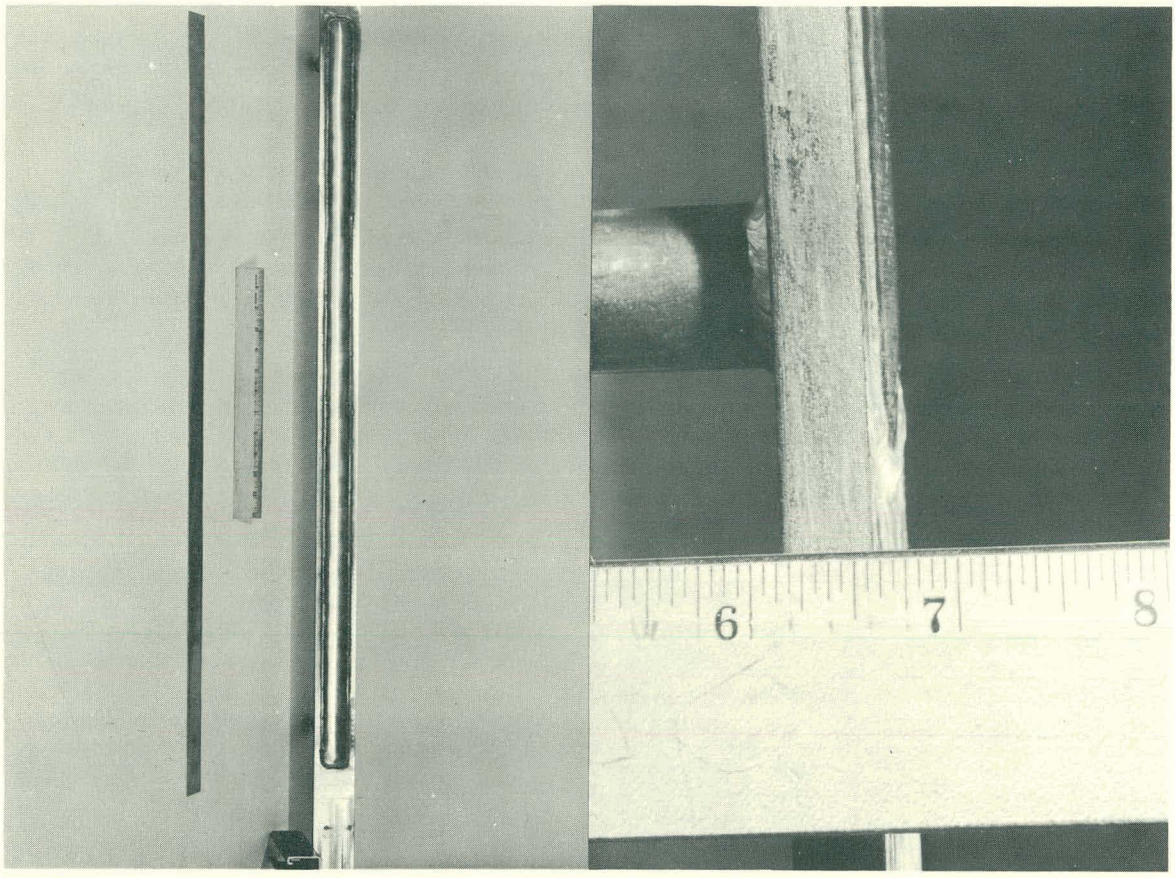

Fig. 17 EOCR fuel plate thermocouple test sections for insertion in the CDTL.

an induction motor. Bearing lubrication and motor winding cooling are provided by recirculation of a small portion of the pumped fluid through the rotor chamber. This recirculated fluid, isolated from the stator and rotor windings by non-magnetic liners (cans), is kept at the proper temperature for cooling by a thermal barrier between the pump casing and the rotor chamber which essentially eliminates heating by the process stream, and by recirculation of the fluid in the rotor chamber through an integral exchanger by an auxiliary impeller on the rotor shaft.

Initial operation and testing (about 18 hr), with a eutectic mixture of biphenyl and terphenyl, showed that the pump was not operating satisfactorily or as intended by its design. Test data showed a high mass transfer of the hot (up to 500°F) pumped fluid from the pump discharge, through the rotor chamber, and back to the pump suction. The high flow of hot pumped fluid through the rotor chamber requires excessive auxiliary cooling to maintain the Class H motor insulation temperature below 360°F and, consequently, results in excessive heat removal from the main process stream. Test data showed that 5.5 kw was removed from the process stream (550°F eutectic mixture of biphenyl and terphenyl) when maintaining the motor winding temperature at a safe level. Figure 19 compares the flow pattern intended by pump design with that experienced during initial testing.

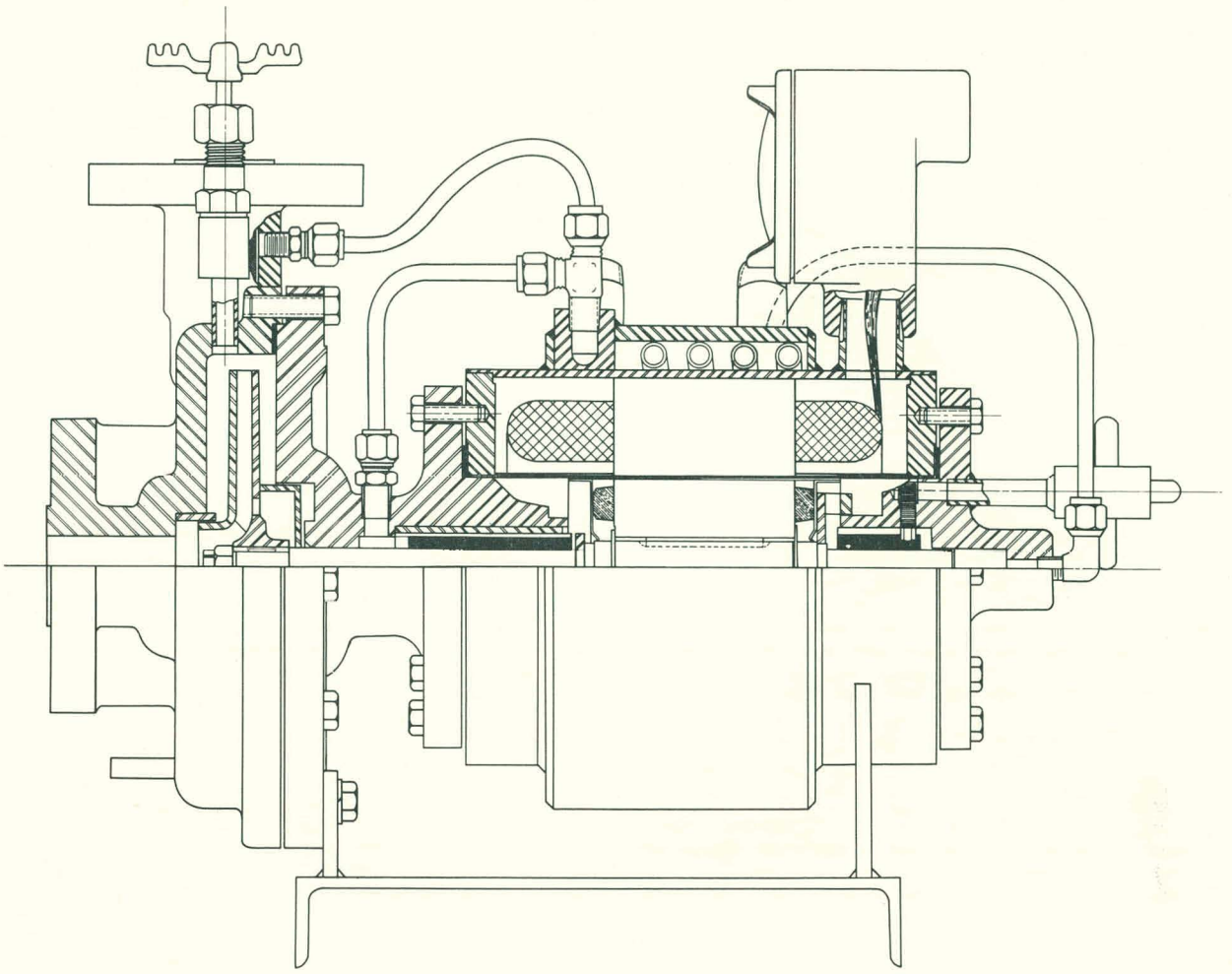

Fig. 18 Chempump cross section.

The excessive flow of hot fluid to the rotor chamber results from the high pressure transmitted from the pump discharge via the pressurizing line, causing a high flow along the shaft back to the impeller suction. The need for this pressurizing line is questionable when using the pump at suction pressures well above the vapor pressure of the pumped fluid. A brief test was conducted to investigate this. The pressurizing line was isolated from the pump discharge by a valve, and the pump was satisfactorily operated for 6-1/2 hr with 500°F Santowax under 150-psig nitrogen pressure. Proper lubricating and cooling flow was maintained. Buildup of vapor or non-condensables in the pump rotor chamber was not evident. Additional operating time should be logged to determine the performance and reliability of the pump operating in this manner.

After being advised of the initial operating experience, the manufacturer recommended modifications (reduction of pressurizing pressure and less clearance along the impeller shaft) to reduce the flow of the hot pumped fluid through the rotor chamber. The necessary parts have been returned to the manufacturer for modifications. Testing of the pump will continue after receipt of the modified parts.

Figure 20 is a photograph of the disassembled Chempump after 25 hr of operation. Some wear, most likely due to thrust, was apparent on the impeller and adaptor faces. Figure 21 is an enlarged composite photograph showing this wear.

1.24 Experimental Program - Ball Valve Test. Tests are being conducted to determine the suitability of ball-type block valves for high temperature (up to 750°F) Santowax service. Table XXXV presents the valve specifications, and Figure 22 is a photograph of the disassembled valve.

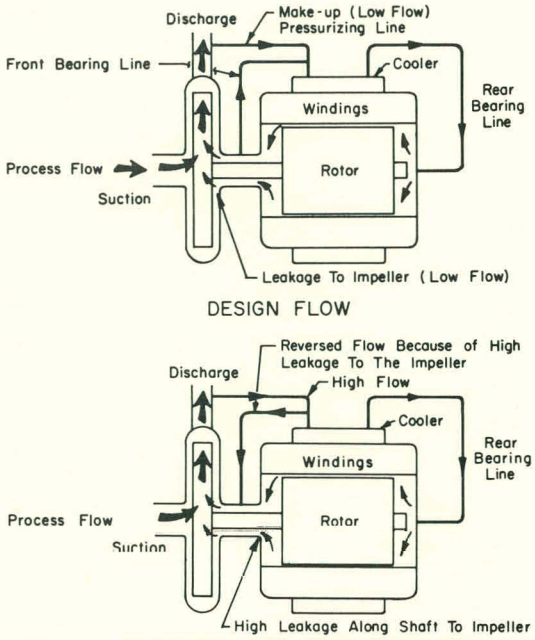

Fig. 19 Chempump flow patterns.

Prior to installation of the test valve in the CDTL, the leakage was measured across the closed valve and found to be unacceptable. Inspection of the valve showed small areas where the ball was not seating on the Graphitar seats. The seats were lapped to correct this condition. Table XXXVI presents the results of the leakage measurements across the closed valve before and after correcting the seating condition. These tests were made with water at room temperature and a pressure differential of 150 psig across the closed valve.

During 17 days of operation in the CDTL with a eutectic mixture of biphenyl and terphenyl, no stem leakage was observed. The valve had operated approximately 40 hr at temperatures of 300 to 600°F and at pressures of 50 to

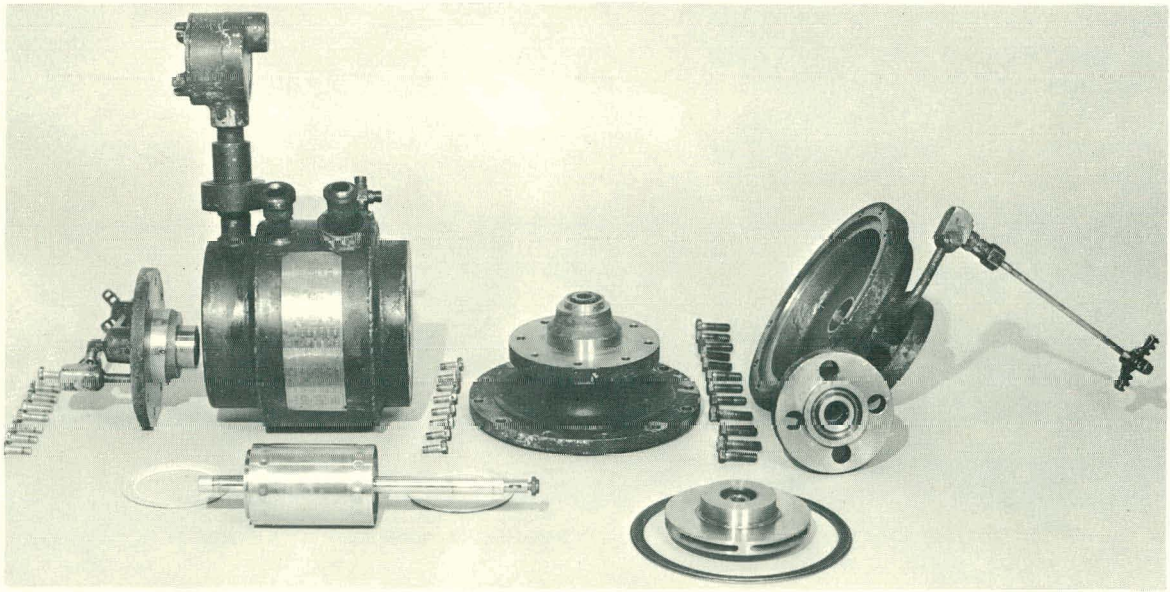

Fig. 20 Disassembled Chempump.

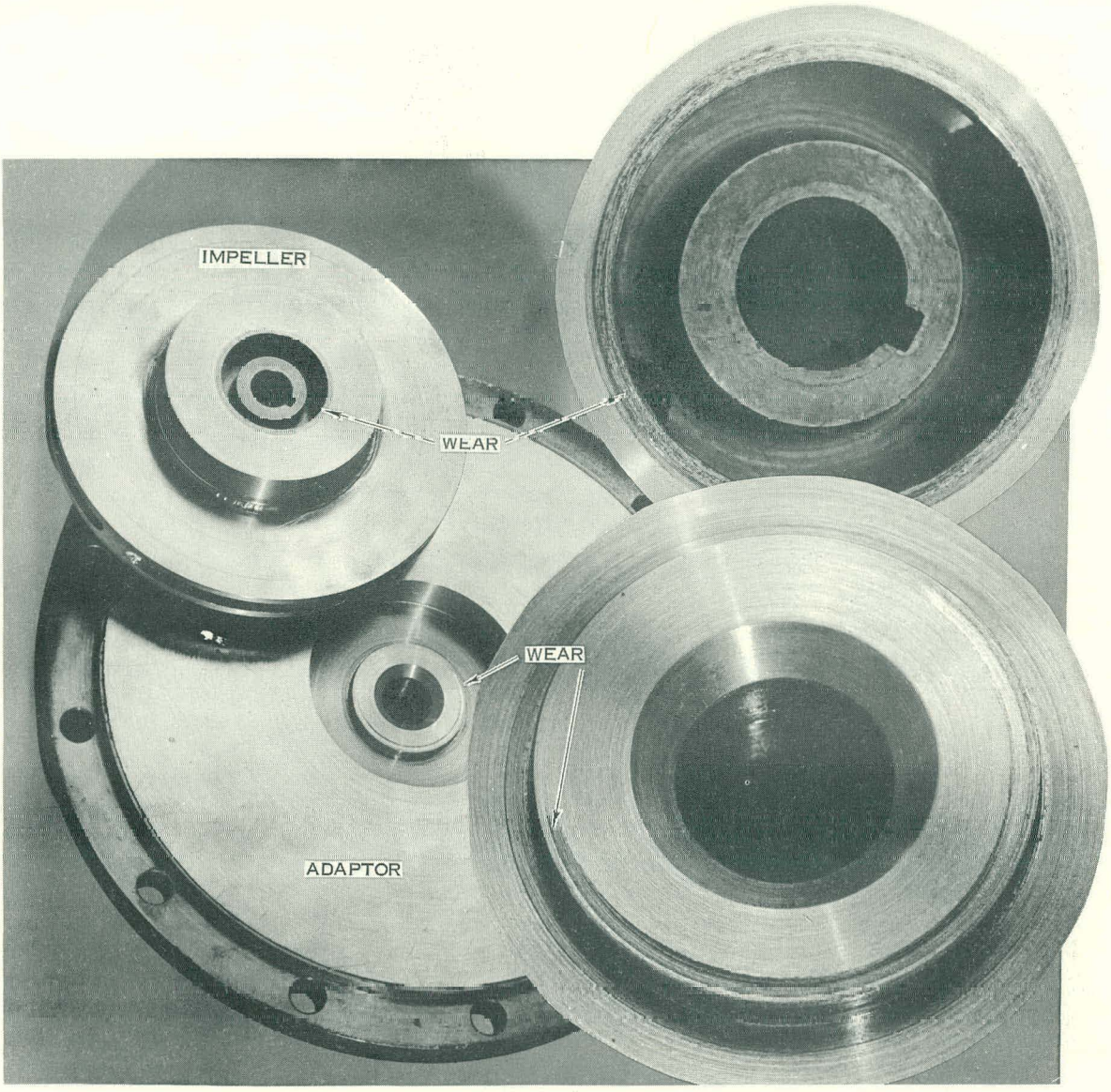

Fig. 21 Chempump adaptor and impeller.

TABLE XXXV

BALL VALVE SPECIFICATIONS

Manufacturer	Hills-McCanna Co.
Type	Ball valve with wedge seat design
Size	One in.
Pressure rating	300 psi
End connections	Flanged - 300-lb raised face
Body	316 stainless steel
Seat material	Graphitar

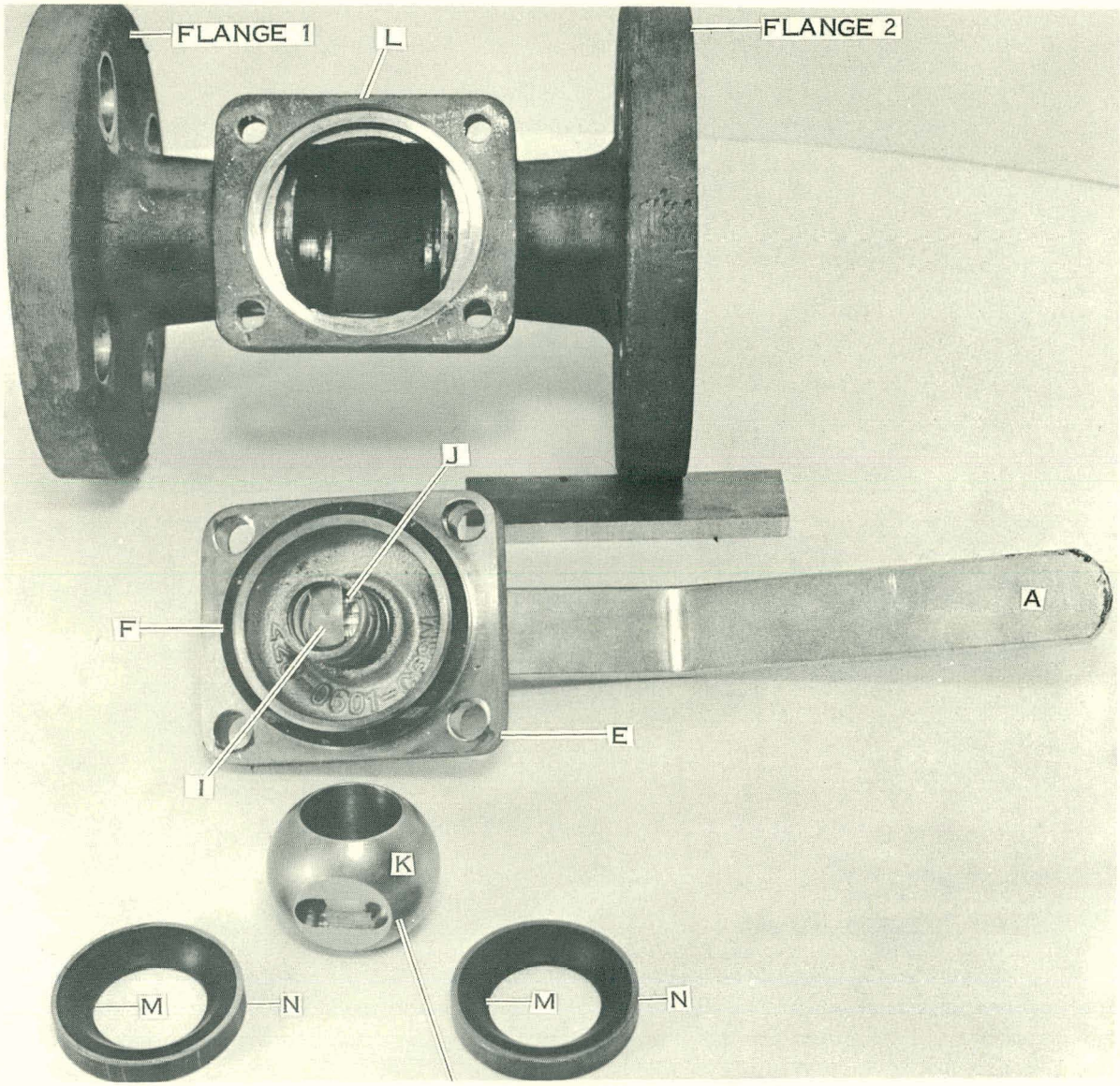

FINISH BETWEEN 16 AND 32 MICROINCHES

HILLS-MCCANNA CO. MCCANNASEAL BALL VALVE WITH WEDGE SEAT CONSTRUCTION

A. HANDLE

B. HANDLE RETAINER NUT (NOT VISIBLE)

C. TRAVEL STOP (NOT VISIBLE)

D. CAPSCREWS (NOT SHOWN)

E. BONNET

F. BONNET GASKET

G. STEM SEALS (NOT VISIBLE)

H. GLAND RING (NOT VISIBLE)

I. STEM

J. NON-FLEXING, NON-TORSIONAL SPRING

K. BALL

L. BODY

M. SEATS

N. SEAT RING

Fig. 22 Disassembled ball valve.

TABLE XXXVI

CLOSED VALVE LEAKAGE TEST

Pressure Side	As Received from Manufacturer	After Lapping Seats
Flange 1	48 cc/hr	none
Flange 2	108 cc/hr	~ 10 drops/hr

150 psig, and was cycled six times from cold to hot operating conditions. However, after CDTL shutdown to atmospheric pressure and room temperature, a few drops of leakage were observed around the valve stem.

Testing of the valve is continuing. After further operation, it will be removed and tested for closed valve leakage across the ball and its seats.

2. EXPERIMENTS

2.1 EOCR Control Rod Latch Reliability Test (S.Cohen, E Burroughs, D. G. Kuper, E. R. Oetken)

Complete details of this test have been published in previous reports [22,23]. The final Vard design latch mechanism and hook for the EOCR control rod drive assembly has been successfully and reliably operated in a hot organic medium containing particulates 100 times the anticipated concentration in the EOCR and with a simulated heavy polymer deposition in all primary latch parts.

2.2 Fuel Technology Loop Nuclear Mockup (D. R. Conkling, R. G. Young)

A conceptual design of the FTL nuclear mockup was completed during this quarter. Its purpose is to provide a dummy section in the L-1 position of the EOCR whenever the FTL in-pile tube is not in position. This nuclear mockup will duplicate the nuclear characteristics of the FTL in-pile tube containing a fuel-follower sample for the A-3 core loading. The mockup is designed to use reactor coolant and will not penetrate the bottom head. It can be used during both low power and high power reactor operation.

The design of the in-core tube and in-core filler blocks of the mockup is essentially a duplication of the FTL in-pile tube, modified to use reactor coolant rather than isolated external coolant. The fueled section is a modified EOCR fuel-follower, orificed to provide proper coolant flow. An extension tube extends from above the core to the top spider and attaches to a standard hold-down mechanism. The bottom of the assembly rests on the reactor grid plate so that all thermal expansion will be upward.

2.3 Fuel Technology Loop Samples for EOCR Approach to Power (D. R. Conkling, R. G. Young)

Detailed design of the approach-to-power samples is nearing completion. All mechanical design has been completed. Work is continuing on the design of the attachment and leadout of sample instrumentation.

Figure 23 shows the core portion of the sample with its proposed instrumentation and leadout. The coolant flow enters the sample inlet extension below the reactor core, flows up through the fueled section, and returns down the passage around the fueled section. The sample is instrumented with a total of 14 thermocouples; there are 8 fuel plate surface thermocouples, 4 plate channel thermocouples, and 2 bulk coolant thermocouples. Two static-pressure probes for measuring sample differential pressure are also provided. The figure also shows the inlet extension, lower transition, fuel plate, fuel box, upper spider, and instrument lead tube.

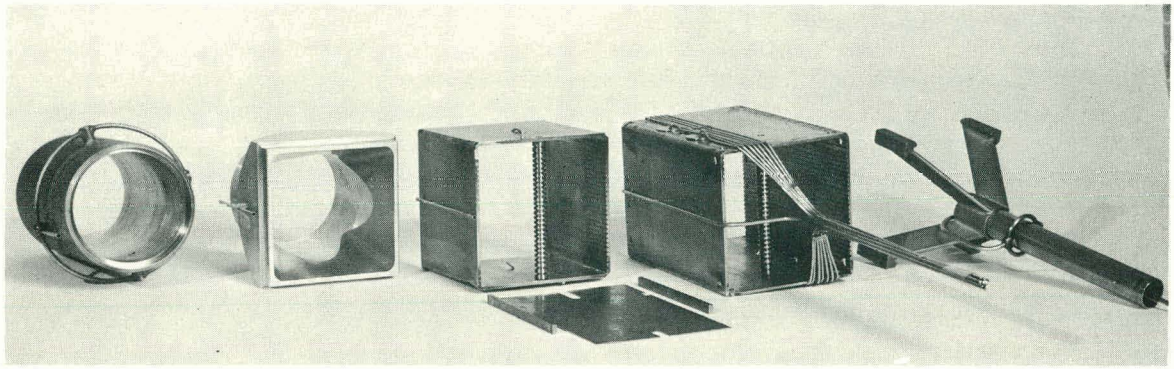

Fig. 23 EOCR approach-to-power sample.

Two methods, brazing and spot welding, are being investigated for attaching the thermocouple junctions to the plates.

2.4 EOCR Fuel Element Instrumentation (D. R. Conkling, R. G. Young)

The proposed instrumentation for EOCR fuel elements is similiar to that previously described for the FTL sample. The eight driver elements being instrumented are D-4, D-6, D-9, D-10, D-11, D-12, D-16, and P-12. These elements were chosen on the basis of coolant flow, flux distribution, core symmetry, and rod programing. Each of these elements has six thermocouples, except D-11 and P-12 which have eight.

Each driver element consists of two rectangular fuel boxes, 3 x 4 in., separated by a gap of 1/2 in. Due to space restrictions, the thermocouple leads are routed in the 1/2-in. gap between the fuel boxes, into the center extension tube, through the upper extension tube, and into the instrumentation channels on the upper surface on the webs of Spider 1. These channels lead over to the instrumentation junction boxes located near the outer periphery of the spider. The junction boxes contain a nitrogen atmosphere and terminate through the side nozzles of the reactor vessel. This concept of instrumentation leadout requires further study.

It is currently planned to terminate the sheathed thermocouples inside the junction boxes. This requires that each instrumented driver element have an appendage of thermocouple lead wires approximately 5 ft long. This undoubtedly will require preforming of the lead wires and preparation of end connections prior to the insertion of the fuel element. This method will require considerable care during handling and insertion of the instrumented elements.

2.5 Fuel Element Wash System Development (E Burroughs, S. Cohen)

The first presentation of this project and initial development work was presented in a previous quarterly report [24].

The scoping laboratory tests with ethylene glycol indicated the glycol would displace the wax from metal surfaces quite effectively. A bench test ethylene glycol fuel element wash loop was designed and built. The loop flow diagram is shown in Figure 24. Figure 25 is a photograph of the complete loop.

Basically, the procedure for operation of the loop is as follows. The fuel element test cell (with test element installed) and the entire loop system are heated to 320°F by circulating hot ethylene glycol. When the system is at temperature, the fuel element wash cell is drained of glycol. The organic in

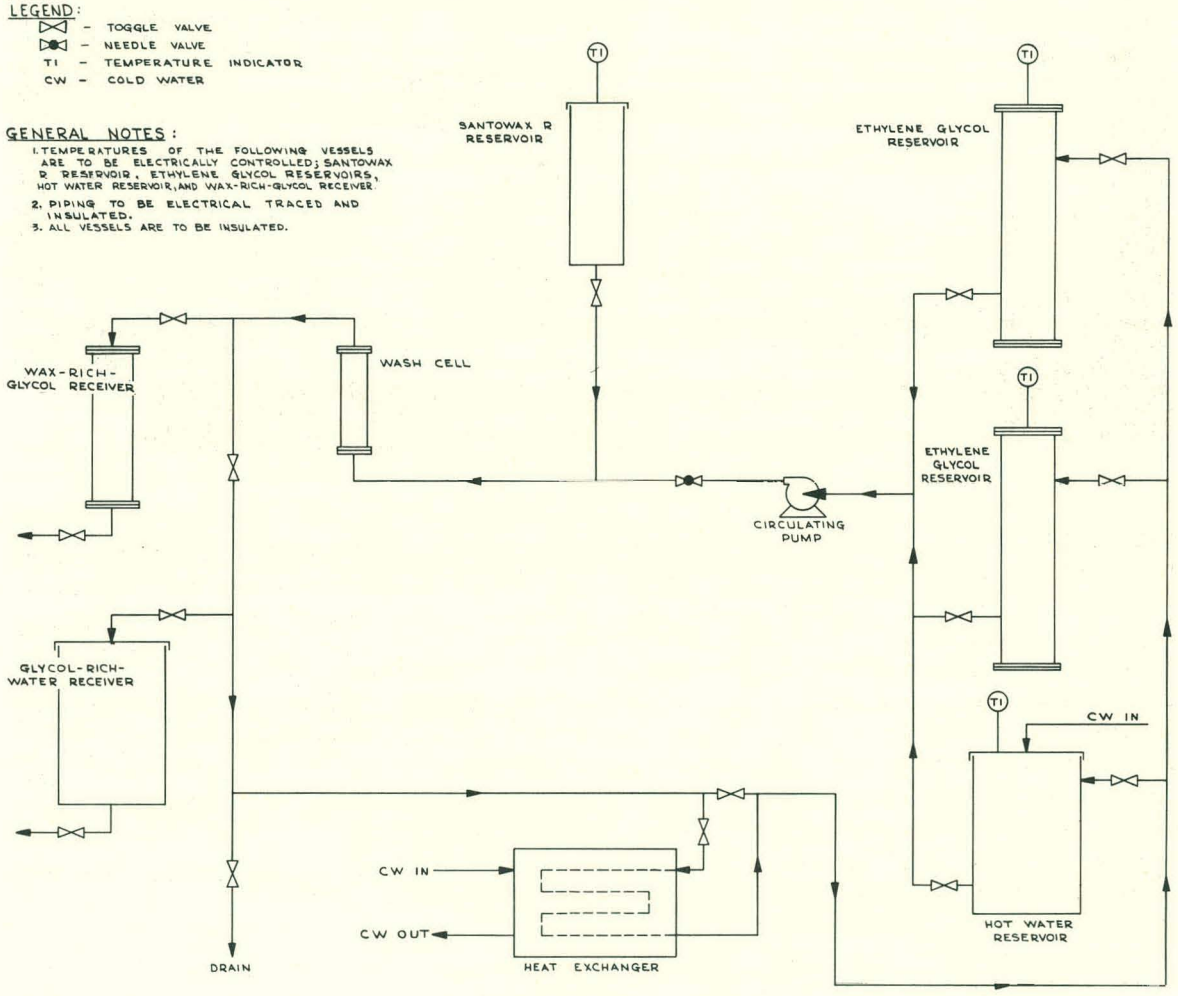

Fig. 24 Loop flow diagram.

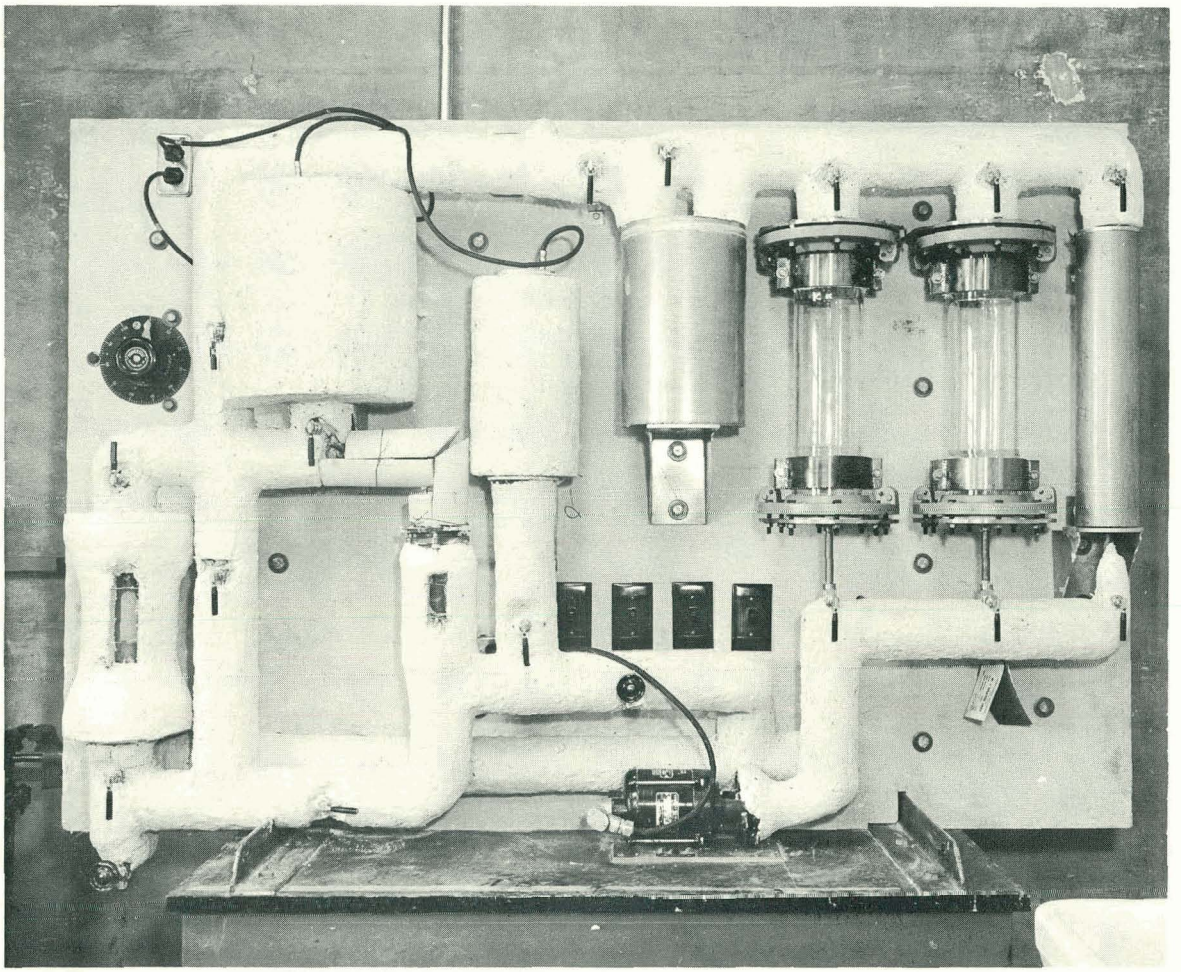

Fig. 25 Fuel element wash system loop.

the terphenyl reservoir is heated to 320°F and allowed to flow by gravity and fill the test wash cell. The pump is started and ethylene glycol from one reservoir displaces the wax into the wax-rich glycol receiver. The remaining glycol is circulated (temperature maintained at 320°F) for a period of time to displace and dissolve any residual wax. The first glycol reservoir is shut in and the glycol in the second reservoir circulated at 320°F. After circulation of the glycol, the heat exchanger is utilized and the temperature of the glycol reduced to 160°F. At that time, the reservoir is shut in. Water, which has been heated to 160°F, is used to wash the glycol from the fuel element wash cell into the glycol-rich water receiver. After washing with the 160°F water, the temperature of the wash water is lowered to room temperature. The test fuel element is removed and inspected for residual wax.

As terphenyl is noted for freezing and plugging lines, the initial runs were made using HB 40 which is a hydrogenated terphenyl mixture, liquid at room temperature, and similar to terphenyl in physical characteristics. These initial tests were successful.

At the time of this report, two runs had been completed using terphenyl (Santowax OMP). With the exception of mechanical difficulties with loop equipment, the loop operated as expected.

After the first run, the fuel element test section was removed. Visual inspection indicated complete removal of the wax, with the exception of one small spot located in a stagnant flow area downstream of a spacer. The spacer was modified to eliminate the stagnant flow area around the fuel test element. When the test element was removed after the second run, visual inspection showed the wax removal was complete. There was no "waxy" feel to the surface of the test element, and all channels between the simulated fuel plates were completely clear.

More testing is scheduled but, based on the above tests, the ethylene glycol process for cleaning the EOCR fuel elements would be satisfactory. Although promising as a fluid to clean fuel elements, by displacement of wax, it does not appear that glycol would be very suitable for washing the reactor head and auxiliary equipment in the dry dock. Since the reactor head and auxiliary equipment will be at room temperature, it is suggested that certain solvents of the trichloroethane group be used instead of the very flammable xylene.

When the fuel element wash process demonstration runs are completed, laboratory fractionation data for terphenyl-glycol and glycol-water systems will be determined. This information is necessary for engineering studies of organic and solvent (displacement fluid) cleanup systems as related to the EOCR. Preliminary studies indicate that conversion of the present coolant and solvent (xylene) cleanup system to a melt displacement liquid such as ethylene glycol would not involve any major modifications or high investment.

2.6 EOCR Chemical Cleaning (E Burroughs, S. Cohen)

The EOCR reactor vessel, piping, and all auxiliary equipment will be chemically cleaned before the organic is charged to the system. The organic power reactor at Piqua, Ohio, was chemically cleaned. The system was inspected after cleaning and heavy rust deposits were found. (Subsequent chemical cleaning of the Piqua reactor has been acceptable). It was decided to bench test the proposed EOCR chemical cleaning method.

A loop was designed and fabricated so that carbon steel (SA 106B) coupons and pipe used in the EOCR could be chemically cleaned and passivated, then visually inspected. The flow diagram of the chemical cleaning test loop is shown in Figure 26.

At this point, the responsibility of the chemical cleaning loop operation, the chemical cleaning tests and evaluation of results was transferred to the Plant Engineering Branch. The two basic procedures tested were as recommended by Dow Industrial Services and the Charles Pfizer Co.

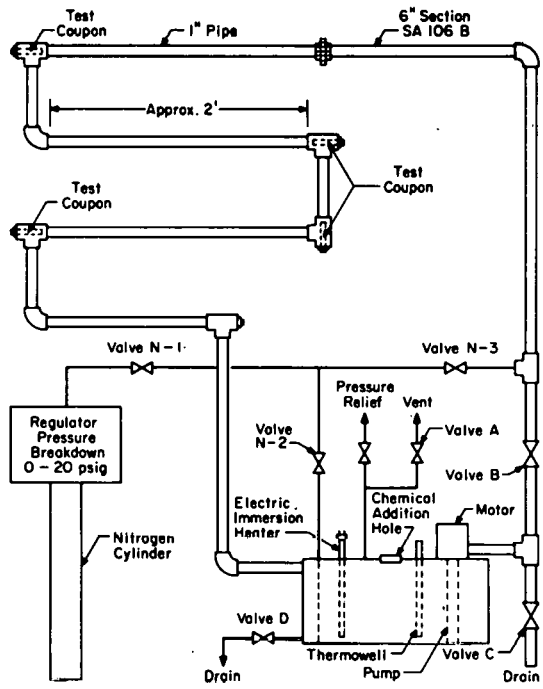

Fig. 26 Chemical cleaning test loop.

The Dow procedure consisted of (a) alkaline degreasing using caustic, sodium metasilicate and detergent solution followed by a water flush, (b) acid derusting using Dow Deruster followed by a dilute citric acid flush, (c) surface passivation using ammonium citrate, and (d) air drying using 300 to 400°F air.

The Pfizer procedure consisted of (a) alkaline degreasing using caustic, tri-sodium phosphate, gluconate ion and detergent solution followed by a water flush, (b) derusting using citric acid followed by ammoniation, (c) surface passivation using sodium nitrate, and (d) air drying using 300 to 400°F air.

The tests indicate the procedure, slightly modified, as recommended by Pfizer (used in cleaning the Piqua reactor) is better than the Dow method with respect to mill scale and rust removal.

The surface of carbon steel pipe after being chemically cleaned has a lightly adhering passivation film which is removed by the circulation of hot organic. Since the passivation film is removed as particulate matter in the hot organic, it is possible that the fouling potential of the organic will increase. Therefore, samples of fresh Santowax OMP, Santowax OMP with pipe passivation film particulates, and Santowax OMP with non-chemically cleaned pipe particulates were sent to the Bartlesville laboratory for fouling tendency tests. These tests will indicate if an appreciable difference in fouling tendency exists. Results are not available for this report. It also should be pointed out that visual inspection of pipe surfaces of chemically cleaned and non-chemically cleaned pipe after exposure to circulating hot organic indicated very little difference in surface appearance.

Whether the Bartlesville tests do or do not show any difference in fouling rates, the fact remains that passivation film particulates will appear in the hot organic charge to the reactor. This means the system organic will have to be completely processed after the initial circulation of the hot organic. Present plans are to run the organic through the purification system before charging the organic to the reactor system. However, due to immediate pickup of the passivation film particulates in the circulating organic, it might be advisable to charge the organic as received directly to the reactor system, circulate it hot, then purify the system organic before further reactor tests are conducted.

2.7 Radiolytic Damage Mechanism Studies (D. G. Kuper, S. Cohen)

2.71 Introduction. It has been generally postulated that radiolysis of polyphenyl coolant results in the formation of free radicals. Such free radicals have been suggested as precursors or causative agents for film formation on reactor fuel plates. Experimental evidence of the type or quantities of free radicals produced is lacking. Identification of the free radicals should prove valuable in elucidating reaction mechanism and in lending information as to possible film-forming agents. Work was started this quarter to identify free radicals generated by gamma irradiation of biphenyl.

2.72 Free Radical Identification. Several publications have described the high efficiency of iodine as a free radical scavenger when employed in aliphatic hydrocarbon systems. To be effective, the iodine must be used in quantities not greater than about 3×10^{-3} M and at temperatures below about 80°C. With these conditions, thermalized free radicals are effectively captured by the iodine. Side reactions due to heat or interreactions of the free radicals

are insignificant due to the low temperature and initially minute concentrations of free radicals.

Use of iodine to identify free radicals in irradiated biphenyl seems justifiable since the biphenyl is liquid at temperatures above 69°C and acts as a good solvent for iodine. The technique involves irradiation in the presence and absence of iodine. Subsequently, product yields and iodine uptake are measured and compared. Identification of specific organic iodides is taken as evidence that the organic portion existed as a free radical. With this technique it must be realized that benzene might function as a partial scavenger so that iodine results may represent less than quantitative values.

An initial irradiation was made using biphenyl and biphenyl with iodine added in the amount of 2.6×10^{-3} mol%. The samples, approximately 12 gm in size, were drawn into evacuated stainless steel tubes closed at either end with a stainless steel hoke valve. The capsules were subsequently purged with helium. One sample each of biphenyl and "biphenyl + I_2" were dropped into a 3-in. dry tube at the MTR gamma facility. A third capsule containing "biphenyl + I_2" was placed in a constant-temperature oven held at 160°F, the ambient temperature within the 3-in. dry tube, to measure any thermolytic effects. Subsequent to the irradiation the resultant gas and solid phases were analyzed by mass spectrography and gas chromatography respectively. The results show air had leaked into the capsules which precludes applying quantitative results to iodine uptake or gas generation.

Table XXXVII lists the results as obtained from the mass spectrometer. Table XXXVIII was derived by subtracting out the component contribution of air using N_2 as a base. The results show that about 50% less hydrogen uptake was obtained with iodine additive while approximatey 50% less CO_2 was generated. These preliminary data suggest, but do not confirm, that as much as 50% of the hydrogen exists for a finite time as thermal diffusion hydrogen atoms and that oxidation proceeds via a free radial mechanism.

Chromatographic analyses of the solid phases showed a barely perceptible amount of quaterphenyl in each of the irradiated samples, with none being detected in the non-irradiated sample.

TABLE XXXVII

COMPOSITION, INCLUDING AIR, OF GASES FROM IRRADIATED SAMPLES

Conditions: Time, 90 hr; initial dose rate and ambient temperature = 6.5×10^6 r/hr ≈ 170°F; final dose rate and ambient temperature = 4.87×10^6 r/hr ≈ 158°F; total dose = 5.25×10^8 r.

Sample	Component Including Air (mol%)							
	H_2	He	N_2	O_2	CO_2	A	Benzene	Toluene
Biphenyl	0.7	0.25	86.8	5.9	3.2	1.15	0.02	trace
Biphenyl + I_2	1.4	0.33	91.6	3.8	1.5	1.26	0.01	0.05

TABLE XXXVIII

COMPOSITION, MINUS AIR, OF GASES FROM IRRADIATED SAMPLES

Conditions: Time, 90 hr; initial dose rate and ambient temperature = 6.5×10^6 r/hr ≈ 170°F; final dose rate and ambient temperature = 4.87×10^6 r/hr ≈ 158°F; total dose = 5.25×10^8 r.

Sample	Component Minus Air Contribution (mol%)				
	H_2	O_2	CO_2	Benzene	Toluene
Biphenyl	2.7	-17.4	3.2	0.02	trace
Biphenyl + I_2	1.4	-20.8	1.5	0.01	0.05
Ratio biphenyl + I_2/biphenyl	0.52	1.12	0.48	—	—

The work shows that a greater dose will be necessary to assign significant figures to experimental results.

2.8 Organic Coolant Pyrolysis Studies (D. G. Kuper, S. Cohen)

2.81 Introduction. Several workers have previously described the pyrolytic stability of biphenyl and terphenyl isomers. The data reported have arisen for the most part from use of various Santowax samples or individual isomers contained in evacuated capsules. The results have not been in good agreement so that a question is left as to the actual stability or reasons for the disparities. Thus, it does not seem unnecessarily repetitious to study the pyrolysis of terphenyl coolant in some detail to include the effect of variable proportions of isomers and the presence of various impurities. On this basis, a study of the pyrolytic stability of terphenyls is being made. The work is expected to provide:

(1) Isomer and coolant stability data with precision limits determined,

(2) Optimization of terphenyl isomer ratios for maximum stability consistent with ease of operational handling,

(3) Provide an accurate base line for distinguishing pyrolytic from radiolytic effects,

(4) Show quantitative effects of various additives; ie, oxygen and H_2O.

2.82 Pyrolytic Equipment. Capsules designed to withstand high pressures at high temperatures (1000 psig/1000°F) are being used. The capsules consist of a high temperature coupling, manufactured by Gamah Corp, Santa Monica, Calif, which is welded to a capped 6- to 7-in. length of 1-1/2 in. schedule-40 stainless steel pipe. The coupling is sealed with a metal O-ring which is deformed against beveled edges when the cap is tightened. Gas and liquid sampling ports have been included to permit intermittent sampling. Thus, the capsule can be used as a reactor from which samples can be withdrawn or as an autoclave for heating smaller capsules. The heating is provided with a tubular heating

element wrapped around the case of the capsule and imbedded in Thermon to provide good heat transfer. The temperature is controlled by a thermocouple probe which extends into the bottom center portion of the capsule. The thermocouple operates a Protect-O-Vane temperature controller. With the system, temperatures are controlled to ± 1.5%. The maximum diameter of the capsule is 3.5 in. Figure 27 depicts the assembled and disassembled capsule.

2.83 Analytical Technique. Analyses of the liquid or solid phases are made using the F&M Model 500 gas chromatograph equipped with a 5-ft 1/4-in. stainless steel column packed with 30% LiCl on 60-80 mesh Chromosorb P. The instrument is temperature programmed to as high as 500°C.

Number average molecular weights are determined with the Mechrolab osmometer. Melting points are obtained using capillary melting point tubes heated in a silicon oil bath.

2.84 Pyrolysis of Terphenyl Isomers. The work thus far has been principally exploratory to test the equipment and "feel out" the type of problems likely to be encountered. The isomers studied were obtained from Monsanto and were used as received with no further purification.

The ortho-, meta-, and para-terphenyl isomers were scanned for their respective stabilities by subjecting each to varying temperatures in the aforementioned capsules under a helium atmosphere. After charging the capsule and removing air by successively evacuating and purging with helium, temperatures were raised at 1-hr intervals. A liquid sample was taken at the conclusion of each heating interval.

Typical chromatographs of the isomer before and after pyrolysis are shown in Figure 28. Plots of the analytical data are given in Figures 29, 30, 31.

The data plotted in Figure 29 indicate that o-terphenyl did not exhibit a rapid degradation until 900 to 950°F. Biphenyl and quaterphenyls were major degradation products. The melting point data plotted in Figure 30 in general indicate the same threshold temperatures as does Figure 29 with one exception. Melting point data indicate o-terphenyl degrades rapidly at a temperature of 800°F.

Molecular weight data were so scattered that a single line was plotted through the mass of points for all of the isomers. Since the osmometer exhibits a high degree of precision, the divergence probably is attributable to non-representative sampling.

A surprising result was obtained in the pyrolysis of p-terphenyl. Upon heating to 900°F for only a few minutes, the sample was turned essentially to coke. A chromatograph of the leached coke is shown in Figure 32. Repeated pyrolysis showed little degradation as is evidenced in Figure 29. The reason for the coking has not been determined.

Meta-terphenyl was pyrolyzed at a constant temperature interval of 785 to 805°F. This temperature was selected as being sufficiently low to avoid the rapid degradation shown in Figure 29 at the higher temperatures. Three samples were pyrolyzed. Two samples were provided with a helium blanket and a third was blanketed with helium plus 5 mol% pure oxygen. Liquid samples

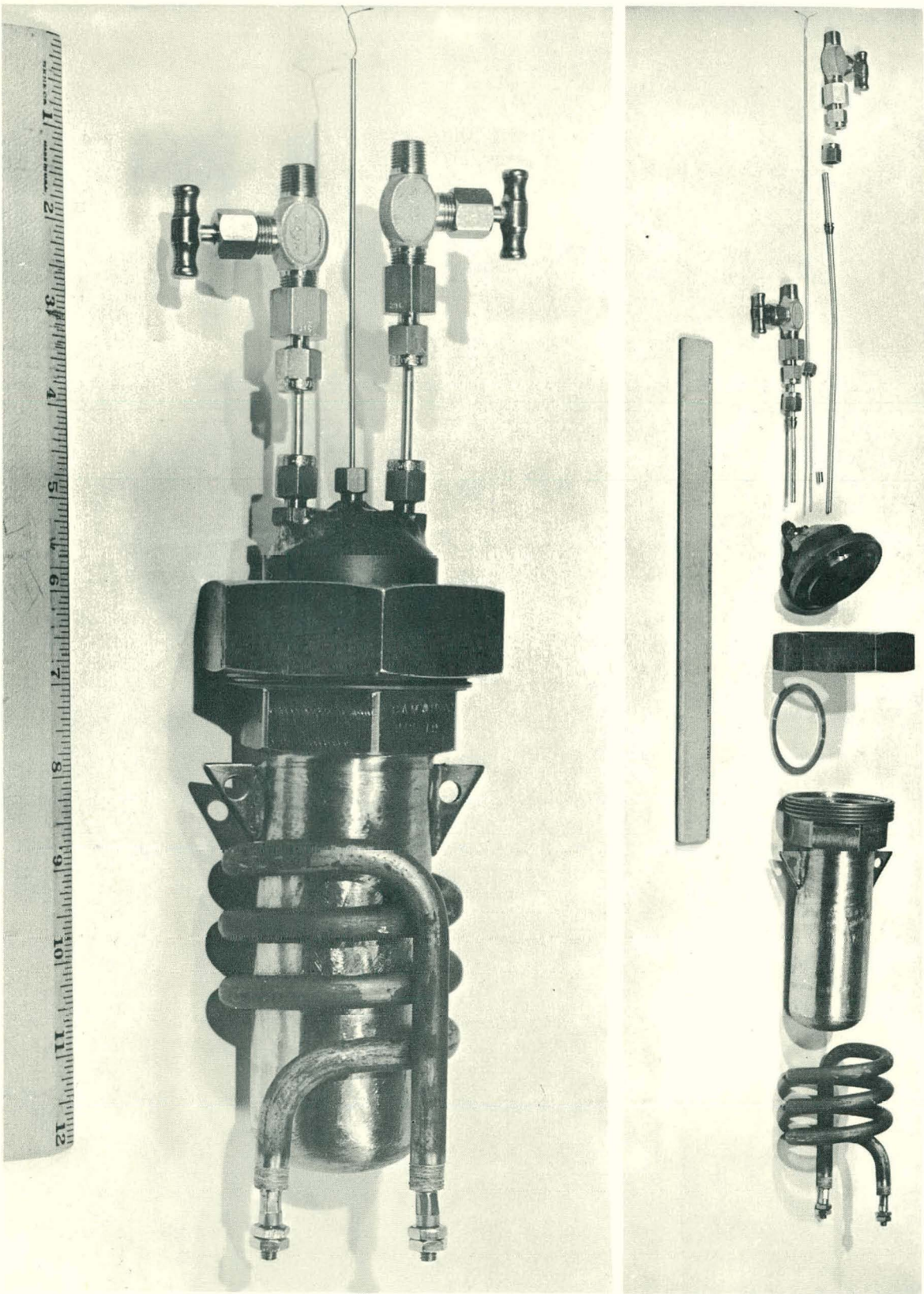

ASSEMBLED CAPSULE

DISASSEMBLED CAPSULE

Fig. 27 Pyrolytic capsule.

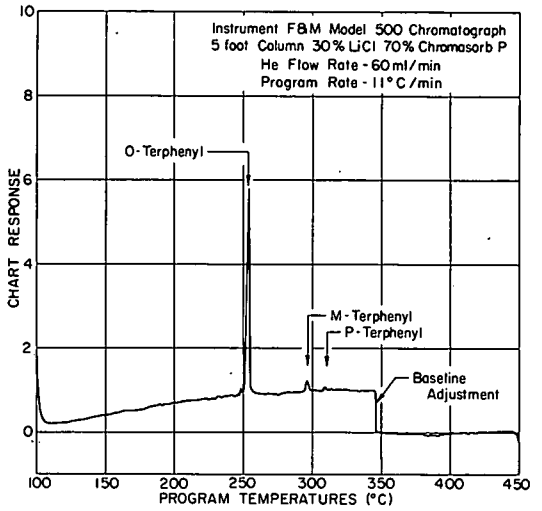

O-TERPHENYL FROM MONSANTO

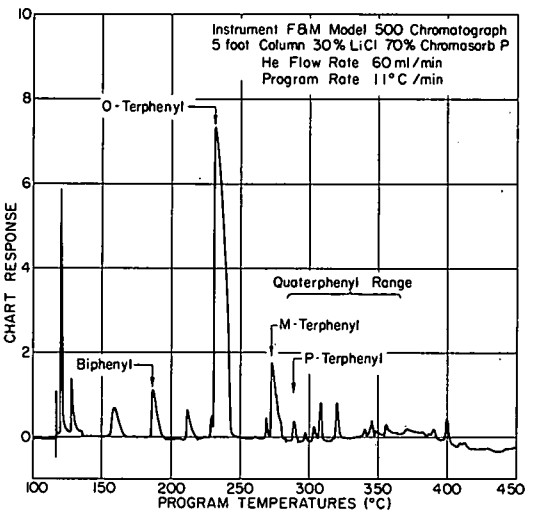

O-TERPHENYL PYROLYZED 50 HR AT 800 °F

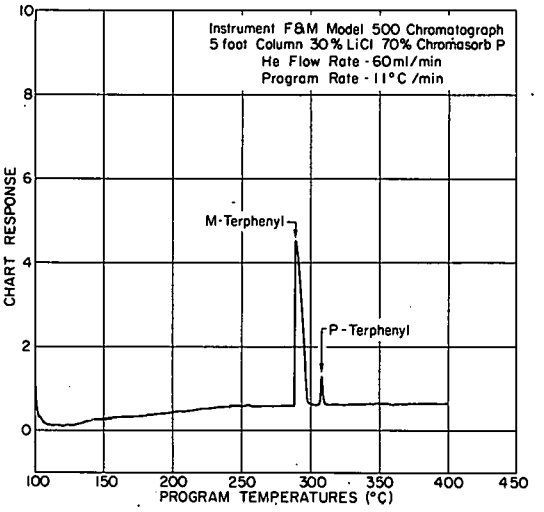

M-TERPHENYL FROM MONSANTO

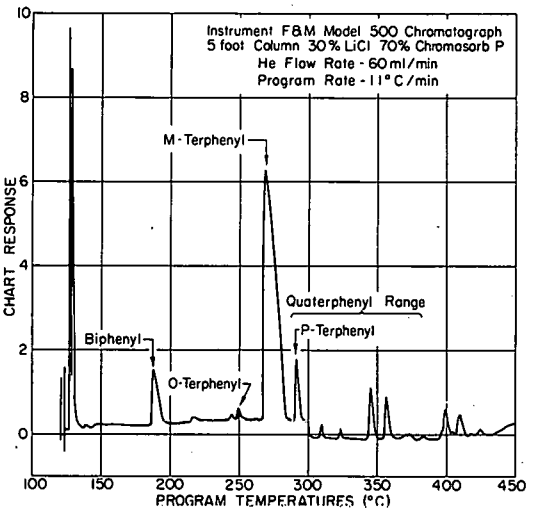

M-TERPHENYL PYROLYZED AT 800 °F

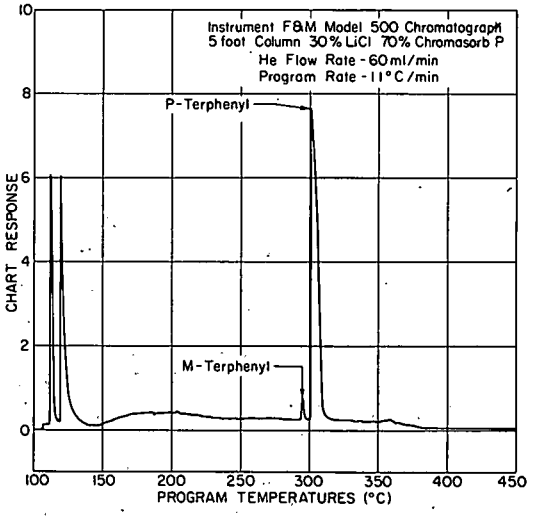

P-TERPHENYL FROM MONSANTO

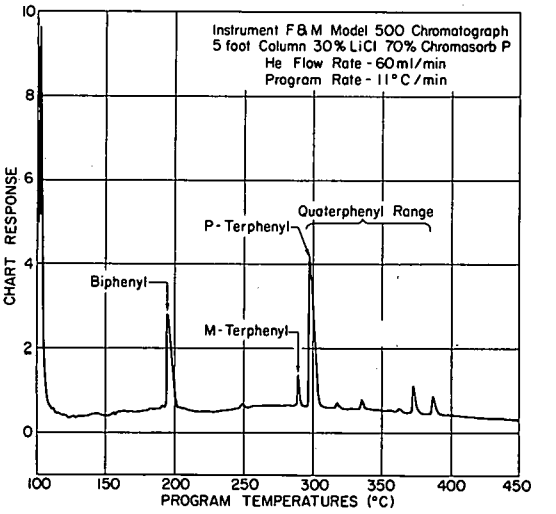

P-TERPHENYL PYROLYZED 1 HR AT 1000 °F

Fig. 28 Typical chromatographs.

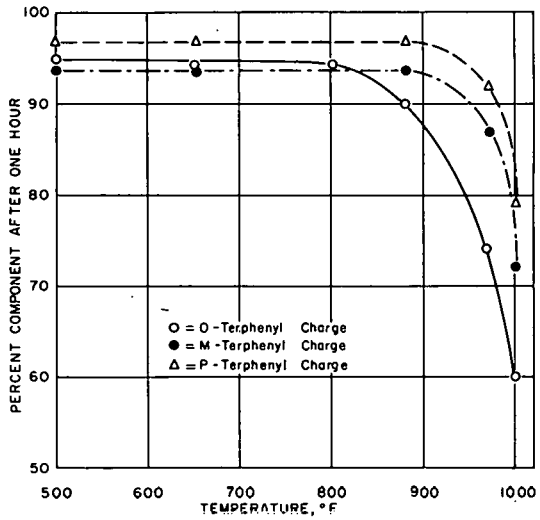

Fig. 29 Pyrolysis of o-, m-, p-terphenyl.

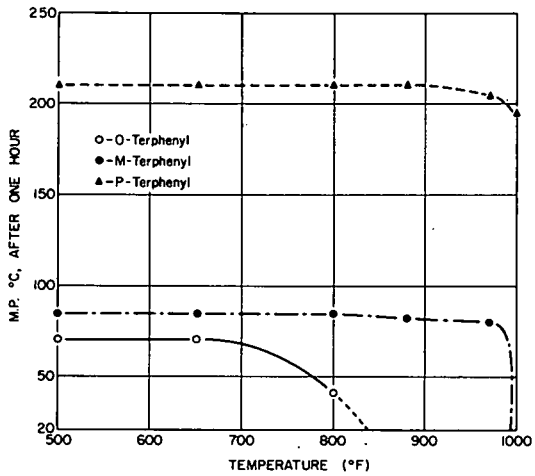

Fig. 30 Melting points of pyrolyzed o-, m-, p-terphenyl.

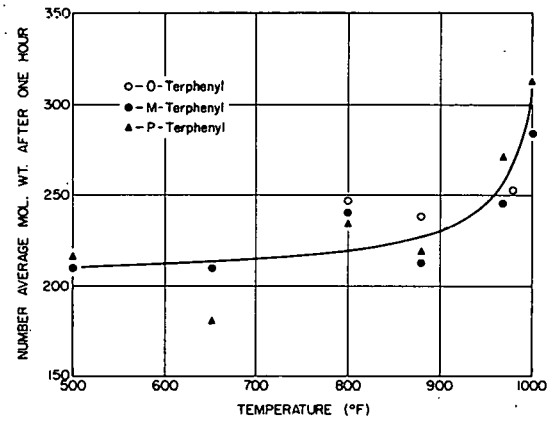

Fig. 31 Number average molecular weights of pyrolyzed o-, m-, p-terphenyl.

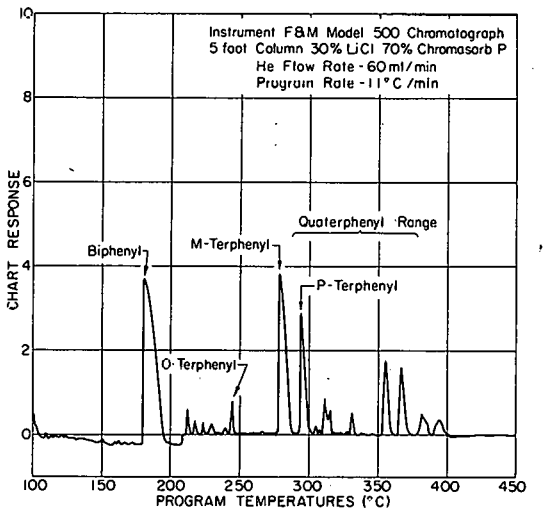

Fig. 32 Benzene leach of carbonized p-terphenyl.

were taken periodically from each capsule during the run and a gas sample was taken at the conclusion of the run.

The sample blanketed with He + O_2 unexpectedly carbonized after about 4 hr. A gas sample was taken and the "coke" was leached with benzene for chromatographic analysis. The chromatograph is shown in Figure 33. Repeated treatments in the presence of even higher amounts of oxygen failed to produce an observable trace of carbonization. As in the case of the p-terphenyl described above, the cause of the coking has not been determined. No carbonization was noted in either of the m-terphenyl samples heated under a helium blanket.

Mass spectrographic analyses of the gases are not yet completed. However, the components identified as present or absent are listed in Table XXXIX.

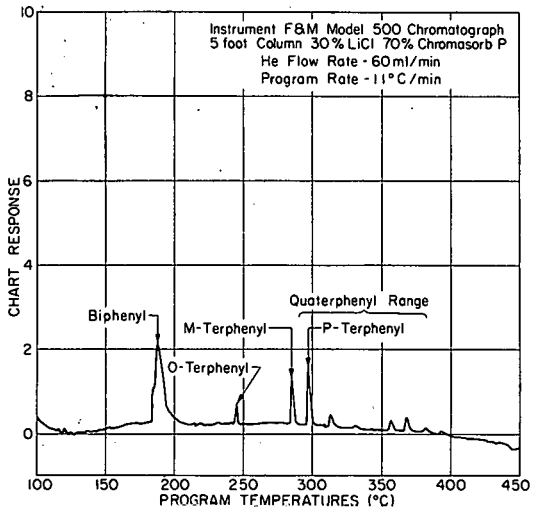

Fig. 33 Benzene leach of carbonized m-terphenyl.

TABLE XXXIX

IDENTIFICATION OF COMPONENTS IN GASES

Component	Helium Blanket	Helium + Oxygen Blanket(a)
Methane	present	present
Ethane	present	present
Propane	present	present
Propylene	present	absent
Benzene	present	present
Toluene	absent	present
Xylene	absent	present

(a) Sample was carbonized.

The presence of alkyl side chains in the coked sample lends suspicion that an acid may have been present to promote alkylation.

The data obtained by pyrolysis of m-terphenyl under a helium blanket are plotted in Figure 34.

The figure shows that duplication was not good. Inspection of Figure 34 suggests that in both cases decomposition rate was not consistent. An apparent time lag of 5 to 10 hr is observed during which little decomposition occurred, followed by a period of rapid decomposition after which the material apparently becomes stabilized. Figure 34 also shows a wide divergence of both melting points and molecular weights. In the first pyrolysis, a sample taken after 23 hr failed to crystallize at room temperature. This material takes on a caramel-like appearance.

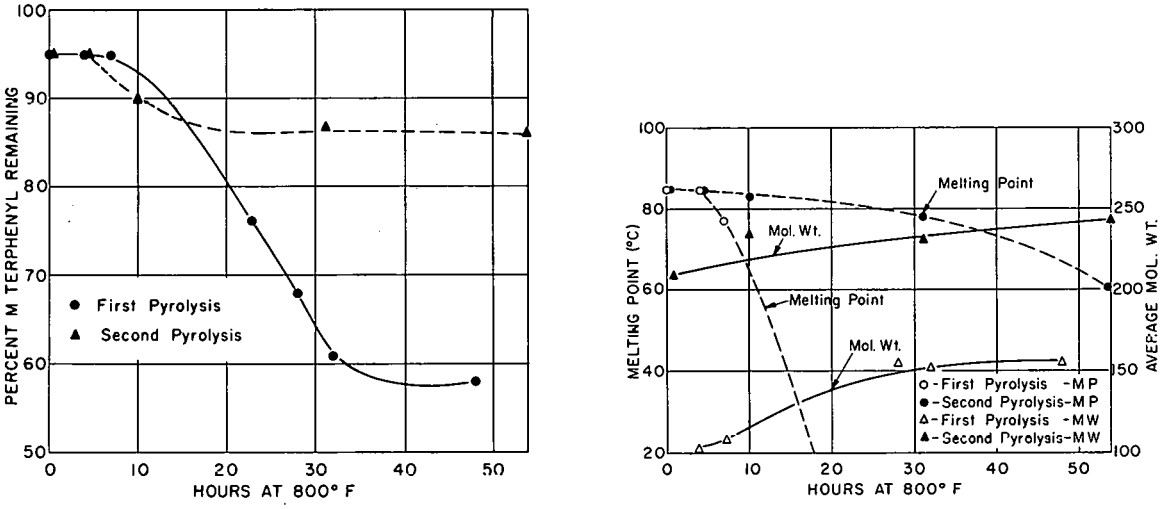

Fig. 34 Pyrolysis of m-terphenyl under helium blanket at 800°F.

The lack of reproducibility shows quite clearly that good control of the environmental conditions was not achieved. Further it demonstrates that the terphenyls can indeed by quite sensitive to their environment so that disagreements among previously reported values are not at all surprising.

Additional work is in progress to improve environmental control and determine what conditions are necessary to provide accurately reproducible data.

2.9 Film Formation Studies - MTR Hydraulic Rabbit Facility (J. R. McGeachin, S. Cohen)

The study of fouling phenomena on heat transfer surfaces, associated with organic coolants exposed to radiation, is presently hampered by the lack of suitable irradiation facilities. The EOCR and associated loops will help fill this need. However, in the interim, much valuable information can be obtained in facilities not specifically designed for organic coolant testing, such as the MTR hydraulic rabbit facility.

The MTR hydraulic rabbit, VH-4, is suitable for this type of irradiation. It is possible to simulate a typical EOCR cycle (100 days) in several hours in this facility. The necessary heat flux on the test surfaces can be obtained, hopefully, with gamma heating of the test specimens.

The purpose of this screening program is to establish which parameters affect the formation of film from organic coolants on heated surfaces under irradiation. Initial irradiations will be made with purified coolants under inert atmospheres at the bulk and surface temperatures produced by the gamma energy absorbed in the test capsule. Subsequent studies of film formation will investigate the effects of adding iron oxides, H_2O, oxygen, and oxygen scavengers to the bulk organic. In addition, film formation on various types of heat transfer surfaces will be studied. The radiation exposure times and rates can be varied by the time in the reactor and the vertical location in the facility. In all experiments, the coolant will be analyzed for decomposition products.

The typical capsule used (Figure 35) will have an outside dimension of 1-1/16 OD x 6 in. long. A cross section of the capsule is shown in Figure 36. A cylinder will be symmetrically located inside the capsule forming an annulus in which organic fluids will be used as a thermal bonding agent. Since the surface of the cylinder will be a higher surface temperature than the containment tube,

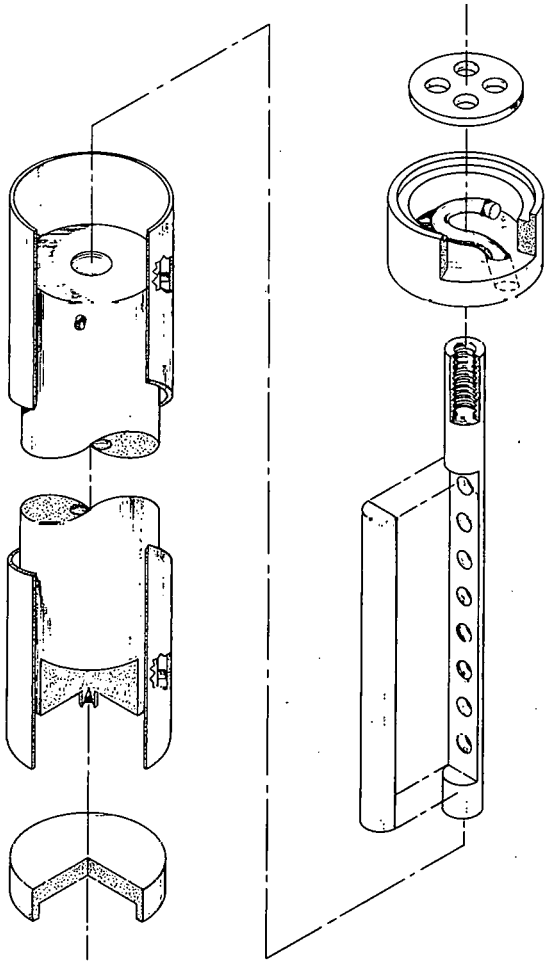

Fig. 35 Film formation rabbit capsule.

natural circulation of the organic fluid will occur. This natural circulation takes the place of the forced convection present in the reactor. Construction of exploratory type capsules has started.

Initial pressure and composition of the gas covering the organic coolant will be carefully controlled. Equipment is being assembled to purge, fill, and seal capsules for reactor use. Hot cell equipment will be used for post-irradiation gas sampling, removal of organic material for analysis, and removal and analysis of film deposits.

Temperature monitoring is accomplished by inserting a number of plugs into holes drilled into the gamma-heated cylinders. The plugs are made of materials having different melting points covering the temperature range of 361 to 800°F. Post-irradiation examination will establish which plugs have melted and which have not. This will determine upper and lower limits of the surface temperature of the cylinder. The limits are within 50 degrees of each other. The plugs, which are made of pure metals and binary eutectics, have been tested and their melting points have been checked. Runs with temperature monitors are necessary to establish that gamma heating is indeed sufficient, and that the capsule annulus is properly designed to give the desired convection circulation.

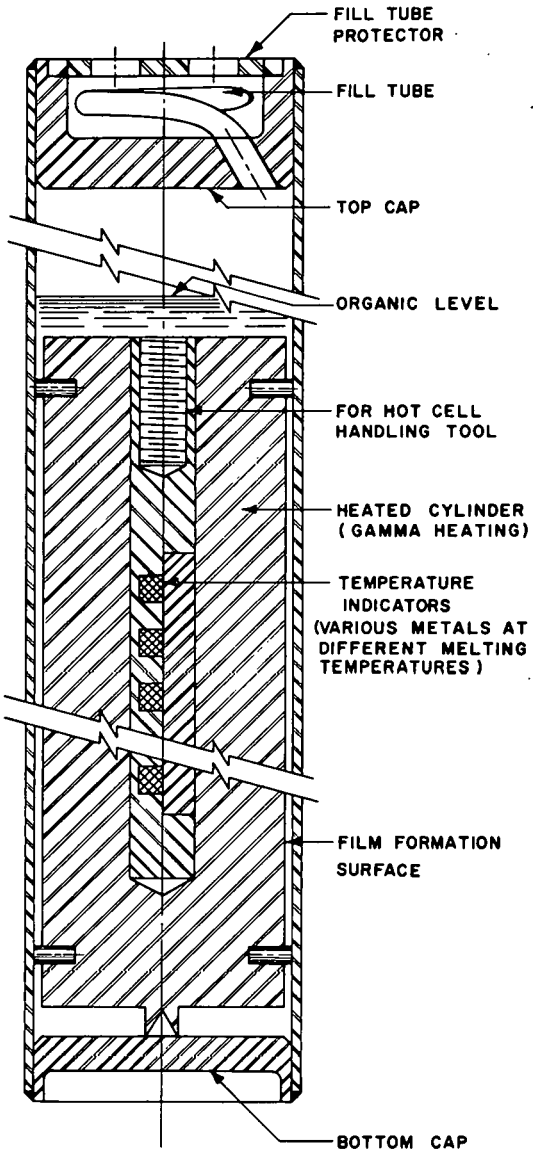

Fig. 36 Cross section of film formation rabbit capsule.

Reliable heat transfer data on natural convection in vertical enclosed annular spaces, using a liquid with the same L/D as the film formation capsules, is not available. Therefore, preliminary tests will be made to measure the overall convection heat transfer coefficient of organic material in an annulus.

The preliminary irradiations to be made will determine the gamma flux at a certain time during the MTR cycle, so the succeeding test can be made at approximately the same flux. The thermal and fast neutron flux will be determined by the use of flux wires. The gamma heat will be determined by using a capsule similar to the one used for film formation, with the exception of a smaller annulus filled with helium. Chemical dosimetry also is being considered to determine gamma heat available in the rabbit facility.

2.10 Radiation Dosimetry (J. R. McGeachin, S. Cohen, W. B. Lewis) A calorimeter has been designed and is being fabricated for the purpose of measuring gamma and neutron energies absorbed in organic coolants. This information is necessary in the study of film formation, radiation damage and radiolytic effects.

The power produced by a radiation field has been measured by the temperature difference created by heat flow through a thermal resistance. The radiation power is absorbed in a mass, and the absorbed power leaks off as heat creating a temperature gradient along a path of known thermal resistance.

The principle on which the new calorimeter is designed is different. Three cylinders of different masses and different composition are enclosed in a cylindrical capsule. Each cylinder is supported by a stem which serves as the principal conductor for heat from a cylinder to the capsule. Each cylinder has enclosed within it an electrical heater. The external dimensions of the three cylinders are identical. The cylinders are symmetrically disposed within the capsule, and all stems are as nearly identical as possible. Consequently, the thermal leakage paths for the cylinders are essentially the same.

When the capsule is placed in a radiation field, the absorption is not the same for the three cylinders. Consequently, they would come to equilibrium at different temperatures were not the power inputs equalized by electric power from the heaters. This is done and the condition of equal values of power is recognized when the three cylinders are brought to the same temperature. The value of this temperature is of casual interest only. The unknown values of gamma-induced power, and neutron-induced power are obtained from the known values of power supplied by the electric heaters.

It is worthwhile to emphasize the difference in design principles in order to determine the advantages of this design over the more conventional design. The older design determines the power absorbed per unit mass by measuring a temperature difference created by heat flow across a member of known thermal resistance. The method does not differentiate between power induced from different types of radiation.

The new calorimeter uses thermocouples only to establish a condition of equal temperature among three elements. The only potential difference needed to any precision is zero. This limitation removes any need for premium grade thermocouples. The radiation-induced power is obtained by comparing it with values of electric power. These values can be obtained with great precision. The new calorimeter distinguishes between power from gamma absorption and power from neutron moderation.

The calorimeter consists of three cylinders supported rigidly from a common base plate. Figure 37 shows an assembly drawing of the capsule. Each cylinder contains a heater for power-balancing purposes. Internally each cylinder is dissimilar. One cylinder has very thick walls which form a small hole to accommodate its heater. The two remaining cylinders are identical, with the exception that one contains an organic. The complete detection unit is incased so that the atmosphere surrounding the cylinders can be controlled. This calorimeter is designed to operate in the EOCR and in the MTR gamma facility.

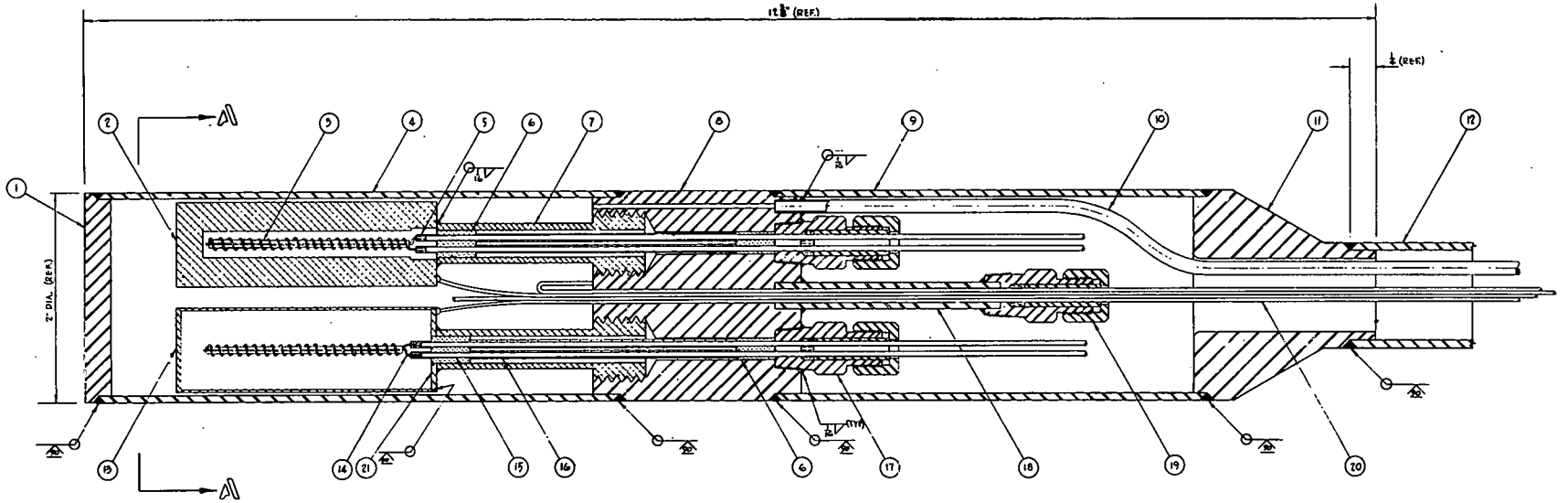

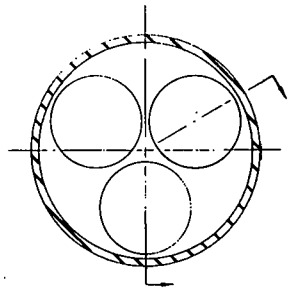

ITEM	DWG. NO.	MATERIAL	DESCRIPTION	QTY.
1	EOCR-E-1169	304 S.S.	BOTTOM TUBE CAP	1
2	EOCR-E-1169	MG	PEDESTAL	1
▷ 3	COMM.	CERAMIC	INSULATOR	3
4	EOCR-E-1169	304 S.S.	BOTTOM TUBE	1
5	EOCR-E-1169	NI	HEATER WIRE SPLICE	6
▷ 6	COMM.	CERAMIC	INSULATOR	6
7	EOCR-E-1169	MALLO AMC595	PEDESTAL LEG	3
8		304 S.S.	BULK HEAD	1
9			TOP TUBE	1
10			⅛" O.D. x .028 WALL TUBING	
11	EOCR-E-1169		REDUCER	1
12	COMM.		1" O.D. x .065 WALL TUBING	
13	EOCR-E-1169	MG	PEDESTAL	2
14	COMM.	NI-CHROME	24 GA. WIRE	
15		NI	18 GA. WIRE	
▷ 16		CERAMIC	INSULATORS	
▷▷ 17		306 S.S.	THERMOCOUPLE GLAND	3
18			¼" TUBING x .065 WALL x 2⅝ LG.	1
▷ 19			THERMOCOUPLE GLAND (MOD.)	1
20		Pt-Pt Rh 304 S.S. SHEATH	40 MIL GROUND JUNCTION THERMOCOUPLE WIRES	
21	EOCR-E-1169	MG	PEDESTAL CAP	2

GENERAL NOTES:

1. STRAIGHTNESS TOLERANCE SHALL NOT EXCEED ⅛" IN ENTIRE LENGTH.

REFERENCE DRAWINGS:

EOCR-E-1169, EOCR GAMMA-NEUTRON HEAT CALORIMETER DETAILS

▷ TO BE FURNISHED BY EOCR EXPERIMENTAL PROJECTS BRANCH

▷▷ CONAX CATALOG NO. 1-20-75
CONAX CORPORATION
2300 WALDEN AVE.
BUFFALO 25, N.Y.

▷▷ CONAX CATLOG NO. MTG-20-A2 (SPECIAL)

Fig. 37 Gamma neutron heat calorimeter assembly.

The three cylinders have different total masses. The cylinders and their legs are made of pure magnesium which will not absorb neutron energy. In the reactor, gamma energy is absorbed in the magnesium, and both neutron and gamma energies are absorbed in the organic. Because of the symmetrical arrangement of the cylinders and because each leg is identical, the thermal leakage is the same for all cylinders if they are all at the same temperature. This condition can be reached by adjusting the heater powers until the temperature differences between each pair of cylinders are zero. Therefore, during steady-state conditions, the total power input (electrical and gamma neutron) to each cylinder will be the same.

The exposed Nichrome-V-type element heater design has the advantage of controlled construction in the laboratory with accurately measured resistance after fabrication; whereas, commercial envelope-type heaters introduce errors caused by the electrical resistance uncertainty. Type "A" nickel is used for the heater element extension through an electrical-insulated, pressure-sealed Conax fitting.

The instrumentation selected for this experiment was done with two primary purposes in mind: (a) all errors that could be attributed to instrumentation would be eliminated if possible, and (b) the instrumentation must be functional and available without excessive delays. Existing equipment was used where available. Figure 38 gives a wiring diagram of the power supply, measuring system, and temperature-measuring system, plus a diagram of the instrumentation for controlling the atmosphere inside the capsule.

Direct current was chosen for the heater power because of the ease of control and measurement. A null-type precision differential dc voltmeter will be used to measure the IR drop across the heater leads and a potentiometer will be used to measure current flow in the system by measuring the IR drop across a precision shunt. Thermocouple emf will be measured with a precision K-3 L&N potentiometer.

After the calorimeter has been assembled, a series of calibrations must be made.

(1) Calibration in Isothermal Bath (See Figure 39)

The emf across Junction 1 and Junction 2 = $E_2(T)$

The emf across Junction 1 and Junction 3 = $E_3(T)$

These will be determined for a series of temperatures. Should there be no source of emf other than the thermal junctions themselves, $E_2(T)$ and $E_3(T)$ should be identically zero. However, should any non-vanishing emf be observed, these are recorded, and their values used to indicate that a pair of junctions are indeed at the same temperature.

(2) Calibration of Ratios of Leakage Paths

These calibrations also are made in an isothermal bath. Power w_1 is given to the heater in cylinder 1. Then the power w_2 to

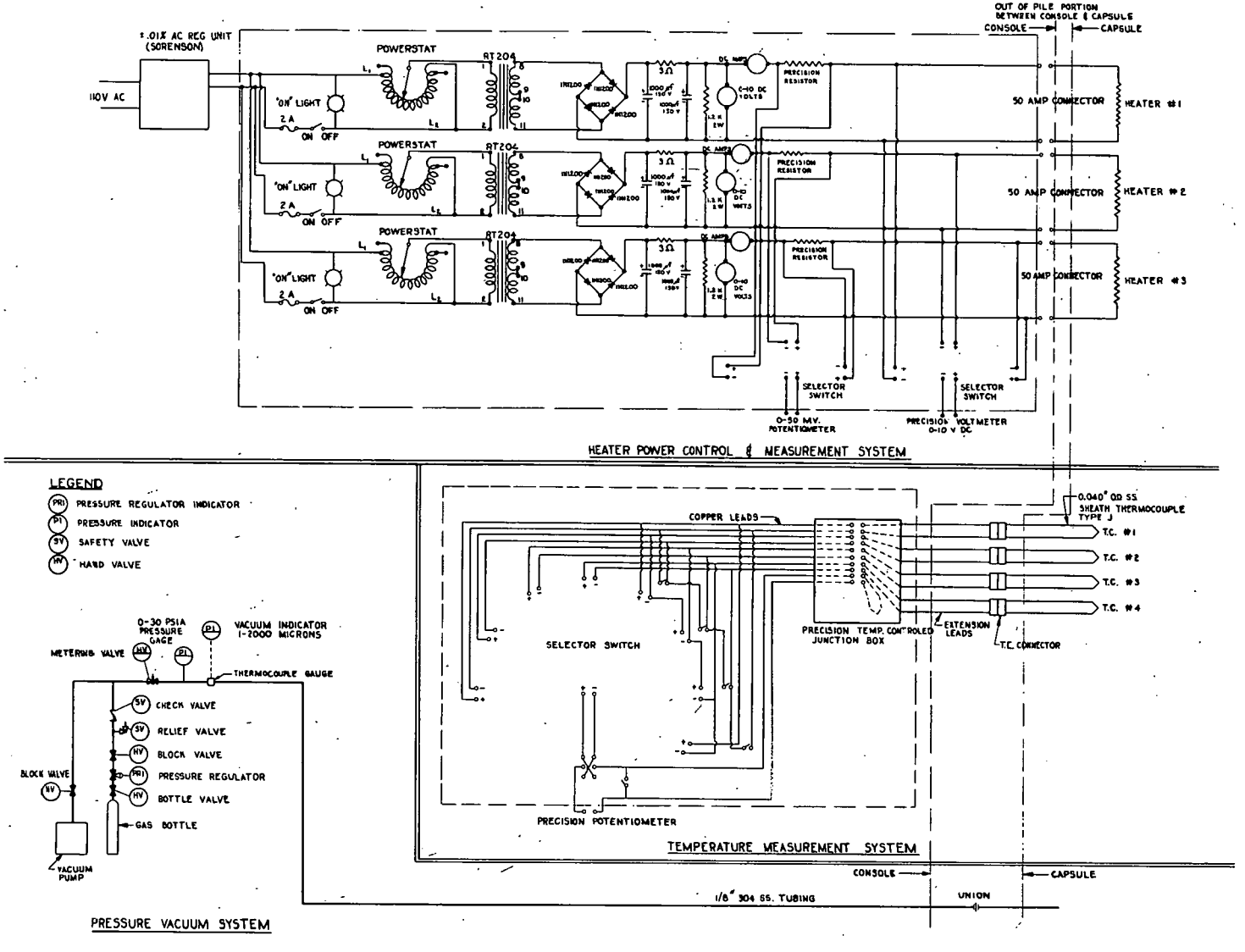

Fig. 38 Gamma neutron calorimeter instrumentation.

cylinder 2 is determined so as to bring the emf of junction 1 and 2 to the previously obtained value $E_2(T)$.

The same process is then followed for cylinder 3.

As a result:

$$w_1 = \frac{T_1 - T_0}{R_1} \; ; \; w_2 = \frac{T_2 - T_0}{R_2} \; ;$$

$$w_3 = \frac{T_3 - T_0}{R_3}$$

Hence $R_1 w_1 = R_2 w_2 = R_3 w_3$ and

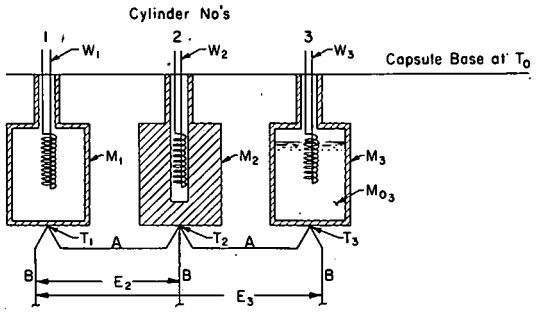

Wj = Heater Power Input To Cylinder j, Watts:
Mj = Mass Of Magnesium Cylinder j, Grams:
Mjo = Mass Of Organic in Cylinder j, Grams:
Rj = Thermal Resistance Of Cylinder j, Watts/°F

Fig. 39 Calorimeter calibration.

$$\rho_2 = \frac{R_2}{R_1} = \frac{w_1}{w_2} \quad \text{and} \quad \rho_3 = \frac{R_3}{R_1} = \frac{w_1}{w_3}$$

where R_j is the overall thermal resistance of cylinder j to the outer capsule.

(3) Calibration in Gamma Facility

The power per unit mass due to the absorption of gamma energy may not be the same for magnesium and organic material. Since two of the cylinders are constructed of magnesium only, and one contains magnesium and organic, measurements in the gamma facility will establish quantitatively the difference in power per unit mass for the two materials.

From cylinders 1 & 2:

$$\gamma m_1 + w_1 = \rho_2 (\gamma m_2 + w_2)$$

Hence

$$\gamma = \frac{w_1 - \rho_2 w_2}{\rho_2 m_2 - m_1}$$

And from cylinders 1 & 3:

$$\gamma m_1 + w_1 = \rho_3 (\gamma m_3 + \gamma_0 m_{30} + w_3)$$

So

$$\gamma_0 = \frac{\gamma\,(m_1 - \rho_3 m_3) + w_1 - \rho_3 w_3}{m_{30}}$$

Where m_j = mass of magnesium cylinder $_j$

m_{jo} = mass of organic cylinder $_j$

γ = gamma watts/gram (Mg)

γ_0 = gamma watts/gram (organic)

Note: only capsule 3 contains organic.

After these calibrations have been made the instrument can be used to differentiate absorbed energies from gamma rays and fast neutrons.

2.11 Pyrolytic Capsule Fouling Test under Irradiation (E Burroughs, S. Cohen, W. B. Lewis)

The pyrolytic capsule fouling test under irradiation has a dual purpose: (a) to study the film formation from a terphenyl mixture on a heated platinum surface under gamma irradiation, and (b) to correlate the rate of film formation to the change in power necessary to maintain a constant ΔT between the heated surface and the bulk terphenyl by resistance thermometry. In addition, the results of the test will indicate the feasibility of an on-stream instrument for determining rate of film formation in an operating organic reactor.

The test capsule is made of Pyrex, heavy-walled glass which can safely withstand the vapor pressure of the terphenyl mixture at 500°F (Monsanto Data Book, Santowax R, 1.3 psia at 500°F). The capsule is designed with a thermo siphon harp, so that, as the bulk terphenyl is heated externally, fluid flow is established over the platinum heater strip. In the laboratory, the equipment is operated behind a safety shield. In the gamma facility, the capsule will be in an aluminum cannister. A sketch of the test capsule is shown in Figure 40.

The individual platinum heater strips are of chemically pure platinum suitable for resistance thermometry. The platinum strips are approximately 6 in. long; the width is 0.125 in. with a tolerance of $\pm$ .005 in. The thickness of the heater strips is 0.002, 0.004 or 0.006 in. The quoted tolerance on the thickness is $\pm$ 0.0003 in; however, actual micrometer readings on the strips indicate the tolerance is $\pm$ 0.0001 in.

Power to the heater strips will be supplied through tungsten electrodes sealed in the glass. A test section is theoretically isolated for test purposes by attaching 0.002- or 0.004-in.-diameter platinum potential leads approximately 4 in. apart on the heater strip. These platinum leads are sealed through the glass. Isolation of a test section in this manner will reduce end effect errors of the current and resistance measurements.

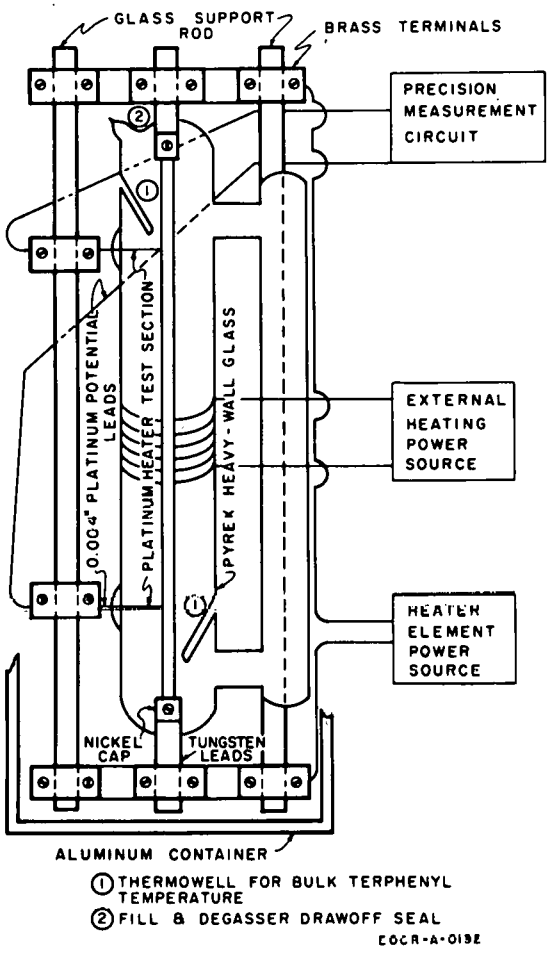

Fig. 40 Radiolytic film formation test capsule.

The bulk terphenyl temperature is measured and controlled with a standard temperature controller attached to the external heater. The bulk terphenyl temperature will be cross-checked by using the heater test strip as a resistance thermometer. The plate temperature of the heater strip is determined by a precise null balance potentiometer circuit measurement of the voltage and current being supplied to the unit. A simple diagram of the circuit is shown in Figure 41.

A temperature differential of 350°F between the bulk terphenyl and plate temperature is planned for initial tests. As a film is deposited or formed on the plate surface, the heat transfer between the plate and bulk coolant can be expected to decrease. It should be possible to correlate the rate and extent of film formation to the change in power necessary to maintain the established ΔT. After the test, the film on the platinum heater strip can be studied by cutting the glass capsule and removing the test section.

It is anticipated the work discussed in the preceding paragraphs will lead to further investigation of heat transfer data from a heated surface to terphenyl mixtures in the range of nucleate and film boiling.

Most of the necessary test equipment has been purchased. The tungsten electrode rods have been silver-soldered to the platinum strips. The platinum potential leads have been resistance-welded to the platinum strips. The width between the two points of contact of the potential leads has been measured. Construction of the measurement circuitry has started.

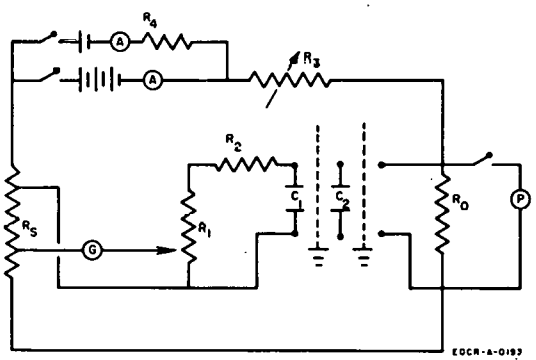

Fig. 41 Radiolytic film formation test circuit.

A dummy capsule was made, filled with terphenyl, and fitted with an external tape heater. The temperature was brought up to 500°F. The thermo siphon design of the capsule creates a very visible flow rate, estimated to be 0.5 to 1.0 ft/sec. At present, resistance measurements of the platinum strips at the ice point and boiling point of water are being determined. Upon completion of these measurements, complete capsules will be fabricated.

3. EOCR HAZARDS ANALYSES AND SUPPORTING STUDIES

3.1 Radiological Hazards Analysis for the EOCR (O. L. Cordes)

3.11 Introduction. The radiological hazards associated with the operation of the EOCR for power levels up to 40 Mw have been analyzed and are presented below. Radiation dose rates arising from normal power operations, fuel unloading, operation with abnormal coolant activity, and the unloading of ruptured fuel assemblies are discussed. It is concluded from these analyses that operation of the EOCR at these power levels does not present serious radiological hazards.

3.12 Coolant Activity. Radiation from activated organic-coolant impurities and from fission products generated from the small amount of U-235 on the fuel element surfaces produces moderate radiation dose levels in the EOCR in addition to those caused by the reactor fuel and radioactive core components. The EOCR has two systems which remove radioactive impurities from the reactor coolant. One of these, the purification system, controls the level of high boiler residue (HBR) in the organic system by distillation. As the HBR is removed in the purification system still, a portion of the radioactive impurities is automatically removed along with the HBR. The second system, for particulate removal, lowers the level of radioactivity in the organic coolant by reducing both the amount of particulate impurities and the residence time of these impurities in the reactor flux zone.

The expected activities in the main coolant stream of the reactor with only the purification system in operation and with a HBR concentration of 30% are shown in Table XL. With both systems functioning during normal reactor operation, it is expected that the total coolant activity will be reduced to approximately 0.03 μc/cc.

3.13 Radiation and Air Concentration Levels During Normal Reactor Operation. All walls bordering on continuously occupied personnel areas have been designed and constructed with sufficient shielding to reduce expected radiation levels to less than 2.5 mr/hr [25, 26, 27]. Calculated radiation levels throughout the EOCR for 40-Mw normal operation with both purification systems in operation are presented in Table XLI.

The quantity of radioactive fission product gases discharged to the stack will be about 10 millicuries per day. Even without including stack-to-ground diffusion, the concentrations of radioactivity in the stack effluent are far below the recommended concentration guides $(RCG)_a$ for continuous breathing. In addition, the rate of production and discharge of argon-41 is calculated to be approximately 100 millicuries per day. Again without taking credit for the stack-to-ground diffusion, the A-41 concentration in the stack effluent is only 20% of the $(RCG)_a$ for continuous breathing. Calculated quantities of radioactive isotopes released from the stack under normal conditions are shown in Table XLII [28].

The maximum quantity of Pu-239 in the core is expected to be less than 0.1 curie. This, however, will be contained within the fuel element cladding and will not present a radiological hazard. Pu-239 released to the process system during a cladding failure will be removed by the purification systems along with the HBR and sent to the burial grounds.

TABLE XL

EXPECTED ACTIVITIES IN THE MAIN COOLANT LOOP WITHOUT A PARTICULATE-REMOVAL SYSTEM

Conditions: The bases for these expected activities are continuous EOCR operation at 40 Mw, OMRE experimental data, computed values for recoil corrosion, and computed values of activities from coolant impurities [27, 29, 30]. It was assumed that there are no breaks in the fuel elements and that there are about 125 mg of U-235 on the fuel-element cladding surfaces.

Radio-Isotope	Decay Mode	Half-Life	Activation Source	Coolant Concentration ($\mu c/cc$)
Cl-38	β,γ	37.3 min	Coolant impurity	0.023
As-76	β,γ	26.5 hr	Coolant impurity	0.022
Sb-122	β,EC,γ	2.75 day	Unknown	0.0095
Na-24	β,γ	14.9 hr	Coolant impurity	0.0072
S-35	β	87 day	Corrosion product coolant impurity	0.0324
P-32	β	14.2 day	Coolant impurity	0.198
Sb-124	β,γ	60.0 day	Unknown	0.001
Mn-56	β,γ	2.6 hr	Corrosion, recoil	0.217
Cr-51	EC,γ	27.8 day	Corrosion	0.025
Fe-55	EC	2.60 yr	Corrosion, recoil	0.068
Co-60	β,γ	5.24 yr	Corrosion, recoil	0.00028
Co-58	EC,β^+,γ	71.3 day	Recoil	0.00077
Mn-54	EC,γ	300 day	Corrosion, recoil	0.0029
Co-58m	γ	9 hr	Recoil	0.040
C-14	β	5568 yr	Organic coolant blanket gas	0.00036
Fe-59	β,γ	44.3 day	Corrosion, recoil	0.0064
Fission products	β,γ	—	U-235 on cladding	Negligible
	Total activity in coolant without a particulate-removal system			0.654

The amount of radioactivity discharged from the plant via the HBR will be less than one curie per day. During the initial operation of the EOCR, the HBR will be discharged to drums after a suitable decay and stored in the burial grounds. The normal direct radiation from the HBR drums is expected

TABLE XLI

RADIATION LEVELS DURING 40-Mw NORMAL REACTOR OPERATIONS

Location	Radiation Level (mr/hr)
First Floor and Upper Levels	
Reactor top area	0.3
Canal containing equivalent of two 220-Mw cores	
Exterior walls	0.25
Water surface with 14-ft submergence	0.1
Water surface after canal drainage to pit	2.5
West wall of reactor building	0.5
Exterior faces of purification room walls	0.25
Utility room	0.25
Boiler room	0.1
Emergency generator room	0.25
Office areas	0.1
Inside purification room	2-50
Inside degassification room	2-50
Roof of degassification room	10
Process control room	0.25
Switch gear room	0.1
Basement Level	
General basement area	0.25
Primary valve cubicle	10-40
Primary coolant trench	10-40
Decay loop room	2-10
Walls of canal	0.25
Sub-Basement Level	
Dump tank and pump room	10-50
Canal sump pump room	7.5
Outside subpile room door	40
Subpile room	
General dose rate	50,000-100,000
Gamma through reactor bottom head	30,000
Thermal and fast neutron through bottom head	1
Streaming around fission chambers	1,000
Streaming from vessel and cavity liner annulus, fast neutron	80,000
Outside Areas	
Primary cooler area west of reactor building	
At fence	20
At pipe surface	50
HBR storage vessel	
At surface	200
At 10 ft	24

TABLE XLII

NORMAL EOCR OFF-GAS ACTIVITIES[28]

Nuclide	Stack Exit Concentration (μc/cc air)(a)	$(RCG)_a$ (μc/cc)(b)	Ratio $\frac{\text{Exit Conc.}}{(RCG)_a}$
Kr-83m	1.86×10^{-10}	—	—
Kr-85m	2.7×10^{-10}	6×10^{-6}	4.3×10^{-5}
Kr-85	3.44×10^{-15}	1×10^{-5}	3.4×10^{-10}
Kr-87	9.21×10^{-10}	1×10^{-6}	9.2×10^{-4}
Kr-88	2.30×10^{-10}	—	—
Kr-89	1.16×10^{-10}	—	—
Xe-131m	1.32×10^{-15}	2×10^{-5}	6.6×10^{-11}
Xe-133m	4.78×10^{-11}	—	—
Xe-133	6.67×10^{-11}	1×10^{-3}	6.7×10^{-6}
Xe-135m	1.09×10^{-9}	—	—
Xe-135	5.12×10^{-10}	—	—
Xe-137	7.93×10^{-10}	—	—
Xe-138	1.47×10^{-9}	—	—
H-3	9.80×10^{-13}	2×10^{-3}	4.9×10^{-10}
C-14	4.78×10^{-14}	4×10^{-6}	1.2×10^{-8}
I-131(c)	1.3×10^{-15}	3×10^{-7}	4×10^{-9}
I-133(c)	1.1×10^{-10}	3×10^{-8}	4×10^{-6}
I-135(c)	1.6×10^{-9}	4×10^{-7}	4×10^{-3}
Br-82, -83, -87	—	—	—
A-41	7.85×10^{-8}	4×10^{-7}	.2

(a) Based on a stack exit rate of 27,250 cfm.

(b) CFR 8595, September 7, 1960.

(c) Iodine release expected to be less than calculated due to reaction with coolant.

to be less than 30 mr/hr at contact. Since the closing of the drums and the moving of the filling hose are momentary operations, no radiation hazard is expected in connection with the normal HBR disposal. Research and development work is in progress to effect more economical disposition of the HBR and its contained activity.

Areas in which the normal radiation levels are greater than 2.5 mr/hr will be under operational control to prevent overexposure to personnel. Access

to areas such as the subpile room which are expected to have very high radiation fields during operation of the reactor will be denied while the reactor is operating.

3.14 Radiation Levels During Fuel Unloading Operations. Fuel and other radioactive components are to be removed from the EOCR with the aid of a reactor extension vessel which, when filled with organic coolant, will provide an additional 11 ft of axial shielding above the core. Twelve portable magnetite concrete shielding blocks will be temporarily installed around the extension vessel to provide radial shielding.

Radiation dose rates in the vicinity of this extension tank will arise both from the radioactive impurities in the organic coolant and from radioactive fuel and core components which are lifted up into the extension tank prior to discharging to the wash cell. These two sources are considered separately in the following discussion.

The highest radiation dose rate from the fuel-handling operation occurs when the control rod assemblies are raised into the extension tank. The control rod assemblies must be raised into the extension tank a minimum of 24 in. above the operating floor for insertion into an unlocking holder. Since the reactor defueling operation cannot begin until about six hours after final shutdown, and since the maximum washing rate is two assemblies per hour, it is unlikely that the most radioactive fuel assemblies located in the center of the reactor will be removed before 20 to 24 hr decay time has elapsed. Under these conditions the defueling operation is expected to produce momentary axial dose rates of approximately 30 mr/hr to the operating platform above the tank, less than 100 mr/hr outside the temporary shielding blocks, and approximately 25 mr/hr outside the extension tank above the shielding blocks. The maximum dose to an operator from the defueling operation for an 8-hr shift is expected to be less than 40 mr.

Although fresh, nonradioactive coolant will be added at the time the extension tank is installed, radioactive coolant from the primary coolant system will mix with the new material and produce a continuous background gamma dose around the reactor extension vessel. The dose rate to the operating platform from this source is expected to be less than 20 mr/hr under normal conditions and should decay to less than 10 mr/hr 24 hr after shutdown. The operating platform will furnish additional shielding which will further reduce these dose rates. The dose rate above the shielding outside the reactor tank extension from the coolant will be approximately 5 mr/hr.

Combined dose rates from the core components and coolant impurities on the operating platform and around the reactor top will not be excessive under normal conditions at 6 hr after shutdown. If required, the dose rates on the bridge can be reduced by the addition of portable shielding, by increasing the time allowed for radioactive decay and by reducing the residual coolant activity with the purification systems.

Normal canal operations during shutdown result in negligible dose rates except for the transfer operation from the deep well section across the bulkhead threshold into the canal. During transfer of a driver fuel element across this threshold, the maximum momentary gamma dose rate expected at the water surface is less than 50 mr/hr. Similarly, the dose rate for the transfer of a combined fuel follower and poison section which has been irradiated for

one year in the central region of the core is expected to be less than 150 mr/hr. The maximum 8-hr shift gamma dose postulated for a single operator under normal transfer conditions is about 35 mr, or one-third of the permissible weekly dose.

Dose rates throughout the EOCR during fuel unloading, except those connected with the subpile room and those mentioned above, should not change significantly from those listed in Table XLI for normal operations. During normal 40-Mw operations, the general dose rate in the subpile room is expected to be between 50 and 100 r/hr. Shortly after the reactor is shut down, this dose rate is expected to drop to less than 3 r/hr, dropping to around 100 mr/hr about 4 hr after shutdown. With access denied to the subpile room during operations and shortly after, and with short duration exposures after that, these dose rates will be acceptable.

3.15 Radiation Levels During Abnormal Operating Conditions. Abnormal operating conditions for the purposes of this section are those which occur due to an increase in the concentration of radioactivity in the reactor coolant. Two different cases of abnormal coolant activity are examined below; one with a coolant activity of 0.6 μc/cc resulting from an inoperative particulate removal system, and the second case with a coolant activity level of 12 μc/cc resulting from a moderate fission break.

An increase of radioactivity in the coolant will occur if the particulate removal system becomes inoperative. Without this system the concentration of activity is expected to rise to 0.6 μc/cc with an effective photon energy of about 0.9 Mev. The important walls of the process system will continue to limit the increased dose rate to below 2.5 mr/hr with only two significant exceptions. The sub-basement dump tank wall permits a dose rate of about 5 mr/hr to personnel at the nearest point of normal access, the stair landing. In addition, the main coolant lines at the primary cooler can be expected to produce dose rates up to 500 mr/hr at their surfaces. This will, in turn, raise the dose rate through the west wall of the reactor building to about 10 mr/hr. These dose rates will require operational control and partial evacuation of the main floor and cooler area. Access to other areas, such as the inside of the purification room, will continue to be under operational control as during normal operation. A tabulation of calculated radiation levels for an abnormal coolant activity of 0.6 μc/cc is presented in Table XLIII.

A fission break in the reactor is another way in which the activity of the coolant can increase to abnormal levels. Since a fission product release of 1200 curies (which is six times the release in the OMRE fuel meltdown and is of the same order of magnitude as some of the larger ones that have occurred at the MTR and ETR) would produce a coolant acitivity of 12 μc/cc, the preceding discussion of radiation levels and Table XLIII can be applied to the abnormal conditions due to a moderate fission break if all dose rates arising from the process system are multiplied by a factor of 20. In the event of a fission break the reactor will be scrammed and access to areas of high radiation will be controlled until the radiation levels are reduced by radioactive decay and the coolant purification systems.

The fission break will, however, present air activity problems in addition to the direct radiation problems discussed above. The degasifier system can be turned off if necessary in order to prevent the fission gases from leaving

TABLE XLIII

RADIATION LEVELS DURING ABNORMAL OPERATING CONDITIONS
WITH A COOLANT ACTIVITY OF 0.6 μc/cc

Location	Radiation Levels (mr/hr)
First Floor and Upper Levels	
Reactor top area	0.3
West wall of reactor building	10
Exterior faces of purification room walls	5
Utility room	2.5
Boiler room	1
Emergency generator room	2.5
Office areas	0.1
Inside purification room	10-500
Inside degassification room	10-500
Roof of degassification room	200
Process control room	2.5
Switch gear room	1
Basement Level	
General basement area	2.5
Primary valve cubicle	100-400
Primary coolant trench	100-400
Decay loop room	100-420
Sub-Basement Level	
Dump tank and pump room	40-700
Canal sump pump room	7.5
Outside subpile room door	40
Subpile room general	50,000-100,000
Outside Areas	
Primary cooler area west of reactor building	
At fence	200
At pipe surface	600
HBR storage vessel	
At surface	200
At 10 ft	24

the primary cooling system until they decay to particulate daughters and become trapped in the organic coolant. However, since radioiodine reacts with the organic coolant and is not readily off-gassed, it is expected that during all but the most severe fission breaks and weather conditions the degasifier can be left operating without exceeding the recommended concentration guides for continuous breathing in the reactor area.

The activity in the main coolant pipes from either a fission release or lack of an operational particulate-removal system will produce rather high levels of radiation around the primary cooler. If access to this area is absolutely necessary, the radiation levels can be reduced by shutting the reactor down and draining the contaminated coolant from the primary cooler into the system dump tank.

It is expected that the organic coolant can be decontaminated with the purification and particulate-removal systems. The radioactivity is expected to remain in the HBR stream and to be carried out to the HBR storage area for decay and disposal. Following a fission break, the HBR storage vessel also will become a source of high-radiation dose rates. However, the location of the HBR storage tank is such that controlled access to this area will reduce personnel exposures to negligible levels. If the production of HBR in the reactor requires that the HBR storage vessel be emptied before the radioactivity decays to acceptable levels, the contaminated HBR can be pumped into drums located behind temporary shielding. When the radiation level has dropped sufficiently, the drums can be sent to the burial grounds.

3.16 Radiological Hazards During the Unloading of Ruptured Fuel Assemblies. The removal of a ruptured fuel assembly from the core will necessitate minor changes in the unloading procedures. The time between reactor-shutdown and top-head-removal will be extended and part of the component wash cycle will be eliminated.

The time between shutdown and top-head-removal must be extended to allow the coolant purification systems sufficient time to reduce the fission product activity in the coolant to acceptable levels for unloading. The wash cycle must be cut short to prevent the accumulation of a large inventory of contaminated solvent which would present both radiation and disposal problems. The wash cycle for ruptured fuel assemblies will be reduced to a once-through displacement of the organic coolant by an organic solvent followed by an abbreviated water wash. The wash cycle can be modified since a ruptured assembly will not be reused and thus does not need to be so thoroughly cleaned. The contaminated coolant will be sent to the system dump tank for reprocessing and any solvent which remains contaminated will be stored in steel drums for radioactive decay. The water from the water wash will be stored or dumped to the aqueous waste system, depending on its level of activity. After the water wash, the ruptured assembly will be transferred to the water-filled canal. MTR-ETR experience indicates that severely ruptured assemblies can be stored in a water-filled canal with only low-level activity being released. Once the ruptured assembly has been placed in the canal, the unloading of the remainder of the core will proceed in the normal manner.

3.2 Heat Transfer and Hydraulics (J. L. Liebenthal)

3.21 Introduction. The controlling factors setting heat transfer limits in organic reactors are burnout, a function primarily of coolant temperature and

pressure and of heat flux; pyrolysis of the coolant, primarily an economic factor; and fouling or coking of heat transfer surfaces, of which the exact causative factors are now being determined. The approach to the heat transfer analysis of the EOCR core, therefore, is based on imposing two limits: (a) burnout margin, the ratio of the departure-from-nucleate-boiling heat flux to the local heat flux in any part of the core; and (b) the maximum surface temperature of a fueled plate.

The burnout margin is so chosen that the maximum heat flux during normal operation is well below the burnout heat flux, in order that the reactor may sustain a sizeable increase in power or decrease in heat transfer rate without overheating or melting of fuel plates. The burnout margin limitation has been set at 2.0 during normal operation. This margin is one that is considered safe in most reactor designs and, since in EOCR there is no known danger of violent metal-coolant reactions and since melting of fuel element plates has been shown by OMRE experience to result in significantly less fission product contamination than a similar accident in a water reactor, this burnout margin is more than adequate.

The safe fuel plate surface temperature limitation, as long as it is well below the nucleate boiling temperature, is primarily a function of the state of coolant development and of the ability to control or predict fouling rates on fuel plates. Present organic coolant knowledge requires a maximum fuel plate surface temperature limitation considerably below the temperature required to cause nucleate boiling. Thus, the major considerations in the choice of a fuel plate temperature are coolant pyrolysis rate and fouling rate, where fouling rate is the only factor of the two which is pertinent to reactor safety. For initial operation of EOCR, the limiting hot spot fuel plate surface temperature has been chosen as 750°F. This represents the present limit of operating experience in organic reactors. OMRE has operated at hot spot fuel plate surface temperatures of 750°F. In addition, one fuel element has been operated in OMRE with a fuel plate temperature of 850°F for a significant period [31, 32, 33, 34]. Fouling on this element was found not to be abnormal compared with the rest of the core. This datum tends to substantiate the 850°F fuel plate temperature upon which the EOCR design was based. To fulfill the development purposes of the EOCR as an experiment, it is anticipated that soon after experience is gained with the reactor system and core properties, the limiting temperature will be raised to explore operation at more severe conditions. Prolonged operation at core temperatures near nucleate boiling temperature (about 1050°F for Santowax OMP) will no doubt await results from EOCR loop experiments. The initial approach to power, utilizing fuel plate surface thermocouples in the core and a monitored sample in the central loop, will clarify the operating limits allowable with the present core design. The monitored sample will operate at coolant conditions existing in low flow elements, but will operate at heat fluxes beyond those in these elements.

The calculation of expected values of hot spot temperatures referred to above takes into account the maximum deviations from the nominal values of all fuel element dimensional and material tolerances, variations in coolant effectiveness and coolant operating conditions, and reactor control accuracy. A large factor is included to account for the degree of fouling found in previous experience. All of these factors will undoubtedly be reduced in the future when further experience with fuel element fabrication, reactor operation, coolant properties, and especially fouling rates has been gained. The present calculations

are based on hot spot factors considered conservative despite ignorance in these areas. For example, at a coolant inlet temperature of 500°F, a hot spot temperature of 850°F reflects a nominal temperature at the hottest point in the core of about 620°F. A projection of conservative hot spot factors and reactor power which may be expected to obtain after sufficient experience, but without redesign of the core, is presented in Tables XLIV and XLV and Figure 42.

TABLE XLIV

PROJECTED FUTURE EOCR FUEL ELEMENT HOT-SPOT HOT-CHANNEL FACTORS

	Variable Affected									F_t	F_θ	F_ϕ
Source of Factor	P_e	f_c	f_p	Lp_h	W	V	a	D_e	B	Hot Channel Factor	Hot Spot Factor	Hot Flux Factor
Flow orifice error					1.14	1.14				1.14	1.12	
Power control error	1.10									1.10	1.10	1.10
Meat thickness error		1.05									1.05	1.05
Flux prediction error	1.05	1.10	1.05							1.06	1.10	1.10
h Correlation error									1.25		1.25	
Meat area error				1.02						1.02	1.02	1.02
Channel dimen. error					1.24	1.21	0.98	1.14		1.24	1.17	
Flow distribution					1.05	1.10				1.05	1.08	
Fuel/plate error		1.02		1.02						1.02	1.02	1.02
				Total Factors						1.80	2.34	1.32

TABLE XLV

PROJECTED FUTURE EOCR CONTROL-ROD FUEL-FOLLOWER HOT-SPOT HOT-CHANNEL FACTORS

	Variable Affected									F_t	F_θ	F_ϕ
Source of Factor	P_e	f_c	f_p	Lp_h	W	V	a	D_e	B	Hot Channel Factor	Hot Spot Factor	Hot Flux Factor
Flow orifice error					1.14	1.14				1.14	1.12	
Power control error	1.10									1.10	1.10	1.10
Meat thickness error		1.05									1.05	1.05
Flux prediction error	1.05	1.10	1.05							1.06	1.10	1.10
h Correlation error									1.25		1.25	
Meat area error				1.02						1.02	1.02	1.02
Channel dimen. error					1.24	1.21	0.98	1.14		1.24	1.17	
Flow distribution						1.05					1.04	
Fuel/plate error		1.02		1.02						1.02	1.02	1.02
				Total Factors						1.72	2.25	1.45

3.22 Steady-State Heat Transfer Calculations - Calculation Method. The calculation of steady-state heat transfer in the EOCR core follows principles and methods presently used by Phillips Petroleum Co for other reactors [35]. The method for estimating the severity of heat transfer conditions in the core

is essentially the usual hot-spot hot-channel analysis. In the EOCR each element and control rod is orificed in order to make the maximum use of the available flow. Thus, the heat transfer calculations require that, for any power and flux distribution, flows for each element be calculated and summed to obtain the minimum reactor flow. The bases for the results presented in this section are the two flux distributions for beginning- and end-of-core-life for Core A-3, presented in Figures 43 and 44. To obtain the total active core flow for any reactor power, flow rates for each element were calculated for both beginning- and end-of-life for a selected maximum hot spot temperature. The higher flow for each element from either case was the flow assigned to this element for the entire core life. Thus, the calculated hot spot temperature reaches the selected value for part of the elements in either the beginning- or end-of-core-life if the core power is held constant throughout the cycle, which is the assumed method of operation. Flows for control rods were calculated on the same basis as the fuel elements, and then the assigned flows were increased over those calculated in order to account for future changes in power distribution within the core.

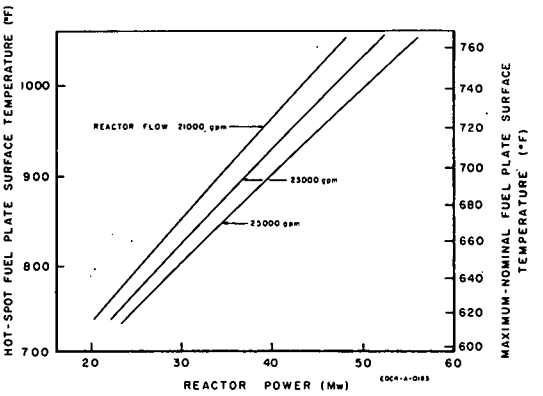

Fig. 42 Core A-3 calculated power levels (based on projected future hot spot and hot channel factors).

The equation by which the hot spot plate temperatures were calculated is:

$$T_w = T_{bl} + \Delta T_b + \Delta T_f$$

where

T_w = fuel plate surface temperature

T_{bl} = coolant core inlet temperature

ΔT_b = coolant bulk temperature rise

ΔT_f = laminar film temperature rise

In terms of reactor and coolant characteristics, this equation becomes, for the hot spot:

$$T_w = T_{bl} + \frac{P_r f_{ei} f_{ci}}{N_p}\left[\frac{f_1 f_p N_c F_t}{W_i C} + \frac{f_{si} f_2 f_a F_\theta (\rho a)^{0.80} (D_e)^{0.20}}{Lp_h B (W_i)^{0.80}}\right]$$

where

P_r = reactor power

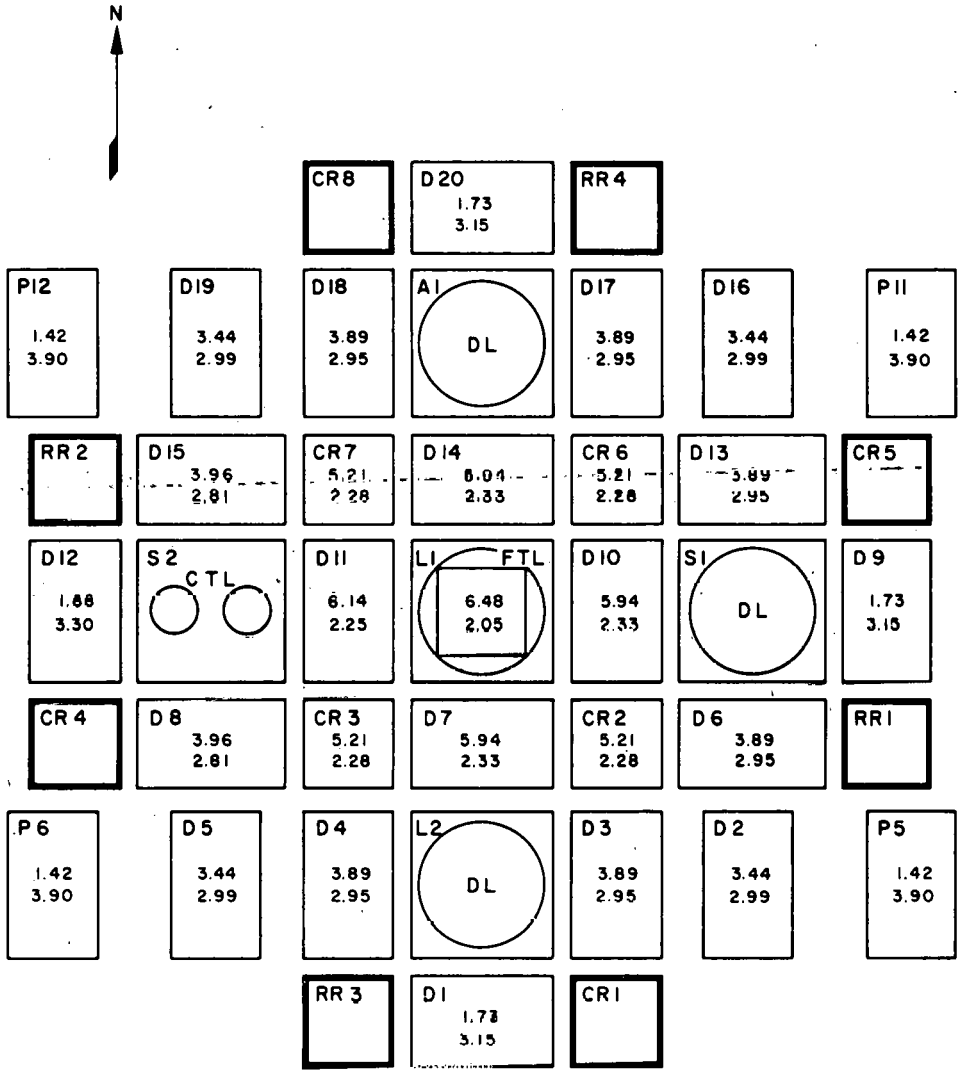

Fig. 43 Maximum and average power generation in Core A-3 at 1-Mw core power, beginning-of-core life with four control rods withdrawn.

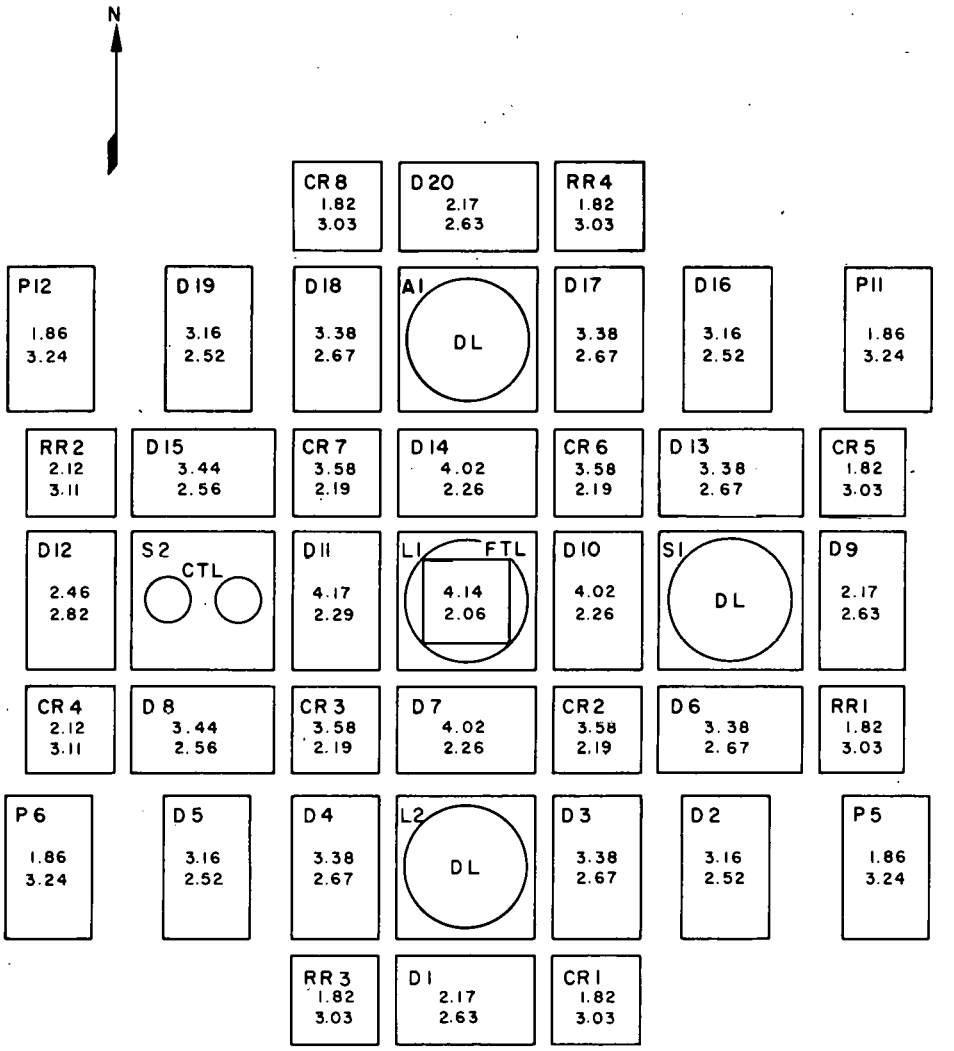

Fig. 44 Maximum and average power generation in Core A-3 at 1-Mw core power, end-of-core life.

f_{ei} = fraction of core power generated in element i

f_{ci} = radial ratio of hot channel power density to element average power density in element i

N_p = number of fueled plates per element i

Thus,

$\frac{P_r f_{ei} f_{ci}}{N_p}$ = power generated in the peak-power channel

f_1 = fraction of core power generated in, or transferred to, coolant

f_p = fraction of power generated below (upstream) of hot-spot elevation

N_c = number of channels per element i

F_t = hot channel factor

W_i = mass flow rate through element i

C = specific heat of coolant

Thus,

$W_i C/N_c$ = the heat capacity per unit time of flowing coolant in a single channel,

$\left(\frac{P_r f_{ei} f_{ci}}{N_p}\right)\left(f_1 f_p\right)$ is the power added up to the hot spot in a single channel, and

$\left(\frac{P_r f_{ei} f_{ci}}{N_p}\right)\left(\frac{f_1 f_p F_t N_c}{W_1 C}\right)$ is ΔT_b

f_{si} = ratio of peak-to-average power density in the hot channel

f_2 = fraction of reactor power generated in fuel plates

f_a = axial (vertical) maximum-to-average power density

F_θ = hot spot factor

L = heated length of a channel

p_h = heated perimeter of a channel

Thus,

$\left(\frac{P_r f_{ei} f_{ci}}{N_p}\right)\left(\frac{f_2}{Lp_h}\right)$ is the average heat flux in the channel, and

$\left(\frac{P_r f_{ei} f_{ci}}{N_p}\right)\left(\frac{f_{si} f_2 f_a}{Lp_h}\right)$ is the peak heat flux in the element.

ρ = coolant density

a = flow area per element i

D_e = hydraulic diameter of a channel

$\frac{W_i}{\rho a}$ = coolant velocity

The film heat transfer coefficient, h, is obtained from a Dittus-Boelter [36] type relation based on bulk coolant properties.

$$h = B\left(\frac{W_i}{\rho a}\right)^{0.8}\left(\frac{1}{D_e}\right)^{0.2}$$

where B is a function of the coolant properties. A plot of B as a function of coolant temperature is shown in Figure 45.

Thus, the hot spot film temperature rise is

$$\Delta T_f = \left(\frac{P_r f_{ei} f_{ci}}{N_p}\right)\left(\frac{f_{si} f_2 f_a F_\theta (\rho a)^{0.8} D_e^{0.2}}{L\, p_h\, B\, W_i^{0.8}}\right)$$

The values for terms in the equation are given in Table XLVI. The Dittus-Boelter equation was used on the recommendation of the core designer, Atomics International [37]. A linear approximation of B, accurate to less than $\pm$ 1% was used to simplify computer calculations.

3.23 Hot-Spot Hot-Channel Factors Based on EOCR Design Information. Hot-spot hot-channel factors are given in Tables XLVII and XLVIII. Detailed

factors which apply to appropriate variables are given and then combined to give the factors classified as hot channel, hot spot, and hot-spot heat-flux factors. These combined factors are applied directly to the bulk coolant temperature rise, the film temperature rise, and heat flux, respectively.

The following section describes how these factors were derived and gives values for the fuel element to aid in understanding the description. Factors for the control rod were arrived at in the same way.

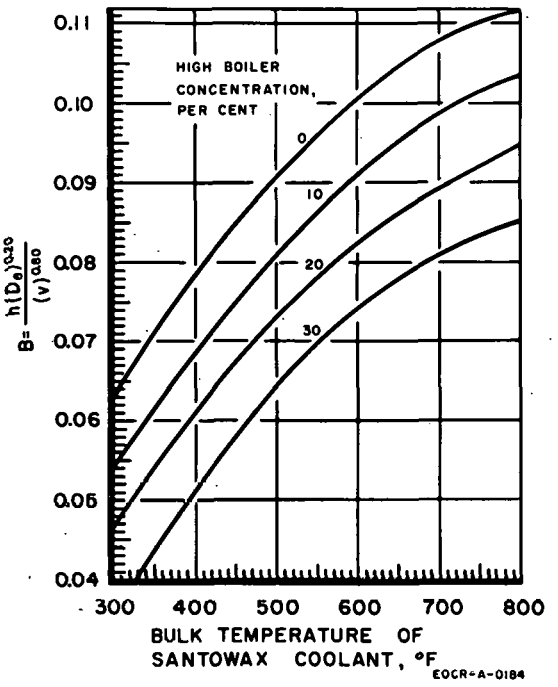

Fig. 45 Santowax heat transfer correlation.

Errors in Flow Orificing. Flow orificing affects the flow for the whole assembly. It may be monitored by measuring the pressure drop across the orifice. Some of the coolant leaves the element through the side slots in the extension tube and some through the orifice. The error in area of the slots may vary from about 1% for a high-flow element up to 4% for a low-flow element. The flow for an orifice-slot combination will be determined in the EOCRT flow test facility. The error in the flow determined in EOCRT is assumed as $\pm$ 10%. The total error in flow is thus assumed to be $\pm$ 14%.

Reactor Power Control. Reactor power is controlled by a servo system which operates from ion chambers sensing core neutron level. The setpoint for the servo system is based ultimately on core heat power calculated from the flow rate and temperature rise of the total reactor coolant flow. An analysis of a similar system in MTR [38] has resulted in an estimate of $\pm$ 10% error in the controlled power. It is assumed the same accuracy is obtained in EOCR.

Fuel-Meat-Thickness Deviation. The specified tolerance of fuel meat thickness, 0.020 $\pm$ 0.003 in., is assumed to be the local deviation of uranium density from the average value for the plate. The specifications also require, "the uniform distribution of the fuel matrix in each square centimeter of the plate; this shall be within 5% of the average area density of the fueled portion of the plate". Obviously, a requirement of 5% maximum deviation in uranium area density requires a similarly small deviation in meat thickness. The presently planned check on uranium area-density is by fuel plate radiographs. Densitometer measurements of the entire area of a fuel plate would be excessively expensive unless done only on a spot-check basis. Thus, the fuel-meat-thickness tolerance has been chosen as an attainable and probable maximum local uranium density tolerance. The error is thus $\pm$ 15% and is considered only a local effect. Variations over a whole plate are accounted for by the factors for meat area and fuel content per plate.

Flux Prediction. The power densities used in the heat transfer calculations are calculated power densities. The calculation results are a set of relative

TABLE XLVI

CHARACTERISTICS OF A-3 CORE

Core A-3 Loading	
Fuel elements	24
Control rods	12
Heat Transfer Areas (ft^2)	
Per fuel-element fuel plate	1.202
Per 56-plate fuel element	67.3
Per 24 fuel elements	1615
Per control rod fuel plate	1.702
Per 26-plate control fuel assembly	44.3
Per 12 control rods	531.0
Core heat transfer area:	
Startup: 4 rods withdrawn	1792
Shutdown: all rods withdrawn	2146
Flow Areas (ft^2)	
Fuel element	0.1143
Control rod	0.0796
Channel Hydraulic Diameters (ft)	
Fuel element	0.0158
Control rod central channel	0.0162
Core Active Length (ft)	
Channel heated length	3.0

power densities at the reactor midplane. Power outputs for volume sources were based on the assumption that the vertical flux and power distribution is chopped cosine function. Errors are implicit in this assumption, and there are errors involved in the flux calculations. Point deviations from the chopped cosine assumption are estimated to be $\pm$ 5%. It is assumed that the same error can be applied to the integral of the cosine flux distribution up to the hot spot, about half the length of the section. Errors in the original calculations are estimated by assuming the error in a single point on the flux map to be 10%, divided into a systematic error of 5% and an error of 5% which has a normal probability distribution. The error in the average flux in coolant channel was assumed to be 6%. The error in a 4- x 6-in. fuel assembly was assumed to be 5%.

TABLE XLVII

EOCR FUEL ELEMENT HOT-SPOT HOT-CHANNEL FACTORS BASED ON DESIGN INFORMATION

	Variable Affected									F_t	F_θ	F_ϕ
Source of Factor	P_e	f_c	f_p	Lp_h	W	V	a	D_e	B	Hot Channel Factor	Hot Spot Factor	Hot Flux Factor
Flow orifice error					1.14	1.14				1.14	1.12	
Power control error	1.10									1.10	1.10	1.10
Meat thickness error		1.15									1.15	1.15
Flux prediction error	1.05	1.10	1.05							1.06	1.10	1.10
h Correlation error									1.33		1.33	
Meat area error				1.02						1.02	1.02	1.02
Channel dimen. error					1.24	1.41	1.14	1.14		1.24	1.37	
Fouled channel dimen.					1.53	1.75	1.14	1.14		1.53	1.64	
Flow distribution					1.05	1.10				1.05	1.08	
Fuel/plate error		1.02		1.02						1.02	1.02	1.02
					Total Factors - new element					1.80	3.19	1.45
					Total Factors - fouled element					2.22	3.82	

TABLE XLVIII

EOCR CONTROL ROD FUEL FOLLOWER HOT-SPOT HOT-CHANNEL FACTOR BASED ON DESIGN INFORMATION

	Variable Affected									F_t	F_θ	F_ϕ
Source of Factor	P_e	f_c	f_p	Lp_h	W	V	a	D_e	B	Hot Channel Factor	Hot Spot Factor	Hot Flux Factor
Flow orifice error					1.14	1.14				1.14	1.12	
Power control error	1.10									1.10	1.10	1.10
Meat thickness error		1.15									1.15	1.15
Flux prediction error	1.05	1.10	1.05							1.06	1.10	1.10
h Correlation error									1.33		1.33	
Meat area error				1.02						1.02	1.02	1.02
Channel dimen. error					1.24	1.41	1.14	1.14		1.24	1.37	
Fouled channel dimen.					1.51	1.72	1.14	1.14		1.51	1.63	
Flow distribution						1.05					1.04	
Fuel/plate error		1.02		1.02						1.02	1.02	1.02
					Total Factors - new element					1.72	2.95	1.45
					Total Factors - fouled element					2.09	3.51	

h Correlation. The correlation used for calculating h is the Dittus-Boelter type correlation with a 0.0243 constant, rather than the usual 0.023, namely:

$$\frac{hD_e}{K} = 0.0243 \left(\frac{VD_e}{\nu}\right)^{0.8} \left(\frac{C\mu}{K}\right)^{0.2}$$

where

h = film coefficient

D_e = hydraulic diameter

K = heat conductivity

V = linear velocity

μ = viscosity

C = heat capacity

ν = kinematic viscosity

$= \mu/\rho$

This correlation was obtained by Atomics International for several polyphenyls [36, 37]. The accuracy of the correlation is stated in the references to be $\pm$ 25%. In a plot of the data and the correlation, data for Santowax R fall almost exclusively below the values predicted by the correlation. The possible error in calculated h has been taken as 25%.

Meat Area Deviation. This factor is based on the tolerances required by Drawing No. 5942-EOCR-601-MS-43. Together with the fuel per plate, meat area per plate determines the average heat flux, and the amount of meat area below the hot spot determines the bulk coolant temperatures at the hot spot.

Deviations in Channel Dimensions. The tolerances required by drawings for plate spacing and channel tolerances are shown in Figure 46 for the fuel elements and control rods. The hot channel and hot spot factors were determined from the effect on:

(1) Mass flow rate, W, from

(a) The effect on D_e, proportional to thickness, and its effect on V, proportional to $D_e^{2/3}$;

(b) The effect on area, proportional thickness.

(2) Local D_e, affecting the heat transfer film coefficient by $D_e^{-0.2}$.

(3) Local area, reducing channel velocity by the ratio of local area to channel average area. Local velocity affects the heat transfer film coefficient by $V^{0.8}$.

The ratio of nominal to minimum thickness for the present fuel elements is 0.098/0.086 or 1.14:1. The ratio of maximum to minimum thickness is 1.12/0.086 or 1.30:1.

It was assumed that the average thickness of the hot channel was the minimum permitted by the tolerance. At the hot spot, it was assumed that this channel widened to the maximum permitted by the tolerance.

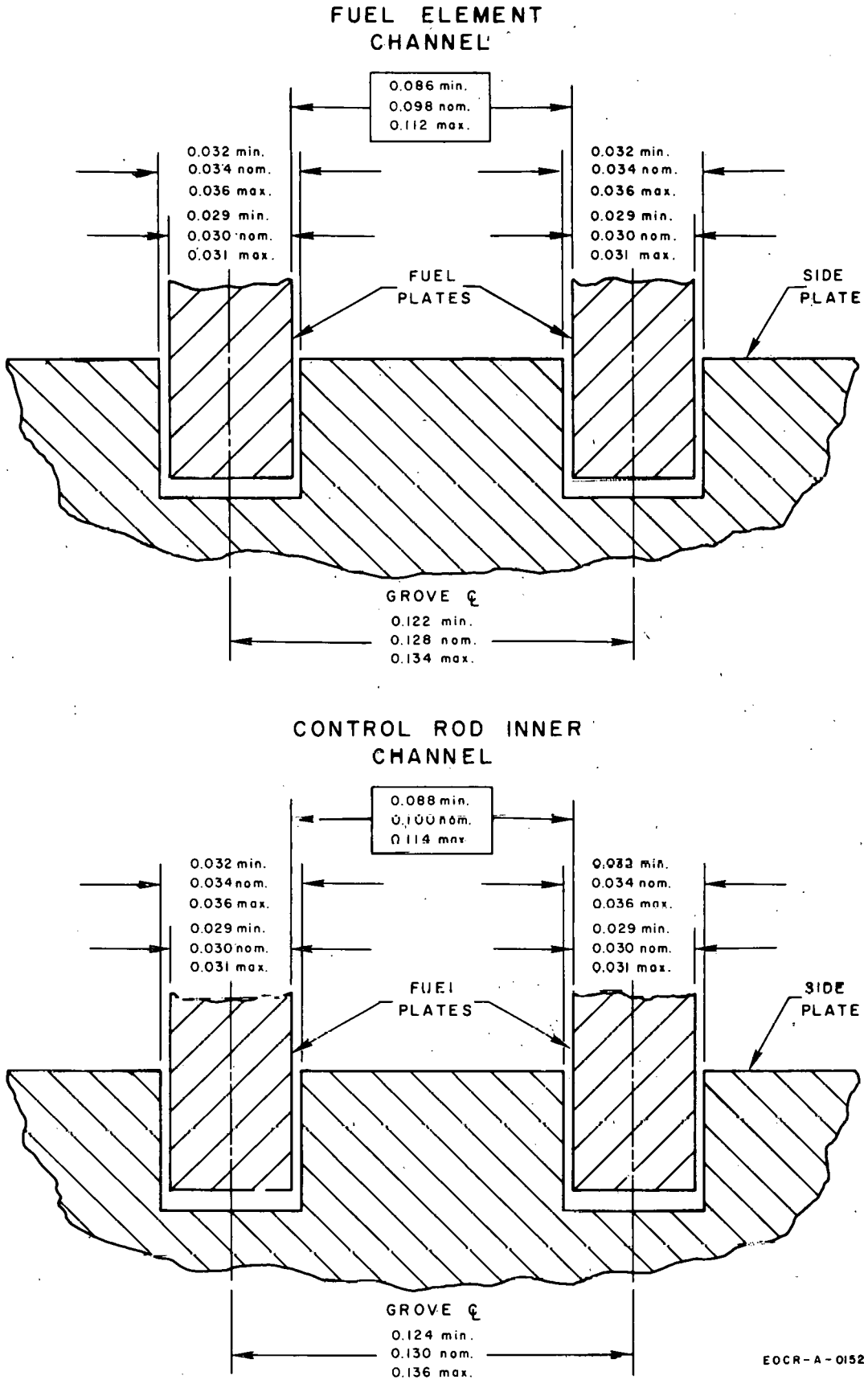

Fig. 46 Channel thickness tolerances.

Dimensions of Fouled Channel. This factor replaces the factor for clean channel dimensions for calculation of hot spot temperature at the end of the cycle. Since the significant temperature is that of the solid-coolant interface, whether the solid is fuel plate or fouling film, there is no factor for the resistance of the fouling film to heat conduction. The factors account only for the change in channel dimensions produced by the fouling film.

It was assumed that a uniform fouling film of the same surface smoothness as the surface of the fuel plate is formed. Since the fouling is rougher than the fuel plate, a thicker film than those found in OMRE elements was assumed (see Table XLIX). The film is assumed to be 5 mils thick on each plate bounding a channel of hot channel dimensions. It is further assumed that at the widest spot in the minimum-sized hot channel (the hot spot) the fouling film flakes off, leaving the wide spot at its original dimensions. This behavior - fouling film buildup, followed by flaking off starting at the hottest spot - has been observed in OMRE.

The hot spot factors, using the fouled-channel dimensions, were obtained in the same way as the channel dimension hot spot factors for clean channels which they replace.

The ratio of original nominal channel thickness to minimum fouled channel thickness is 0.098/0.076 or 1.20:1. The maximum-to-minimum thickness ratio is 0.112/0.76 or 1.47:1.

TABLE XLIX

OMRE FOULING RESULTS [39]

Fuel Element No.	Core No.	Exposure Length		Coolant Ash Content During Exposure (ppm)		Fouling Thickness (mils)	
		Core (Mwd)	Time (mo)	Average	Maximum	Average	Maximum
3	I	549	6	unknown	unknown	0.25	0.37
33	I	940	11	unknown	unknown	?	6
136	II	442	2	50	70	3	8
106	II	747	$6\frac{1}{2}$	100	220(a)	("0-2 mils")	
103	II	747/34(b)	$6\frac{1}{2}$	100	220(a)	("No thicker than on elements 136 and 106")	
109	II	747/34(b)	$6\frac{1}{2}$	100	220(a)		
123	II	904/40(b)	9	100	220(a)	?	?
130	II	904	9	100	220(a)	(Deposits bridging channel)	

(a) Occurred during shutdown; maximum during power operation, 180 ppm.

(b) Total burnup for fuel element.

Flow Distribution. Since the heat flux peak occurs at the edge of the meat, and since in a rectangular channel the velocity is lower in this region, a hot spot factor is included to account for the deviation from the average velocity in the channel.

A maldistribution of flow among the channels results from disturbances at the entrance and exit sections of a fuel assembly. The low flow occurs in the outer, hottest channels. Since the outer channels in the control rod are widened to correct specifically for the effect of the poison plates on channel-to-channel flow distribution, the control rod calculation was based on the size of a center, thinner channel and no factor was included.

The channel-to-channel velocity distribution of the fuel element is based on a measurement in water of flow through an EOCR fuel element dummy.

Fuel Per Plate. This factor represents the maximum deviation from nominal U-235 content per plate (and consequently heat flux) permitted by fuel element specification, namely 35.8 ± 0.5 g of U-235 per plate.

3.24 Projected Future Hot Spot and Hot Channel Factors. In the future, reactor operating experience and developments in OMR technology may be expected to permit reduction of hot spot and hot channel factors. The purpose of this section is to examine the probable reductions and their effect on reactor power. The factors shown in Tables XLVII and XLVIII will be examined individually. No account is taken of design changes which are possible, although the ability of fuel fabricators to meet or to improve upon specified tolerances is considered. For example, widening the meat or removal of minimum channel size restrictions imposed by the core designer could result in significant power increases. Revised hot spot and hot channel factors are given in Tables XLIV and XLV.

Flow Orifice Error. This factor is considered irreducible because, without drastic redesign of the upper extension of the fuel element, the orifice control is through a system not subject to accurate determination.

Power Control Error. This factor is considered irreducible since it was obtained from the characteristics of power control systems long in use.

Meat Thickness Error. The size of this factor reflects a conflict in the specifications and represents uranium area-density variation larger than specifications permit; control of uranium area-density independent of meat thickness is not possible with present manufacturing controls. An area-density variation of $\pm$ 5% is an obtainable tolerance on uranium density and may be assumed to be obtained in the future with revisions in specifications and adequate control. The reduction in hot spot factor from this cause is 1.05/1.15 or 0.91.

Flux Prediction Error. This factor is considered irreducible because future changes in core and experiment loading will result in flux changes which probably will be calculated due to the difficulty of making flux runs in this reactor.

h-Correlation Error. It is assumed that further work on organic heat transfer can reduce the uncertainty of the film coefficient determination to that of water, particularly in view of the fact that terphenyls have been shown

to be capable of correlation by traditional equations. It is assumed the hot spot factor can be reduced to 1.25, the value currently employed by Phillips Petroleum for water heat transfer. The reduction is thus 1.25/1.33 or 0.94.

Meat Area Error. This factor is considered irreducible because it is sufficiently small as to be not economically reducible.

Channel Dimension Error. Experience has shown that fuel elements may be made more accurately than many of the tolerances require, although the dimensional accuracy of fuel elements varies somewhat from fabricator to fabricator. It is antpcipated that the minimum allowable channel size represents the closest economically attainable tolerance and that the bulge or wide spot in the minimum channel, at which the hot spot occurs, can be held to within 10 mils of the average channel size. The resulting hot spot factor is 1.17.

Fouled Channel Dimensions. In view of the extensive research effort on fouling, it is assumed that channel dimension reduction from fouling may be made negligible. In fact, there is some evidence to indicate that this statement may be true for the EOCR first core. Since this factor affects only flow requirements of part of the elements, those which increase in power during the cycle, the resulting change cannot be accurately estimated without knowledge of future full cycle flux shifts. Based on present flux patterns, the effective reduction in hot spot factors is 0.95.

Flow Distribution. This factor is considered irreducible without redesign of the element.

Fuel/Plate Error. This factor is irreducibly small.

The operating powers possible with a set of hot spot factors based on the above considerations, but employing the same calculation method used in the development of Figure 47, are given in Figure 42.

3.25 Coolant-Flow Distribution. The EOCR is orificed element-by-element to use coolant more efficiently. The fuel elements are orificed so that the calculated hot spot temperature of the fuel plate surface is held to a selected value in all elements. The calculated hot spot temperature which is selected for control is called the limiting temperature and is the temperature used herein as a measure of the severity of core operating conditions. The flow distribution is shown in Figure 48; the actual flow rates reported in Figure 48 are based on a total flow rate of 22,000 gpm to the 24 driver fuel assemblies and 12 control rod fuel followers. The hot spot surface temperature of the control rods was reduced to 790°F relative to a fuel element temperature of 850°F by increasing the flow in the rods. This has been done to allow for future

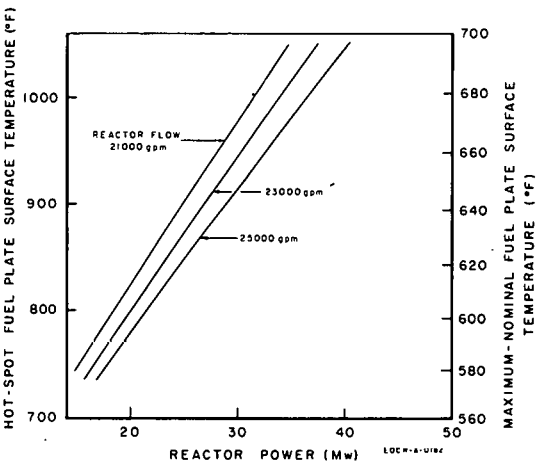

Fig. 47 Core A-3 calculated power levels (based on hot spot and hot channel factors derived from design information).

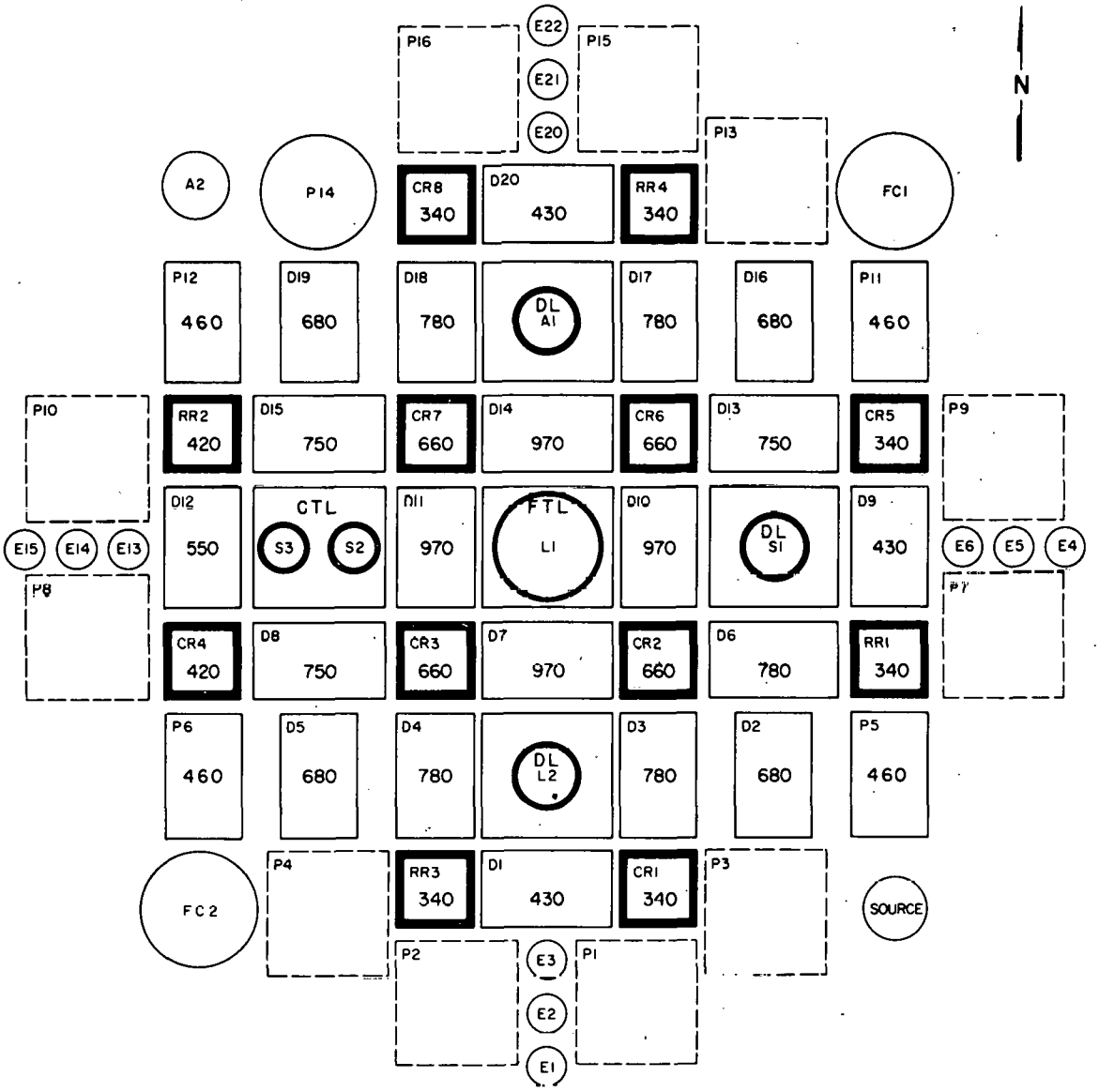

D DRIVER FUEL ASSEMBLY
CR CONTROL ROD
RR REGULATING ROD
L LARGE TEST LOOP
S SMALL TEST LOOP
A RABBIT OR LOOP TEST POSITION
P PROTOTYPE-FUEL TEST POSITION
E CAPSULE & LEAD-TYPE TEST POSITION
FC FISSION CHAMBER

FTL FUEL TECHNOLOGY LOOP
CTL COOLANT TECHNOLOGY LOOP
DL DUMMY LOOP

Fig. 48 Core A-3 flow distribution (gpm per channel). Basis: total coolant flow rate of 22,000 gpm through the 24 fuel elements and 12 control rods.

increases in power density in the control rods up to 20% without changing the control rod flow orifices.

The flow distribution is based on the heat transfer calculations previously discussed. The flow distribution, shown in Figure 48, will be used for low-power operations with the first core loading until experimental flux information becomes

available. Then, if necessary, the flow orifices will be changed prior to high-power operation to achieve the flow distribution suggested by the experimental flux information. This philosophy will be used in establishing the flow distribution for future core loadings which involve major changes. Additional experimental information with various orifice sizes will be obtained, using the EOCR Test Facility in order to assist in sizing the orifices used in the reactor.

3.26 Calculated Power Ratings for Core A-3. Figures 42 and 47 present reactor power as a function of the temperature of the hot elements, those having the maximum fuel plate surface temperature in the core for three coolant flow rates. These curves are based on 500°F inlet bulk coolant temperature and Santowax OMP coolant with 5% HB content. The flows quoted are total reactor flows, including flows through leakage paths around core pieces, filler pieces, and experimental pieces, and flows required for those capsule positions and filler pieces which are cooled by primary coolant. The total requirements for this cooling and for leakage are estimated at 1200 gpm.

Figure 47 is based on hot spot factors from Tables XLVII and XLVIII. Figure 42 is based on anticipated future hot spot factors from Tables XLIV and XLV. With extensive temperature instrumentation of the fuel plates, powers higher than indicated by either figure undoubtedly are possible for any selected limiting temperature. The hot spot temperature is the result of the hot-spot hot-channel calculation. The maximum nominal temperature is the temperature calculated from nominal dimensions and operating conditions at the same location as the hot spot temperature. It is the most probable temperature corresponding to the low-probability hot spot temperature. The nominal temperature scale in Figure 47 (and also Figure 42) represents the largest value of nominal temperature associated with the corresponding temperature on the hot spot temperature scale. Since the relationship between the two is not constant for all elements or times in the core life, the actual nominal temperatures corresponding to any hot spot temperature have a range of several degrees. It can be seen in Figure 47, that the most probable peak temperature in an element with a calculated 850°F hot spot plate temperature is about 620°F.

Nucleate boiling should commence at about 1050°F plate temperature, in the absence of low-boiling organic impurities or large amounts of dissolved gases. This represents the upper limit of applicability of these curves. Radiolytic diphenyl is expected to build up in the coolant. Since the equilibrium diphenyl concentration which may be expected (and its overall effect) is unknown, diphenyl will be closely studied during early operations. Pool boiling experiments [40] indicate that diphenyl will affect the temperature of the transition from nonboiling to nucleate boiling, but that it will have little effect on burnout.

All of the curves in Figures 42 and 47 are based on 500°F coolant inlet temperature. The effect of coolant inlet temperature on core power is illustrated by Table L, which lists comparative

TABLE L

EFFECT OF INLET TEMPERATURE ON REACTOR POWER

Conditions: At 850°F hot spot temperature and 23,000-gpm reactor flow.

Core Inlet Coolant Temperature (°F)	Reactor Power (Mw)
500	23
600	18
700	11

powers with an 850°F hot spot temperature and 23,000-gpm reactor flow rate for several inlet temperatures.

3.27 Burnout Heat Flux. Burnout heat flux is compared with heat fluxes at reference points in Core A-3 in Table LI. The assumed reactor power is

TABLE LI

EOCR BURNOUT HEAT FLUX

	Reference Channel	Nominal Value Core Peak Power Point	Core Hot Spot
Pressure (psia)	150	147	147
Coolant velocity (fps)	12.7	18.8	8.4
Coolant temperature (°F)	508	534	561
Heat flux (Btu/hr-ft^2) (Beginning of life)	45,700	175,000	253,000
Burnout heat flux with 5% high boiler (Btu/hr-ft^2)	1.03×10^6	1.04×10^6	870,000
Burnout margin with 5% high boiler	22.5	5.9	3.4

24 Mw, the assumed inlet temperature is 500°F, and the flow distribution is as given in Figure 48. The "reference channel" is a hypothetical driver-fuel-element channel operating at conditions obtained by averaging all channels in the core on the basis of coolant flow and power generation. Tho "core peak point" is the point of maximum heat flux in the core, and the values given under this heading are nominal, or most probable, values. The "core hot spot" values are for the same point with the flow reduced and the power generation increased by the hot spot factors previously discussed.

The burnout heat fluxes are those given by the Griffith Correlation [41] with a minus 33% conservative factor applied. The values quoted were obtained from the graphs by Baumeister [42]. Graphs from these sources are shown in Figures 49 and 50, respectively.

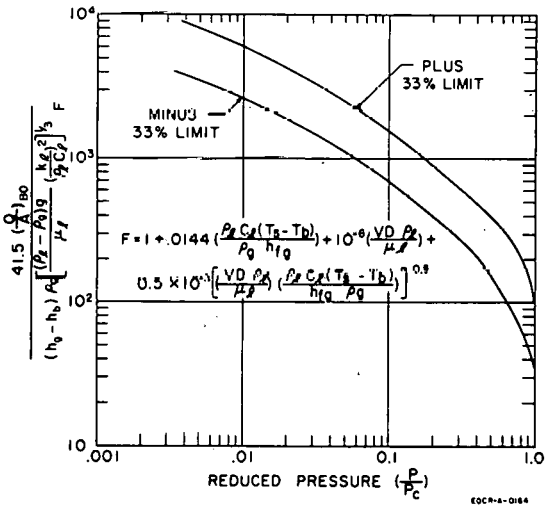

Fig. 49 Griffith burnout correlation.

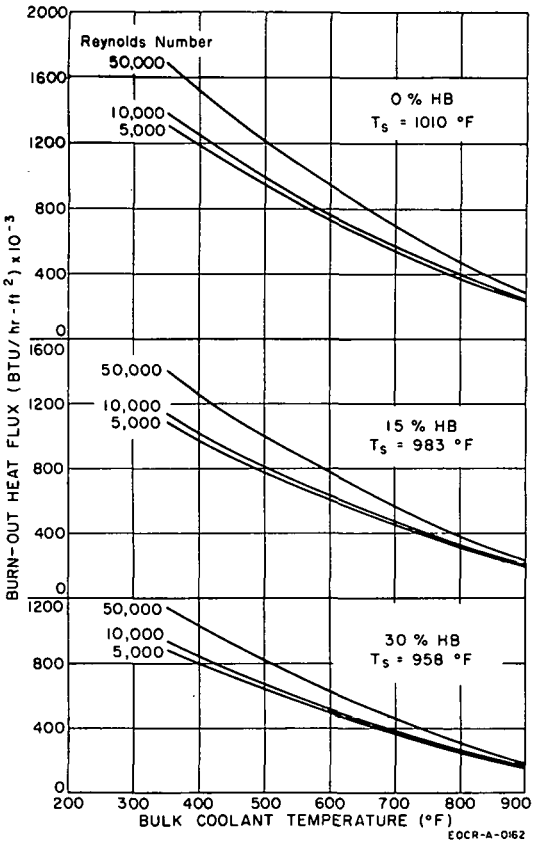

Fig. 50 Burnout heat fluxes for Santowax R at 150 psia.

3.3 Reactor Physics - Operating Lifetime of First Loading (R. W. Goin)

A two-dimensional burnout study has been made on the proposed first EOCR operational core loading (Core A-3, see Figure 51). Based on these calculations, it is expected that the initial EOCR core will have an operating life of 1200 Mwd or more.

Specifically this study was based on the northwest quadrant of Core A-3 shown in Figure 52. Due to imposed symmetry, lattice positions S1 and S2 each contains two 2.875-in. OD tubes, A1 and L2 each contains one 2.875-in. OD tube, and L1 contains a fuel follower.

The first time-step described the core as having the four inner control rods withdrawn and the eight outer rods inserted. This step was operated for 100 Mwd to allow fission product poisons to build into their equilibrium values. The second time-step continued with the same configuration to a total of 1000 Mwd. At the beginning of the third time-step, all eight outer control rods were considered withdrawn, and the time-step was terminated after 1000 Mwd, a total of 2000 Mwd. The fourth time-step continued time-step three to a total of 3000 Mwd.

The calculated values of k at the beginning of each time-step are given in Table LII. From these results it is found that the fission product poisons are worth about 0.056 Δk, fuel burnout accounts for approximately 0.012 Δk per 1000 Mwd, and the outer eight control rods are worth about 0.07 Δk. The value of control rod worth is slightly higher than that given previously [43] due to the flux shift caused by fission product poison. Figure 53 gives a plot of k-excess vs Mwd assuming that the reactor is just critical with the four inner rods withdrawn. Figure 53 indicates a charge life of 1200 Mwd. (The initial k_{eff} of 1.07 is the estimated actual k_{eff} of Core A-3. The development of this estimated actual k_{eff} value is presented in a previous quarterly report [44].) If the reactor were just critical initially with three inner rods withdrawn, assuming an inner rod worth of 0.03 Δk, the charge life would be approximately 3800 Mwd.

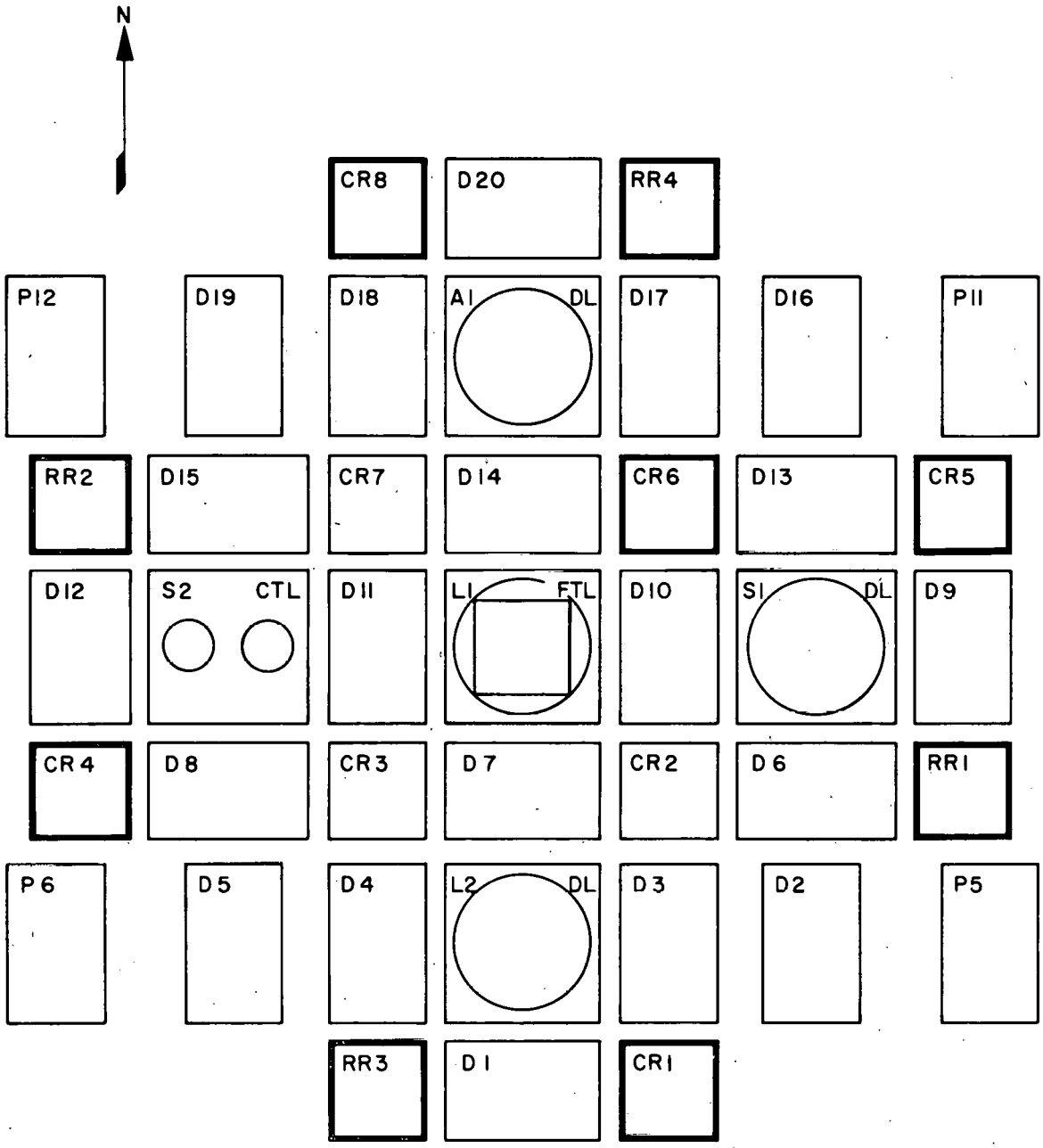

D DRIVER FUEL ASSEMBLY
CR CONTROL ROD
RR REGULATING ROD
FTL FUEL TECHNOLOGY LOOP
CTL COOLANT TECHNOLOGY LOOP
DL DUMMY LOOP

EOCR-B-0125

Fig. 51 Core A-3 cross section at midplane.

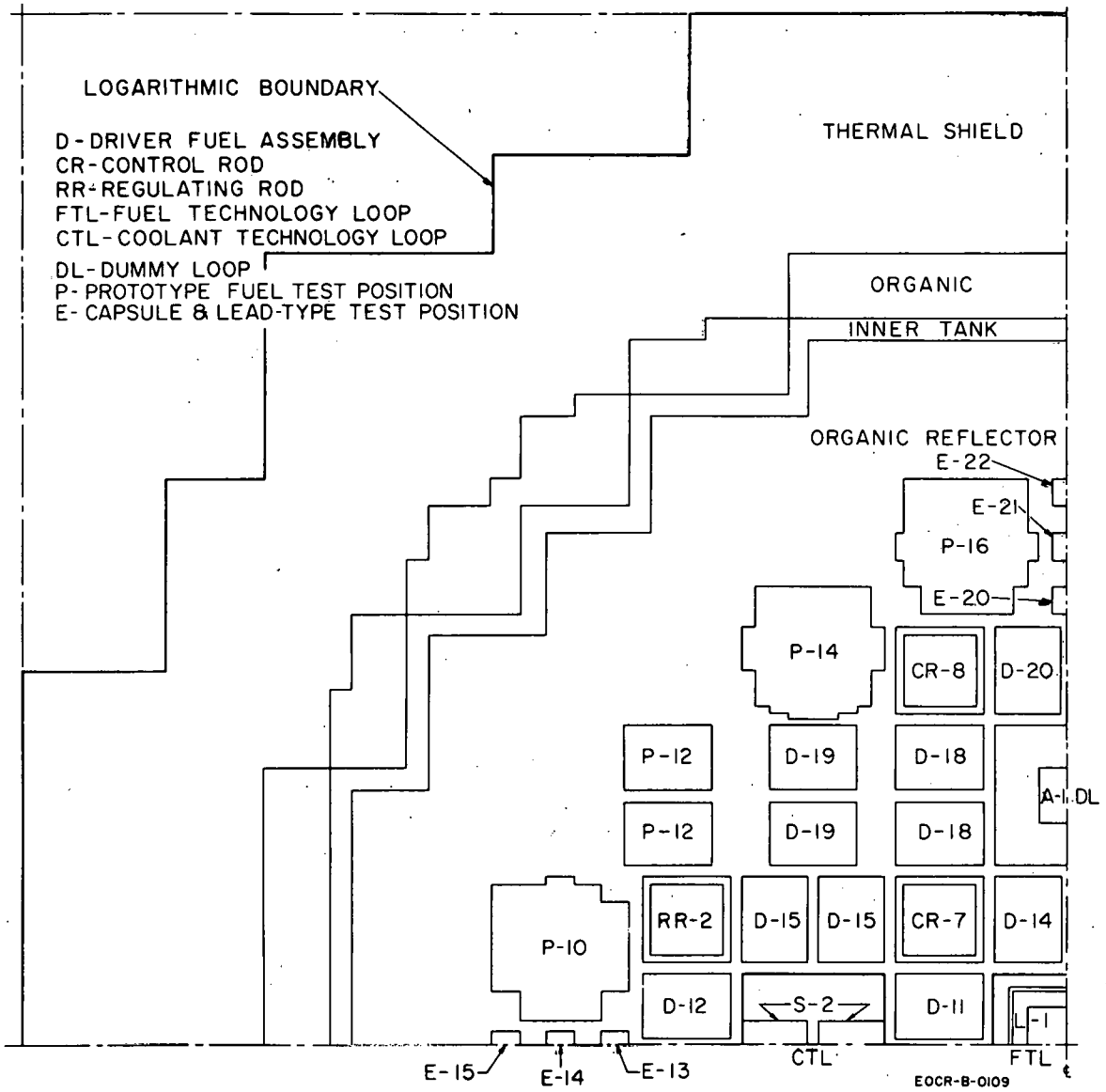

Fig. 52 PDQ model of typical EOCR quadrant.

TABLE LII

TURBO-CALCULATED k_{eff} VALUES FOR OPERATIONS WITH CORE A-3

Control Rod Disposition			
4 Inner	8 Outer	Mwd of Operation	Calculated k_{eff}
Fuel	poison	0	1.113
Fuel	poison	100	1.057
Fuel	fuel	1000	1.116
Fuel	fuel	2000	1.104

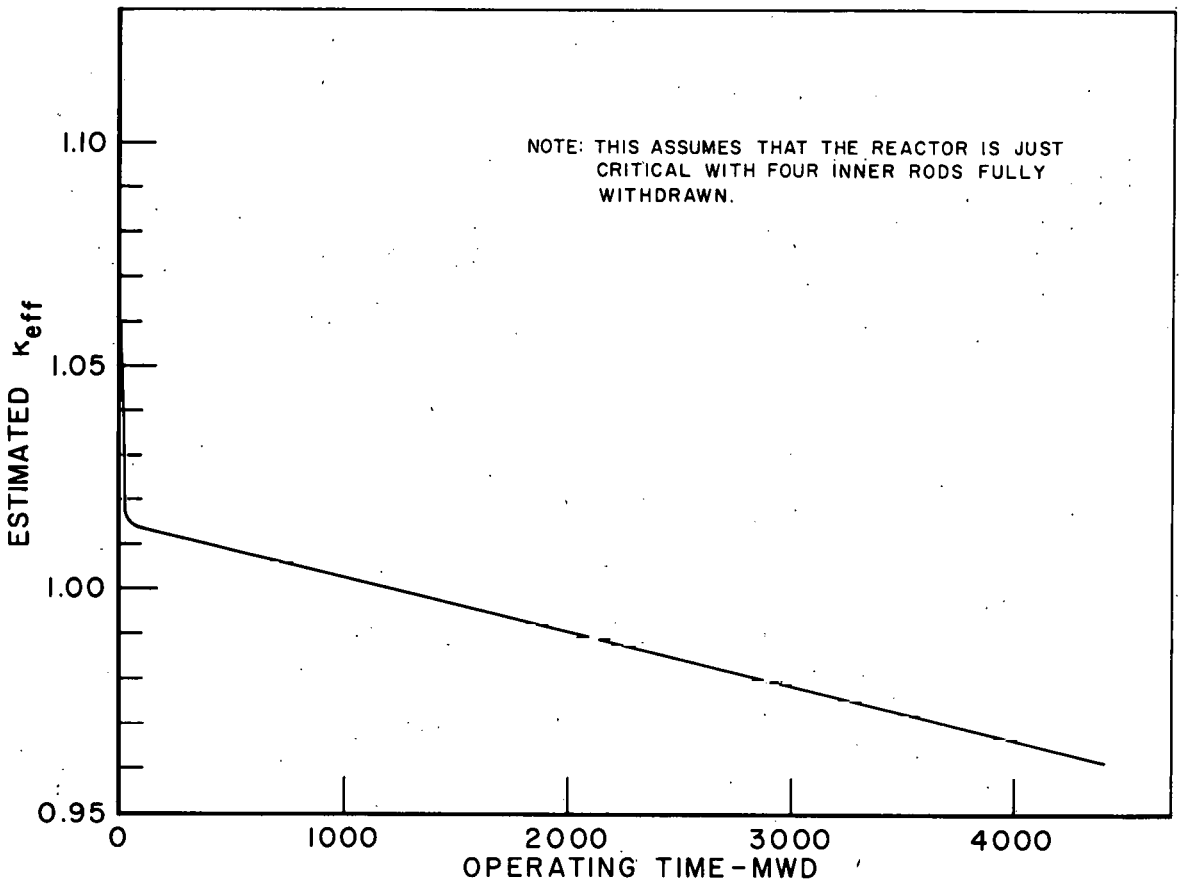

Fig. 53 Estimated k_{eff} vs operating time for EOCR Core A-3.

III. EOCR OPERATIONS

1. INTRODUCTION

Operations Branch personnel, by means of close liaison with the architect-engineer and construction contractor, continued to study and evaluate design and construction of the facility. This evaluation and study was directed toward efficient and safe operation of the EOCR.

Other areas of activity included preparation of portions of the final hazards report and operating manuals. Testing of a prototype control rod and drive mechanism was continued.

2. EOCR DESIGN AND CONSTRUCTION

2.1 Construction Status

The reactor vessel and reactor internal components were received. The vessel was moved to the reactor building main floor for external cleaning and installation of heaters and insulation. It was lowered into position March 26, 1962 for final setting and alignment. Wash cell components were received and pre-assembly testing and check-out was begun. Installation of primary coolant pumps, process piping, and steam tracing lines continued.

Fabrication of control rod poison plate assemblies was completed. The plates were then subjected to ultrasonic testing. Six completed poison assemblies have now been received at the site. Overall completion of the EOCR was approximately 83% as of March 30, 1962.

2.2 Radiography and Inspection of Organic Piping

The extent of radiographic examination of organic process piping was evaluated. Recommendations for additional radiographing and inspection of the organic piping were discussed with IDO-AEC and the additional testing approved. These additional requirements for organic piping welds are tabulated below:

(1) Class 9 piping (organic coolant - 335 psig and 850°F).

Continue radiography with one picture per weld through 4-in.-diam pipe. Take sufficient additional pictures to give 100% coverage on piping 6 in. in diam and larger.

(2) Class 8 piping (organic coolant - 300 psig and 850°F).

Since none of this piping is larger than 2 in. diam, and is all socket weld, no additional testing is required.

(3) Class 6 and 7 (organic coolant - vacuum to 80 psig, 850°F).

One radiographic picture will be taken at each weld on piping above 2 in. diam throughout the system. Dye-penetrant test the root pass of all uncompleted piping.

2.3 Reactor Vessel Bottom Head

As mentioned in the previous quarterly report [22], the reactor bottom head could not be aligned with the grid, spiders, and top head, due to improper location of the bolt holes in the bottom head. This fabrication error was adjusted by rotating the grid, spiders, and top head 33 minutes east of north with reference to the reactor vessel. This corrected the misalignment problem; however, it caused the relocation and slight modification of other minor components.

3. FIELD TESTING

Representatives of the branch witnessed plant equipment component tests (A-tests) performed by the construction contractor, C. F. Braun. These tests are not considered complete as final test data have not been transmitted to Phillips Petroleum. Component tests which were witnessed are:

A-205, overhead bridge crane

A-250, diesel-driven generator

A-211, instrument air compressor

A-217, demineralizer packages

A representative of the branch, along with the representatives of the architect-engineer and construction contractor, traveled to Salt Lake City to inspect and witness testing of the nuclear instrumentation received by Montek, Inc. from Bendix Corporation. Results of this testing are:

(1) Startup channel testing was not witnessed because precision test equipment was not available. Bendix test data will be verified by further acceptance testing at the EOCR site.

(2) The period channel was checked with a period simulator and the response was acceptable.

(3) The flux level amplifier was found to have an insufficient range. Montek agreed to make the necessary changes to enable the equipment to perform within the desired range.

(4) It was found that the scram logic channel would not drop the control rods on some of the tests performed. Montek agreed to make the corrective circuit changes.

C. F. Braun has agreed to release the equipment to Phillips when received at the job site for testing with precision test equipment.

The schedule for performing plant acceptance tests was reviewed with C. F. Braun. It appears that systems testing, which will be performed by Phillips, will be started about the middle of June.

4. OPERATIONAL PLANNING

Operational planning included completing (in initial draft form) portions of the final hazards report and plant operating manuals. A substantial effort is being made forecasting anticipated needs and initiating design and procurement of various items which will be required for operation of the plant. This work is summarized below.

4.1 Final Hazards Report

The initial draft form was completed on the final hazards report. Sections prepared by the Operations Branch included reports on principal EOCR design features, plant and reactor descriptions, reactor control and nuclear instrumentation, reactor operation, and organization and philosophy of operation.

4.2 Operating Manuals

Initial drafts were completed on all portions of the utilities section of the operating manual. This portion of the manual includes reports on the systems for raw water, fire protection, chemicals, demineralized water, diesel oil, boiler fuel oil, condensate, steam, pressurized cooling water, plant and instrument air, aqueous waste, gaseous waste, heating and ventilation, electricity, and evacuation alarm.

Preparation has started on the reactor area portion of the manual. This portion of the manual will cover operation of the reactor primary coolant loop and all allied systems.

4.3 Plant Requirements

Design was completed on the following EOCR equipment or allied facilities: (a) FTL tie-in to primary systems, (b) driver fuel instrumentation, (c) tools for removing mock-up pieces, (d) insulated working platform for top spider, (e) handling tools for individual pieces of equipment, (f) nitrogen and propane piping manifold, (g) equipment required for relocation of EOCRT at EOCR site, (h) facility to burn high boiler residue, and (i) area guardhouse and fencing.

Proposals were initiated for moving the EOCR test facility to the EOCR site and for construction of an HBR disposal facility. In addition, design and engineering were either started or continued on many other projects. Examples of the work underway include (a) neutron source handling tool and cask, (b) handling tools for use in the reactor and canal, (c) handling equipment for flake Santowax, (d) primary coolant sampling stations, (e) tool washing facility, (f) startup chambers, (g) aqueous waste monitoring, (h) rabbit facility, (i) FTL sample, and (j) fuel element storage rack.

4.4 Procurement of Organic Coolant

Specifications for the reactor organic coolant were prepared, finalized, and issued for bid. General coolant requirements as outlined in the specifications are as follows:

Coolant - terphenyl

Terphenyl content - 98% by weight (min.)

O-terphenyl - 10 wt% Min.) - 15 wt% (max.)

M-terphenyl - 55 wt% (min.) - 70 wt% (max.)

P-terphenyl - 20 wt% (min.) - 30 wt% (max.)

Diphenyl content - 1 wt% (max.)

High boiler compounds - 1 wt% (max.)

Melting point - 315°F or less

Maximum allowable impurities were specified as follows:

	ppm		ppm		ppm
Copper	2.0	Boron	0.5	Nickel	3.0
Sodium	0.2	Calcium	10.0	Silicon	3.0
Manganese	0.1	Chromium	1.0	Silver	0.1
Chlorine	3.0	Cobalt	0.1	Tin	1.0
Sulfur	60.0	Iron	10.1	Titanium	5.0
Phosphorus	8.0	Lead	4.0	Zinc	1.0
Aluminum	1.0	Magnesium	1.0	Zirconium	1.0
Arsenic	0.5	Mercury	0.1	Selenium	0.5
Barium	2.0	Molybdenum	1.0	H_2O	500.0

4.5 Reactor Fuel Procurement

A contract has been awarded for the fabrication of the first two core loadings for the EOCR. The fabricator will be Metals & Controls, Inc. of Attleboro, Mass. Deliveries of the driver fuel elements and fuel follower (control) rods are sheduled to begin during the third quarter of this calendar year.

4.6 Estimated Startup Schedule

Based on current plant construction progress, an anticipated pre-neutron testing and startup schedule has been prepared. This schedule, reduced to graphic form, is shown in Figure 54. Problems encountered with plant

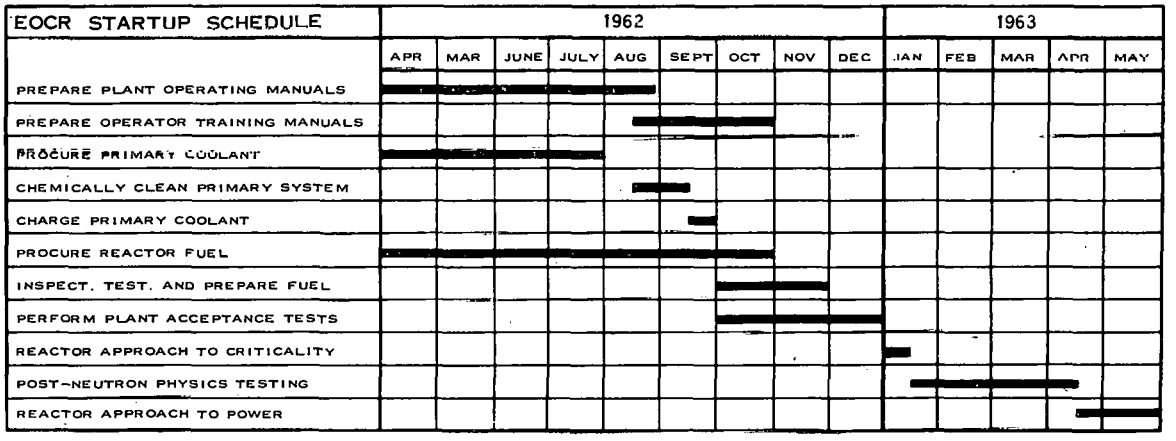

Fig. 54 Anticipated EOCR startup schedule.

acceptance tests or chemically cleaning the primary system, for example, can significantly alter the projected startup date. As indicated, it is anticipated that the approach-to-criticality experiment will not commence until after the first of next year.

5. COMPONENT TESTING PROGRAM

Testing of an EOCR prototype control rod and check-out of reactor control circuitry continued. Status of this work is summarized.

5.1 Control Rod and Drive Mechanism

The test program aimed at evaluating the design of the EOCR control rod drive and driver fuel assembly was suspended for much of the period due to deficiencies demonstrated in the piping of the organic test loop. Urgency of the test program required preparation of the facility for use with water. Preparation procedures involved removal and cleaning of all instrumentation as well as use of solvents in the loop piping for removal of all organic material. Testing was resumed using water at a temperature of 132°F. At this temperature the kinematic viscosities of water and Santowax OMP are essentially the same.

Tests were conducted to obtain flow-vs-pressure-differential data and drop-time data for the control rod.

Control rod conditions were varied by altering and testing the rod in the following manner; (a) as-built rod; (b) rod with scram spring removed; (c) rod with 100-lb weight added; (d) rod with 100-lb weight and modified piston; and (e) rod with 125-lb weight added and modified piston. In addition the rod boot orifices were varied from 15/64 in. diam to 1-1/4 in. diam. As shown in Figure 55 and Table LIII the design maximum flow requirement of 680 gpm was attained with satisfactory rod seating using a 1-1/4-in. boot orifice, modified piston, and 100 lb added ballast.

Additional testing of the control rod with added weight is planned. A program was begun testing the EOCR driver fuel with eight top orifice and slot combinations to control flow rates through the driver fuel.

The initial eight combinations of orifices and slots were those suggested by the reactor designer. The limited test results obtained as of the end of

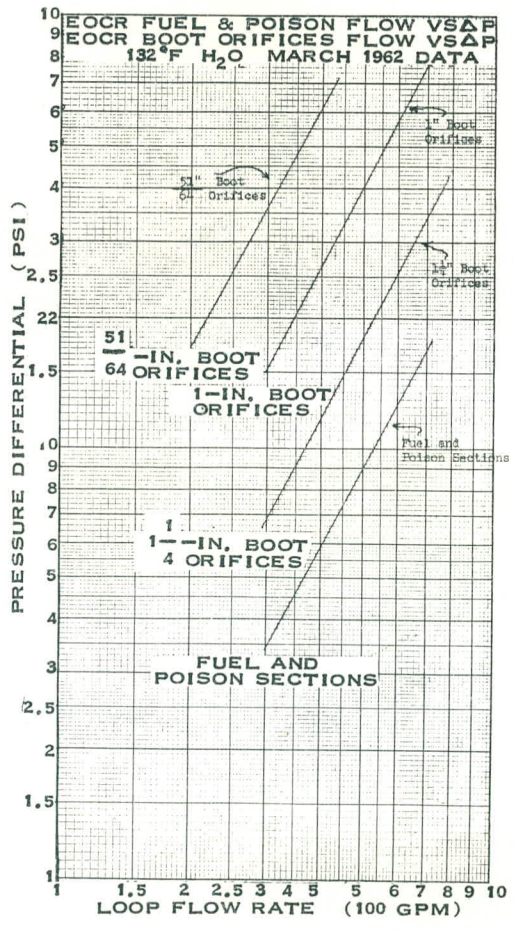

Fig. 55 EOCR control rod hydraulic data.

TABLE LIII

FLOW VS CONTROL ROD DROP TIME

Flow Rate (gpm)	Time for 36 in. Drop (msc)							
	As-built Rod, 1-in. Boot Orifice	As-built Rod, 1-1/4-in. Boot Orifice	Rod Without Scram Spring, 1-1/4-in. Boot Orifice	Rod With 100-lb Weight, 1-1/4-in. Boot Orifice	Rod With 100-lb Weight, Modified Piston, 1-1/4-in. Boot Orifice	Rod With 100-lb Weight, Modified Piston, 1-in. Boot Orifice	Rod With 100-lb Weight, Modified Piston, 51/64-in. Boot Orifice	Rod With 125-lb Weight, Modified Piston, 1-1/4-in. Boot Orifice
0	—	580	650	555	567	560	525	—
300	705	—	910	—	—	683	682	—
400	~ 825	790	1075	783	770	760	750	710
500	1010	966	1615	933	920	925	910 at 475 gpm	808
600	—	—	—	1183	1200	1333	—	1000
660	—	—	—	Time not obtained	1800 at 675 gpm	—	—	1175
700	—	—	—	—	—	—	—	1380
	Flow Rate (gpm)							
Maximum Rate For Seating	540	550	530	660	680	~ 640	—	700
Rod Lift Off	635	680	650	740	750	No lift off	No lift off	No lift off
Rod Back Down	405	385	300	565-545	490			

the report period (Table LIV) indicate that orifice and slot sizing will have to be modified. Test data obtained were extrapolated to a core differential pressure of 40 psig. Orifice number 5 was being installed at the end of the report period.

TABLE LIV

DRIVER FUEL ORIFICE FLOW

Conditions: Data in 132°F water.

Orifice No.	Top Orifices Total Area (in.^{2})	Slot Size (in.)	Predicted Flow Rate (gpm)	Extrapolated Flow Rate (gpm)
8	3.536	1.125 x 3.000	882-892	990
7	3.00	0.750 x 3.000	852	960
6	1.248	0.750 x 3.000	832	915
5	0.400	0.750 x 3.000	815	—
4	3.400	0.291 x 3.000	738-743	—
3	0.252	0.291 x 3.000	534	—
2	3.096	1/4 hole	481	—
1	2.704	1/4 hole	443-447	—

5.2 Reactor Control Circuitry

A control rod drive magnet and carriage identical to that furnished for the EOCR was fabricated and tested. Testing results showed it to be satisfactory.

An electronic scram circuit identical to that to be furnished was made up. Testing showed that the portion of the circuit that is supposed to suppress the high voltage created by the collapsing magnet field during scram failed to function properly. Various circuit revisions are being tested.

IV. REFERENCES

1. Organic Coolant Reactor Program Quarterly Report, 4th Qtr 1961, IDO-16761, p 1 (1962).

2. Ibid, p 7.

3. Organic Coolant Reactor Program Quarterly Report, 3rd Qtr 1961, IDO-16734, p 16 (1961).

4. J. Hoigne and Gaeumann, "Radiation Chemistry of Hydrocarbons", Helv. chim. acta 44, p 2141 (1961) (In German).

5. Organic Coolant Reactor Program Quarterly Report, 3rd Qtr 1961, IDO-16734, p 24 (1961).

6. Organic Coolant Reactor Program Quarterly Report, 2nd Qtr 1961, IDO-16713, p 9 (1961).

7. W. Huckel, Structural Chemistry of Inorganic Compounds 1, p 163, New York, Elsevier Publishing (1950).

8. J. C. Bailar, Chemistry of the Coordination Compounds, p 221, New York, Reinhold Publishing (1956).

9. Organic Coolant Reactor Program Quarterly Report, 4th Qtr 1961, IDO-16761, p 40 (1962).

10. L. Silverman and W. Bradshaw, "Rapid Spot Tests for Identification of Biphenyl, o-, m-, and p-Terphenyl, and Certain Other Polyphenyls", Anal. Chem. 27, p 96 (1955).

11. A. P. Altschuller and S. F. Sleva, "Spectrophotometric Determination of Olefins", Anal. Chem. 33, p 1413 (1961).

12. W. M. Hutchinson et al, Relationship Between Yields of Dimers of a Polyphenyl and Its Partial Reaction Rates, IDO-16706 (August 7, 1961).

13. G. F. Woods and L. W. Tucker, "Synthesis of m-Diarylbenzenes", J. Am. Chem. Soc. 70, p 3340 (1948).

14. G. F. Woods and F. Scotti, J. Organic Chem. 26, p 316 (1961).

15. J. Davidson et al, J. Organic Chem. 2, p 328 (1937).

16. Organic Coolant Reactor Program Quarterly Report, 4th Qtr 1961, IDO-16761, p 32 (1962).

17. Ibid, p 55.

18. Organic Coolant Reactor Program Quarterly Report, 4th Qtr 1960, IDO-16675, p 32 (1961).

19. Organic Coolant Reactor Program Quarterly Report, 4th Qtr 1961, IDO-16761, p 59 (1962).

20. Ibid, p 63.

21. R. J. Wineman et al, Organic Coolant Reclamation, 9th Quarterly Report, March 15 - June 15, 1961, TID-13355, Monsanto Research Corp. report (1961).

22. Organic Coolant Reactor Program Quarterly Report, 4th Qtr 1961, IDO-16761, (1962).

23. E Burroughs and S. Cohen, EOCR Control Rod Latch Reliability Test, IDO-16775 (March 1, 1962).

24. Organic Coolant Reactor Program Quarterly Report, 3rd Qtr 1961, IDO-16734, p 74 (1961).

25. EOCR Preliminary Hazards Report, IDO-24034 (April 1960), Addendum (November 1960), and Addendum No. 2 (April 1961).

26. Letter FL-1244 dated February 15, 1962, from M. R. Dusbabek of The Fluor Corp to H. M. Leppich, Idaho Operations Office, "EOCR Safeguards Report Information".

27. W. P. Schiffries, "EOCR Process Shielding", Atomics International Technical Data Record, No. 5582 (September 15, 1960).

28. Letter FL-1175 dated December 11, 1961, from C. D. Garrelts of The Fluor Corp to H. M. Leppich, Idaho Operations Office, with attachment "EOCR Off-Gas Radioactivity", by F. T. Selleck.

29. L. Baurmash et al, Radioisotopic Investigations of OMR Coolants. Part I. OMRE Operation, January 1958 through August 1960, NAA-SR-5049 (December 1961).

30. Letter 60AT-2185 dated March 8, 1960, from C. W. Wheelock of Atomics International to M. R. Dusbabek of The Fluor Corp, "Radioactivity in EOCR Process Fluids".

31. E. Peters and H. M. Binstock, Fabrication Modification Development of OMRE Third Core Loading, NAA-SR-5616 (July 15, 1961).

32. July-September, 1961, Quarterly Technical Progress Report on Non-Classified AEC Programs, Section III-A, NAA-SR-6777, p 4 (November 10, 1961).

33. October-December, 1961, Quarterly Technical Progress Report on Non-Classified AEC Programs, Section III-A, NAA-SR-6999, p 4 (February 2, 1962).

34. Robert J. Mack, Atomics International, private communication.

35. R. J. Nertney, Ed., Calculated Surface Temperatures for Nuclear Systems and Analysis of Their Uncertainties, IDO-16343 (June 1, 1957).

36. W. R. Martini, "Status of Heat Transfer Development for Organic Reactors", Proceedings of the Organic Cooled Reactor Forum, October 6-7, 1960, NAA-SR-5688, p 45 (December 1960).

37. Letter 61AT-5746 with enclosures dated July 19, 1961, from C. W. Wheelock of Atomics International to H. M. Leppich of Idaho Operations Office, "Organic Fluid Heat Transfer Coefficients and EOCR Power Rating".

38. F. H. Tingey, Error Propagation in Hot-Channel Hot-Spot Analysis, IDO-16588 (October 14, 1959).

39. Evaluation of the Organic Fouling Problem in the OMRE, U. S. Atomic Energy Commission, TID-6882 (March 24, 1961).

40. D. P. Jordan and G. Leppert, "Nucleate Boiling Characteristics of Organic Reactor Coolants", Nuclear Science and Engineering 5, p 349 (1959).

41. P. Griffith, The Correlation of Nucleate Boiling Burnout Data, Tech. Report No. 9, ASME Preprint 5.7-HT-21, NP-6446 (March 1957).

42. E. Baumeister, Calculated Burnout Heat Fluxes for Santowax R, NAA-SR-Memo-3860 (May 14, 1959).

43. Organic Coolant Reactor Program Quarterly Report, 2nd Qtr 1961, IDO-16713, p 54 (1961).

44. Organic Coolant Reactor Program Quarterly Report, 3rd Qtr 1961, IDO-16734, p 62 (1961).